Evaluating The Effects Of Lipopolysaccharides And Hydrogen Peroxide On Human And Mouse Astrocytes *In Vivo* And *In Vitro*, In Relation To Alzheimer's Disease

Author: Anjali Sivaram

Supervisors: Dr. Marie Christine Pardon and Dr. Graham Sheridan

Contents

Abbreviations

Abbreviation	Full form
AD	Alzheimer's disease
APP	Amyloid precursor protein
ATP	Adenosine triphosphate
Aβ	Amyloid beta
BACE1	B-site APP cleaving enzyme 1
BBB	Blood-brain barrier
BSA	Bovine serum albumin
C99	99-residue carboxy-terminal fragment of APP
CD-14	Cluster of differentiation 14
CNS	Central nervous system
COX	Cyclooxygenase
CSF	Cerebral spinal fluid
DAB	3,3'-diaminobenzidine
DMEM	Dulbecco's Modified Eagle Medium-high glucose
DNA	Deoxyribonucleic acid
DPBS	Dulbecco's phosphate buffered saline
ELISA	Enzyme linked immunosorbent assay
FBS	Foetal Bovine serum
GFAP	Glial fibrillary acid protein
i.c.v	Intracerebroventricular
i.p	Intraperitoneal
IFR	Interferon regulatory factors
IKB	Nuclear factor of kappa light polypeptide gene enhancer in B-cells inhibitor
IL	Interleukin
iNOS	Inducible nitric oxide synthase
LBP	Lipid binding protein
LPS	Lipopolysaccharides
MAPK	Mitogen associated protein kinases
MD-2	Myeloid differentiation (MD) 2 protein
MYD88	Myeloid differentiation primary response 88
mRNA	Messenger ribonucleic acid
MTT	3 3-(4,5-dimethylthiazol-2-yl)-2,5-diphenyltetrazolium bromide
NADPH	Nicotinamide adenine dinucleotide phosphate
NF-KB	Nuclear factor kappa light chain enhancer B
NFT	Neurofibrillary tangles
NO	Nitric oxide
NOX-2	NADPH oxidase 2
OD	Optical density
OH^-	Hydroxyl

PBS	Phosphate buffered saline
PRR	Pattern recognition receptors
qPCR	Quantitative polymerase chain reaction
ROI	Region of interest
ROS	Reactive oxygen species
O^{2-}	Superoxide
SOD	Superoxide dismutase
TIR	Toll interleukin receptor
TIRAP	TIR-associated protein
TLR	Toll like receptors
TNB	Trinitrobenzene
TNF- α	Tumour necrosis factor – α
TRAM	TRIF-related adaptor molecule
TREM2	Triggering receptor expressed on myeloid cells 2
TRIF	TIR domain-containing adaptor protein inducing interferon β
Tx-100	Triton X 100

Abstract

Alzheimer's disease is a neurodegenerative disease characterised by gliosis, decreased neuronal cell viability, cognitive impairment, as well as increased amyloid beta levels, cytokine expression and oxidative stress. These symptoms have been seen in *in vivo* and *in vitro* studies that have utilised LPS, inflammatory endotoxins that are derived from gram negative bacteria. Moreover, these are found at elevated levels co-localised with amyloid plaques and astrocytes in the brains of AD patients. Given its ability to mimic or exacberate such neuroinflammatory changes, and its relevance in AD pathology, this study looks at leveraging LPS to stimulate astrocytes *in vivo* using intranasal LPS, and *in vitro,* using the astrocytic SVG-A cells. These models can then be used in the future to test novel anti-inflammatory therapies against AD.

The first part of this study determined the efficiency of delivering LPS intranasally to the hippocampus of C57BL/6 mice. In this double-blind experiment, wild-type C57BL/6 mice were stimulated with 60 µg/ml of LPS given bilaterally in three doses over 24 hours. The effect of this LPS challenge on the hippocampal astrocyte population was analysed 14 days post-treatment, by quantifying and comparing the percentage area covered by DAB-labelled GFAP-positive astrocytes in LPS versus PBS treated mice.

The second part of this study investigated the effects of LPS *in-vitro*, by stimulating immortalised astrocytic SVG-A cells with 0 µg/ml to 10 µg/ml of LPS. The levels of pro-inflammatory IL-6 and IL-1β secreted after 3 hours were quantified by ELISA, and their cell viability after 24 hours was analysed using a MTT assay. Furthermore, the presence of key LPS receptors, TLR-4 and CD-14 receptors were visualised using immunocytochemistry.

In the last part, the effect of oxidative stress on the cell viability of astrocytes was also analysed. This was done by stimulating the SVG-A

cells with 0 µM to 1000 µM of hydrogen peroxide, a pro-oxidant, using MTT assay.

The results showed no difference ($p>0.999$) in the total hippocampal area occupied by the DAB labelled GFAP-positive astrocytes in the mice treated intranasally with LPS (median = 4.617) or PBS (median = 4.979). In the *in vitro* studies, 0 µg/ml to 1µg/ml of LPS did not affect the cell viability of the astrocytes. While the SVG-A cells did express TLR-4 and CD-14 receptors, it was seemingly hyporesponsive to LPS. Only a maximum dose of LPS at 10 µg/ml resulted in a significant increase in the IL-6, however, even at this dose there were no detectable levels of IL-1β that were secreted. Alternatively, stimulating the SVG-A cells with hydrogen peroxide dose-dependently decreased their cell viability.

The results indicate that the intranasal administration of LPS did not have any long-term effects on mouse astrocytes. Further studies are required to see if LPS can be delivered successfully into the hippocampus using this protocol. The *in vitro* stimulation of SVG-A cells with LPS indicates that the SVG-A cells are hypo-responsive to LPS. In contrast, hydrogen peroxide might be a better stimulator in these cells. In conclusion, the SVG-A cells cannot be used with LPS to study AD, rather they are a better model to study hydrogen peroxide induced oxidative toxicity, in relation to AD.

Chapter 1: Introduction

1.1 Alzheimer's Disease

Alzheimer's Disease (AD) is one of the leading causes of dementia, an age-related cognitive and memory disorder. Majority of the cases are late onset and sporadic with no predictable Mendelian patterns of inheritance, affecting individuals over 65. Nevertheless, around 10 % of the incidences represent an early onset version of AD (Cheignon *et al.*, 2018). Hallmarks of the disease include pronounced brain atrophy - especially within the hippocampus - extracellular amyloid plaque deposits coupled with intracellular hyperphosphorylated neurofibrillary tau tangles (NFTs), neuronal cell death, loss of synapses, and gliosis (González-Reyes *et al.*, 2017; Cheignon *et al.*, 2018; Tweedie *et al.*, 2012; Manoharan *et al.*, 2016; Ashraf *et al.*, 2019).

The most documented causative hypothesis of AD is the amyloid beta hypothesis. This hypothesis centres around the insoluble amyloid beta plaques that precede the formation of NFTs and cognitive impairment (Hampel *et al.*, 2021). Amyloid beta (Aβ) is a cleaved portion of the amyloid precursor protein (APP) - a transmembrane protein. In normal conditions, it is cleaved at the Aβ domain by α secretase and then sequentially by two other proteases, the β and γ-secretases. This results in shorter and more soluble products that are non-amyloidogenic. However, in AD, the APP is first processed by B-site APP cleaving enzyme 1 (BACE1), a β-secretase enzyme, and then further cleaved by the γ-secretase complex. This results in the formation of insoluble amyloid beta peptides (Aβ), Aβ 1 – 40 and Aβ 1-42. These can oligomerise to form senile plaques (Hampel *et al.*, 2021). While both have been implicated in AD, Aβ 1- 42 are more capable of forming insoluble aggregates and the main component in the senile plaques. Certain studies have also indicated that Aβ 1 – 40 can be cytoprotective (Lee *et al.*, 2008).

The excessive extracellular amyloid beta deposits form plaques that encourage the formation of hyperphosphorylated NFTs. These have

been found in the neocortex, and their density has been associated with the severity of the cognitive decline and neuronal apoptosis seen in AD (Milton, 2004). NFTs are hyperphosphorylated tau protein, a microtubule-associated protein preferentially located within the axons of neurons. These NFTs are also found within the ageing brain; however, their levels are increased within different brain areas in neurodegenerative diseases (Milton, 2004; Jesus *et al.*, 2004).

Studies have also shown that Aβ plaques can be associated with decreased expression of neurotrophic factors, which leads to decreased neurogenesis affecting long-term potentiation, memory, and learning capabilities (Kahn *et al.*, 2012). However, while there has been a significant interest in the amyloid theory of AD; the prevalence of non demented population with high amyloid and NFT levels, and the failure of amyloid clearing therapies to restore cognitive decline in AD patients indicates that there might be another factor that drives the disease as well (Cunningham and Hennessy, 2015; Perez-Nievas *et al.*, 2013). Over the last decade it has been hypothesised that overstimulation of the innate immune system, both in the central and peripheral nervous systems, could play a part in neurodegenerative disorders like AD. This has been supported by genome-wide association studies that have linked AD to genes associated with immune receptors, such as the Triggering receptor expressed on myeloid cells 2 (TREM2).(Xie, Van Hoecke and Vandenbroucke, 2021; Heneka *et al.*, 2015; Kahn *et al.*, 2012).

1.2 What is neuroinflammation?

Inflammation is the activation of the innate immune system to counteract a harmful stimulus. The key players in inflammation are leucocytes, such as macrophages, which are involved in phagocytosis and antigen presentation. These leucocytes are recruited by endothelial cells or signalling molecules such as cytokines and nitric oxides (NO) at the site of the stimuli (Kinney *et al.*, 2018).

There are two types of cytokines that can be released at the site of inflammation pro-inflammatory and anti-inflammatory cytokines. These

are essentially proteins released by various cells and mediate cell-to-cell interactions. Pro-inflammatory cytokines are involved in propagating and sustaining inflammation by activating the immune cells in the body and mediating the production of other cytokines. Tumour necrosis factor – α (TNF α) interleukin (IL) 1β (IL-1β), IL-8, IL-12 and Interferon gamma (IFNy) are examples of pro-inflammatory cytokines. On the other hand, anti-inflammatory cytokines act against pro-inflammatory cytokines to control and reduce inflammation. These include cytokines such as IL-4, IL-10, and IL-1 receptor antagonist (IL-1RA). Some cytokines such as IL-6 are pleiotropic and can act as either anti-inflammatory or pro-inflammatory, depending on the situation (Zhang and An, 2007; Liu *et al.*, 2021). The dynamic balance between these two categories of cytokines ensures that immune cells and signalling molecules are recruited at the site of an infection or injury, and the inflammation is then regressed once the insult is resolved. However, excessive inflammation due to unregulated pro-inflammatory cytokine secretion can result in chronic inflammation, while excessive anti-inflammatory signalling suppresses the immune system (Liu *et al.*, 2021).

Another pro-inflammatory mediator are reactive oxygen/nitrogen species such as nitric oxide (NO). These add to inflammation by increasing oxidative stress (Zhao *et al.*, 2019). Inducible nitric oxide synthase (iNOS) is another signalling molecule that can promote the deleterious effects of inflammation by catalysing NO synthesis (Kinney *et al.*, 2018). More about reactive oxygen species (ROS) and oxidative stress will be introduced later in this chapter.

The first step in inflammation is the recognition of damage-associated molecular patterns or pathogen-associated molecular patterns by pattern recognition receptors (PRRs) present on the surface of the intracellular domain of immune cells. These PRRs recruit other cells that then oligomerise and release signalling molecules such as TNF α and IL -1β. These can stimulate endothelial cells at the site of injury to present adhesion molecules that can attract leucocytes to the site of the injury.

This way, inflammation is propagated and maintained (Lyman *et al.*, 2014; Newton and Dixit, 2012).

Chronic inflammation due to an imbalance between pro-inflammatory and anti-inflammatory mechanisms, results in sustained inflammation. When this occurs within the central nervous system, it is termed as neuroinflammation and it is propagated and characterised by the activation of innate immune cells of the central nervous system (CNS) (Ashraf *et al.*, 2019; Kinney *et al.*, 2018).

Strong systemic inflammation by infectious agents can lead to neuroinflammation as such seen in sepsis-induced encephalopathy (Xie, Van Hoecke and Vandenbroucke, 2021). Here, sepsis induced peripheral inflammation can induce lead to neuronal loss, activation of the brain's immune cells, and increase in IL-1β and TNF-α in the brain (Semmler *et al.*, 2008).

The blood brain barrier (BBB), the cerebral spinal fluid (CSF) and the arachnoid barrier protect the CNS from the periphery. The tight junction between the capillary and the endothelial cell in the BBB typically only lets in small lipids (0.4 to 0.6 kDa) through (Xie, Van Hoecke and Vandenbroucke, 2021). However, pro-inflammatory signalling molecules like TNF-α, peripheral leucocytes, as well as microbes and their endotoxins can disrupt these barriers, increasing the permeability of the brain or circumventricular organs. These regions do not have tight junctions and are hence more permeable. Once in the brain, these molecules can then activate the immune cells within the brain triggering neuroinflammation which can result in neurodegeneration, as discussed below. Apart from leading to an inflammatory positive feedback loop, these cytokines can also encourage cognitive impairment, decreased BBB permeability, the production of Aβ, hyperphosphorylation of tau and neuronal cell death (Xie, Van Hoecke and Vandenbroucke, 2021).

While the influx of white blood cells is not typically seen in the inflammatory state presented in AD, increased levels of pro-inflammatory cytokines in the serum, CSF, and AD brains as well as increased

incidents of mutations in TREM 2 receptors that supress the activation of macrophages (Cunningham and Hennessy, 2015), support the inflammatory role in AD. Moreover, several animal models of the disease have also shown improvement in response to nonsteroidal anti-inflammatory drugs (Lee *et al.*, 2008; Kinney *et al.*, 2018).

1.3 Key players in Neuroinflammation and Alzheimer's disease

1.3.1 Brain immune cells

The brain's immune cells are made up of microglia and astrocytes. Microglial cells are monocyte-derived cells involved in neuroprotection and neuroplasticity in the brain. They are the primary immune cells within the brain, essentially the macrophages within the CNS (Blasko *et al.*, 2004; Lyman *et al.*, 2014). In their resting inactivated state, they are highly branched with elongated projections and a small soma. They are constantly surveying the microenvironment of the brain and communicating with other cells using their branches (Kinney *et al.*, 2018). They also provide tissue support, are involved in synaptic pruning, and release trophic factors such as brain-derived neurotrophic factors that are involved in synaptic remodelling and memory formation (Guo, Wang and Yin, 2022).

Much like the peripheral macrophages, their activation in response to an insult or peripheral inflammatory mediators results in two different phenotypes: the proinflammatory 'M1' phenotype and the immunosuppressive 'M2' phenotype. The M1 phenotype is more reactive, proinflammatory and can be induced by infections. The M2 phenotype is induced by anti-inflammatory mediators and releases anti-inflammatory cytokines, and trophic factors are involved in phagocytosis and neuroprotection. In normal ageing models, it has been shown that the microglial cells lean more towards an M1 phenotype and upregulate PRRs such as Toll Like Receptors (TLRs), therefore any inflammatory insult results in a more exaggerated inflammatory response compared to that in younger models (Fenn *et al.*, 2012; Guo, Wang and Yin, 2022). This preference is also seen in neuroinflammation, where the cells

remain activated for an extended period (Lyman *et al.*, 2014). There is a phenotypic polarisation of microglia to the M1 phenotype, which subsequently turns into microgliosis within the cortex in response to either a central or a peripheral insult. It can be maintained even if the systemic inflammation may have resolved, resulting in gliosis characterised by hyperproliferation of activated glial cells (Trzeciak *et al.*, 2019).

Astrocytes are another member of the glial cells and the most abundant cell type in the brain (Preston, Cervasio and Laughlin, 2019; Liddelow *et al.*, 2017). They are now known to fulfil multiple functions within the CNS, such as maintaining the pH and supporting the BBB. They have a spongiform morphology and have multiple branches that interact with other cells like neurons. They enrich the formation of synapses and are involved in the uptake and recycling of neurotransmitters. They support the neurons immunologically and are capable of processing and storing glycogen to support the neuronal metabolic demand. These non-neuronal cells influence the formation of perivascular channels that remove metabolic waste and soluble proteins while ensuring the efficient transfer of nutrients through the vasculature. They also express a high number of Aquaporin 4 which helps maintain the cell membrane potential (Monterey *et al.*, 2021).

Like the microglial cells, in response to an immune challenge, these star-shaped cells undergo hypertrophic morphological changes and become reactive (Monterey *et al.*, 2021; Rodgers *et al.*, 2020). The astrocytes also have an ‘A1’ and ‘A2’ phase, expressing destructive or protective genes, respectfully. Infections, Aβ peptides, infiltrating cytokines, and cytokines released by activated microglia can encourage astrocytes to adopt the more reactive A1 state. When activated, they produce molecules like inflammatory cytokines like TNF-α, neurotrophic factors and cytotoxins (Lyman *et al.*, 2014; Li *et al.*, 2019). These changes in the glial cells are proinflammatory and neurotoxic, which can trigger acute or prolonged neuroinflammation that can propagate AD (Pardon *et al.*, 2016; Wang *et al.*, 2021; Lyman *et al.*, 2014). The A1 astrocytes lose their general

maintenance abilities and the ability to prune and form synapses. They are also toxic to neurons and oligodendrocytes (Liddelow *et al.*, 2017). The cytoskeleton of astrocytes is made up of several fibrils composed of the glial fibrillary acid protein (GFAP) and vimentin (Li *et al.*, 2019). In neurodegenerative diseases, there is an upregulation in the expression of these protein. Therefore, increased expression of GFAP, the most abundant of the intermediate filament proteins, is often used to identify reactive astrocytes (Li *et al.*, 2019).

The importance of astrocytes in neurodegenerative diseases such as AD has been shown in multiple *in vivo* and postmortem studies. Not only do reactive, type A1 astrocytes co-localise with amyloid beta plaques, they precede neuronal cell death and are one of the earlier markers of AD (Li *et al.*, 2019). In AD, reactive astrocytes can directly and indirectly induce the formation of Aβ plaques. Studies have shown that reactive astrocytes highly express β secretase enzyme, BACE 1, and APP. In AD, their increased expression is accompanied by an increased production of pro-inflammatory cytokines. These cytokines can also encourage the production of senile plaques by increasing the expression of APP and β secretase. This will be discussed further in later section 1.4.3. Furthermore, their hyperplasia positively correlates with increased cognitive decline (Li *et al.*, 2019). This could be attributed to the diminished ability of A1 astrocytes to help form synapses and phagocytose them. Along with their inability to support neuronal growth, they have also been found to induce the secretion of neuronal apoptosis by secreting an unidentified neurotoxin (Liddelow and Barres, 2017). Severe reactive astrocytes are also capable of producing hydrogen peroxide that induce neurodegeneration. (Li *et al.*, 2019; Ogunmokun *et al.*, 2021; Chun *et al.*, 2020; Monterey *et al.*, 2021).

1.3.2 Cytokines

In neurodegenerative diseases, levels of proinflammatory cytokines, such as TNF-α, IL-1β and IL-6, are reportedly elevated and associated with the senile plaques in AD (Ogunmokun *et al.*, 2021; McGeer and McGeer, 1997; Kinney *et al.*, 2018). TNF-α drives inflammation and can

be released by glial cells. Furthermore, it can self-regulate its expression by these cells and increase the production of APP protein. This cytokine, along with IL-6 and IL-1β can also increase the secretion and activity of β secretase enzyme, further implicating them in augmenting the deposition of amyloid beta plaques (Lee *et al.*, 2008). Additionally, these cytokines can also cross the BBB from the periphery, compromise calcium homeostasis and disrupt the integrity of the barrier, resulting in the infiltration of peripheral neutrophils and monocytes (Ogunmokun *et al.*, 2021).

1.4 Lipopolysaccharides (LPS)

Lipopolysaccharides (LPS) are glycolipids found on the external membranes of most gram-negative bacteria. While different species of gram negative bacteria produce structurally heterogenous LPS, they usually consist of three core components: an immunostimulatory glycolipid moiety called lipid A, bound to polysaccharide chains of hexose sugars and a polysaccharide composed of repeating subunits called the O-Antigen. This is demonstrated in figure 1.1 (Page, Kell and Pretorius, 2022; Beom Seok *et al.*, 2009). The Lipid A component is the most evolutionarily conserved region of the LPS; yet the post translational modifications of the Lipid A structure can vary considerably with different gram-negative bacterial species and even show micro heterogeneity amongst different bacterial strains. These changes are namely in the number of phosphate groups and acyl groups. As the Lipid A determines the immunogenic potential of the LPS, these post translational modifications can determine the extent of inflammatory response to a particular LPS challenge. For example, the *Escherichia coli (E. coli)* have six acylated chains in their Lipid A moiety making them one of the most potent strains of LPS, thereby inducing a strong inflammatory response (Saha *et al.*, 2022).

The toxicity of LPS can be attributed to the downstream activation of the immune system that it brings about. It is a potent ligand of the PRRs called Toll-Like Receptors (TLRs). These are evolutionarily conserved proteins expressed in most cells, especially in the immune cells (Page,

Kell and Pretorius, 2022; Kumar, Kawai and Akira, 2009). LPS is highly potent to TLR-2 and TLR-4, both of which are expressed in microglia and astrocytes (Rodgers *et al.*, 2020).

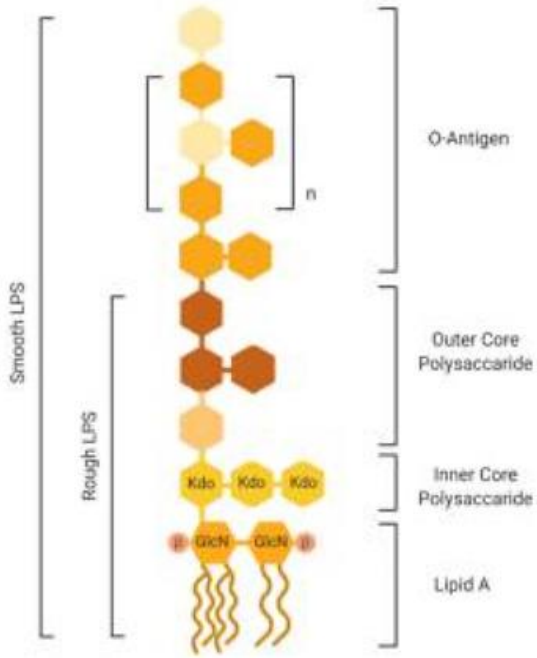

Figure 1.1: Structure of LPS *(Source: (Page, Kell and Pretorius, 2022). LPS contains an oligosaccharide spine attached to an O antigen and a Lipid A structure. The lipid A structure determines the endotoxic activity of the glycolipid and is essential for its interaction with the TLR4-MD2 complex (Beom Seok et al., 2009).*

1.4.1 Mechanism of action by LPS

While LPS is normally produced by the gram-negative bacteria within the gut of healthy humans, their levels are considerably low in the plasma. This is because, in physiological conditions, any LPS that enters the blood stream through the gut or the hepatic portal vein, is removed by the liver.

However, with age, the plasma levels of LPS increase due to an increased gut permeability (Kim *et al.*, 2016; Ghosh *et al.*, 2015). Additionally, during active infections, the levels of gram-negative bacteria can increase and overpower the hepatic clearance pathway (Wassenaar and Zimmermann, 2018).

These circulating LPS binds longitudinally to the Lipid binding protein (LBP), a glycoprotein that facilitates the transfer of LPS to the TLR-4 – MD2 complex. It carries the LPS micelles to the cluster of differentiation 14 (CD-14), a glycophosphatidylinositol anchored protein found on the macrophage membranes. CD-14 binds to the LBP-LPS micelle complex, where LBP transfers an LPS molecule to CD-14. CD-14 then transfers the LPS molecule to the hydrophobic pocket of the Myeloid differentiation 2 (MD-2) protein. MD-2 protein is expressed on the cell surface in association with TLR-4 receptors. When LPS binds to MD-2, it facilitates an interaction with another TLR-4/MD-2 complex as well. This triggers the dimerisation of two TLR-4/MD-2 complexes. (Nagai, Takatsu and Watson, 2014; Page, Kell and Pretorius, 2022; Ryu *et al.*, 2017; Beom Seok *et al.*, 2009; Tan and Kagan, 2014).

Following the structural change undergone by the TLR-4/MD-2 complex because of LPS, they recruit several toll interleukin receptor (TIR) domains containing cytoplasmic proteins. These are the myeloid differentiation primary response 88 (MYD88) protein, TIR-associated protein (TIRAP), TIR domain-containing adaptor protein inducing interferon β (TRIF), and TRIF-related adaptor molecule (TRAM). The recruitment of TRIF and MYD88 proteins leads to the activation of transcription factors such as nuclear factor kappa light chain enhancer B (NF-KB), mitogen associated protein kinases (MAPKs) and interferon regulatory factors (IFR) (Tan and Kagan, 2014; Akira, Uematsu and Takeuchi, 2006; Page, Kell and Pretorius, 2022).

Activation of the NF-KB pathway is relevant in the pathogenesis of AD. Activation of the NF-KB pathway involves the phosphorylation and degradation of the nuclear factor of kappa light polypeptide gene enhancer in B-cells inhibitor (IKB). The IKB exists in multiple isoforms within the cytoplasm and is bound to dimers of the NF-KB, sequestering them, and rendering them incapable of their transcriptional activity. Astrocytes constitutively express NF-KB, and its activation by LPS leads to astrocyte-mediated TNF-α, IL-1, IL-6 and NO secretion. Furthermore, activated NF-KB is found in the neuronal and glial cells associated with

the senile amyloid plaques (Sun *et al.*, 2022; Choi *et al.*, 2007; Kinney *et al.*, 2018). This mechanism is summarised below in figure 1.2.

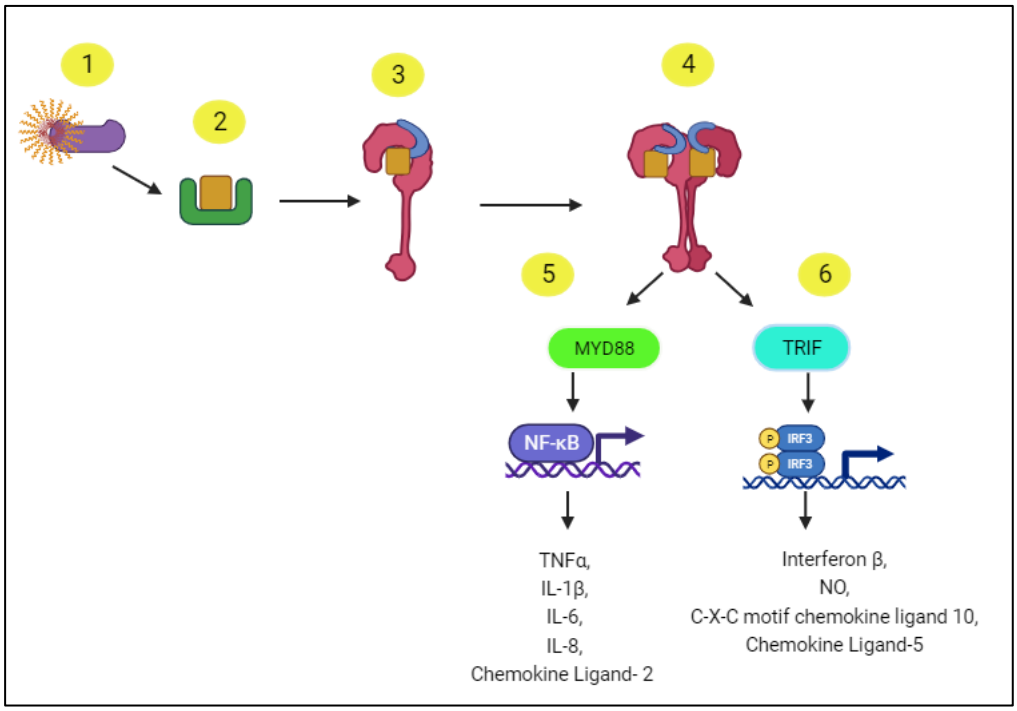

Figure 1.2: Mechanism of LPS signalling. 1) LBP carrying LPS micelles. 2) LPS is transferred to CD-14. 3) CD-14 then transfers this to the TLR-4/MD-2 complex. 4) These triggers two activated TLR-4/MD-2 complex to form homodimers. 5) This results in the MYD88 downstream signalling and 6) the TRIF mediated signalling, resulting in the transcription of several pro-inflammatory cytokines and chemokines, the latter are Image adapted from (Page, Kell and Pretorius, 2022) and created on bio render.

1.4.2 Role of LPS in AD

As stated earlier, there are different ways how the levels of LPS in the human body start to increase to pathological levels as seen in AD. Compared to the non-AD population, the plasma levels of LPS in the AD population are reportedly 3 to 6 times higher. Changes to the gut permeability or infections such as sepsis and periodontitis, are risk factors for the development of AD. Additionally, in conjunction to an altered gut microbiome with respect to gram negative bacteria, several gut derived gram-negative bacteria have also been found within the CNS

of AD patients (Kim *et al.*, 2021). (Brown, 2019) has reviewed several gram-negative bacterial infections that are more common in AD patients, that could give an insight into where LPS possibly arises from. Furthermore, inflammatory diseases like diabetes are also associated with elevated levels of LPS in the periphery and are also seen as a co-morbidity to developing AD (Brown, 2019; Cunningham and Hennessy, 2015). This increase in LPS can possibly prime the body's immune cells, making them more reactive to subsequent exposures, triggering elevated and sustained inflammation (Brown, 2019).

According to a study by Zhang R. *et al*. (2009), the plasma levels of LPS in 18 healthy volunteers were quantified to be around 21 pg/ml (Zhang *et al.*, 2009). In the same study, 18 patients with Alzheimer's disease were shown to have a higher level of plasma LPS levels of about 61 pg/ml. Increased gut permeability within the ageing population accounts for the increased plasma LPS levels. This is supported by recent data which suggests that this perturbation within the gut microbiome is also seen in mild cognitive impairment (MCI), the prodromal stage of AD (Zhao *et al.*, 2022; Jemimah *et al.*, 2023).

LPS has also been detected in the brains from cognitively normal participants as well as AD patients. In the study by Zhan *et.al* (2016), *E.coli* derived LPS was detected in both the superior temporal gyrus grey and the frontal lobe white matter within both control and AD brains of the same age. These LPS were shown to be localised within neurons, microglia, oligodendrocytes, and their progenitor cells. While their levels were significantly higher within the AD patients, it's important to note they were also co-localised amyloid plaques that stained for $A\beta_{1\text{-}40/42}$ and were surrounded by astrocytes in the cortex. LPS was also found associated with perivascular $A\beta_{1\text{-}40/42}$ in AD brain (Zhan *et al.*, 2016). Complimenting this study, gut-derived *E.coli* and *Bacteroides fragilis* LPS were also detected within AD's hippocampal and neocortical regions (Zhao *et al.*, 2022).

How this LPS enters the brain and localises with the amyloid has not been completely understood. While the brain is normally impermeable to LPS, as seen in the study by Banks and Robinson (2010); age, genetics, pre-existing brain pathology and systemic inflammation and inflammatory illness, can alter the permeability of the BBB (Galea, 2021). In the study by Banks and Robinson (2010), they were able to show that systemic administration of LPS derived from a Salmonella strain, was relatively impermeable through the murine BBB.

A few methods by which LPS enters the brain or increases the brain permeability has been suggested in literature. Firstly, LPS can disrupt the permeability of the blood brain barrier by affecting the tight junctions (Kim *et al.*, 2021). This is supported by Banks *et al.* (2015) where a high dose of LPS was required to affect the brain permeability. In this study, Salmonella derived LPS at doses ranging from 0.03 mg/kg – 3 mg/kg injected intraperitoneally, led to symptoms of sickness like behaviour in mice. However, only the highest dose of 3 mg/kg was able to increase the permeability of the BBB, in specific regions, by damaging the tight junction proteins like occludin (Banks *et al.*, 2015). Secondly, immune cells that are secreted in response to an LPS challenge can transport LPS through the BBB through phagocytosis. Thirdly, LPS can bind to LBP and be transported across the BBB by receptors such as APOE receptor 2 or the CD14/TLR4 receptor complex on the endothelial cells. Finally, it can be transported along with the gram-negative bacteria, in outer membrane vesicles.

1.4.3 Neuroinflammatory and neurodegenerative role of LPS

In vivo studies aimed at understanding the effects of LPS in the brain have shown that LPS administration result in decreased cognitive performance and an increased neuroinflammatory state, regardless of whether it was administered centrally or peripherally (Hou *et al.*, 2016; Herber *et al.*, 2006). These models have shown that LPS can activate glial cells within the brains, resulting in excessive production of pro-inflammatory cytokines, reactive oxygen species and Aβ deposits. This is accompanied by a loss of neurons and synapses which induces

cognitive impairment (Zhao *et al.*, 2019). However, while this has been seen in both *in vivo* and *in vitro* studies, it is worth noting that LPS stimulation results can be different based on the species, route of administration, type of cell, dose used, and duration of stimulation.

Central administrations of LPS have often utilised intrahippocampal and intracerebroventricular injections to administer the LPS into the brain. One such study which looked at the short term and long-term changes in the brain showed neuroinflammatory markers within the hippocampus, that lasted for at least 28 days, because of a single bilateral intrahippocampal injection. In this study, LPS (4 µg) was administered into non transgenic 5- to 6-month-old APP/PS1 mice, an increase in CD-45 – the marker of microglial activation used, as well as GFAP, was observed within 6 hours of the treatments. The expression of these markers peaked on 3rd and 7th day respectively, however, while the microglial activation persisted, the increase in GFAP was shown to be resolving, yet still moderately elevated by the 14th - 28th day. Apart from increases in the markers mentioned, there were also morphological changes seen in the glial cells. The microglia cells changed from a highly ramified cell with thin processes, to a busy phenotype, with shorter processes and other time dependent morphological changes. Similarly, thicker processes accompanied the increase in GFAP expression in astrocytes. Parallelly, an increase in the messenger ribonucleic acid (mRNA) expression of TLR-4, CD-14, as well as the cytokine IL-1β and to a lesser extend TNF-α too was also seen within the hippocampus. At this dose a decrease in neuronal survival was not noted, indicating an absence of neurodegeneration due to the neuroinflammation.(Herber *et al.*, 2006).

A more recent study, that utilised a similar dosing method but a higher dose of LPS, looked at even the cognitive effects LSP can have. In this study, a single bilateral intrahippocampal injection of LPS (40 µg) administered to 8-week-old male C57BL/6 mice decreased their spatial working memory and learning capabilities, as assessed by the Y maze, 9 days after the LPS administration and Morris water maze test, 15 days

post LPS administration. However, their locomotor activity that was tested using the Y maze test as well, showed no significant change due to LPS (Hou *et al.*, 2016). These mice also had increased activated microglia and astrocytes, and an elevated expression of TNF-α and IL-1β within their hippocampus 21 days post-administration (Hou *et al.*, 2016).

When 11-12 week old male mice of the same strain were given 12 µg of LPS through the intracerebroventricular (i.c.v) route, it induced sickness-like symptoms, which included anorexia, weight loss, and decreased movement – possibly associated to the sickness that developed after LPS administration. Similar to the intrahippocampal administration model of LPS, Morris water maze test, as well as passive avoidance test and a motor co-ordination test, showed cognitive impairments in these mice, up to 7 days post administration. These cognitive impairments were concurrent with a significant loss of neurons within the hippocampus too. Neuroinflammatory markers such as activated hippocampal microglia, and increased expression of pro-inflammatory mediators like TNF-α, IL-1β, COX-2 and nitric oxide (NO) in the brain and serum were also noted 7 days after the LPS challenge. This increase in expression of the pro-inflammatory mediators align with the increased expression of TLR-4, MyD88 and activation of the NF-KB pathway. (Zhao *et al.*, 2019). . An increase in IL-6 and TNF-α was also seen in the cortex and the ventricular infusion zone (region of hippocampus adjacent to the ventricles), of 8 – 10-week-old male C57BL/6 mice, at 4 hours after LPS was (10 µg/µl) injected via the i.c.v route. This study also recorded a slight increase IL-1β solely within the ventricular infusion zone (Beurel and Jope, 2009).

Another study where LPS (2 µg) was administered centrally by a single, unilateral i.c.v injection to 3–4-months old female Wistar rats showed results like that seen in the C57BL/6 mice, with regards to increase in GFAP labelling as well as Iba 1 labelling (Sharma, Patro and Patro, 2016). Iba 1 is a microglial protein, whose upregulation has often been used to indicate reactive microglial cells (Ohsawa *et al.*, 2004). It is worth noting that similar to the study by Herber *et al.* (2016), the number of

GFAP positive astrocytes came down to control levels in Wistar rats by the 21st day, and the Iba1 stained microglia decreased by the 28th day, indicating that the LPS mediated gliosis can be recoverable. The main point in this study however was that Sharma *et al.* (2016) reported an increase in apoptotic cells within the mice treated with LPS. This was seen by an increase in pro-apoptotic caspase 3 immunolabelling. These cells were shown to be mainly astrocytes (76 %), followed by oligodendrocytes, neurons, and microglia. This activation of the apoptosis pathway was shown to co-relate with an increase in the glutamate transporter 1 (GLT1) and a concurrent decrease in the glutamate synthetase (GS). When the aberrant expression of these proteins was reversed, the cells were shown to survive the LPS challenge. This indicates that LPS can lead to astrocyte apoptosis which is mediated by glutamate toxicity. While an increase in glutamate is neurotoxic, due to the neuroprotective role of astrocytes, the apoptosis of astrocytes can also lead to neuronal cell death (Sharma, Patro and Patro, 2016).

A few studies have also investigated repeated administration LPS in mice and rats.

Chronic LPS administration was also studied by Tweedie *et al*. (2012). Here they administered LPS via the i.c.v route for 14 days into 3-month-old Fisher rats. These also showed an increase in activated microglia and astrocytes. The chronic LPS administration also induced changes in genes involved in synaptic plasticity and memory processing. The chronic LPS administration, however, did not affect the anxiety or mobility of these animals. It must be noted, however, that further comparison cannot be made with current literature, as the dose administered was not clarified (Tweedie *et al.*, 2012).

These studies show that the direct application of LPS into the brain can cause memory impairment, gliosis, pro-inflammatory cytokine secretion. They also show that microglia are more susceptible to chronic activation in response to LPS, compared to astrocytes.

Another established route of administering LPS is through peripheral injections like through the intraperitoneal route (i.p). Administering LPS through the i.p route can induce systemic inflammation, resulting in sickness like behaviours and weight loss (Zhao *et al.*, 2019). This was seen in 2-month-old C57BL/6 mice that were administered a single i.p injection of LPS at a dose of 1 mg/kg. They immediately displayed decreased immediately after the LPS administration (Perez-Dominguez *et al.*, 2019). These animals showed a temporary decrease in locomotor activity in open field test and loss of body weight.

I.p administration of LPS has been shown to induce neuroinflammatory changes, along with systemic inflammation. This was seen in 3-month-old male Fisher rats that were administered 1 mg/kg of LPS via the i.p route. This study reported a time dependent increase in TNF-α in the plasma, that peaked at 90 minutes post LPS treatment. TNF-α was also significantly increased within the hippocampus of these mice (Tweedie *et al.*, 2012).

In their study, Perez-Dominguez *et al.* (2019) reported that a single i.p injection of LPS (1 mg/kg) to 2-month-old C57BL/6J mice activated their hippocampal microglia within a week. However, they also assessed the effects of chronic treatment of LPS with weekly injections (1 mg/kg, i.p) for 4 weeks. This new dosing regimen resulted in a more severely disrupted morphology of the hippocampal microglia. This was characterised by a further increase in Iba1 markers, a round body and incredibly thin processes. Surprisingly, a single dose of LPS resulted in moderately active astrocytes, which was absent in the chronic model. This led them to postulate that repeated systemic administration of LPS, does not have any long-term effects on astrocytes. This lack of persistent neuroinflammatory marker was also seen in term of IL-6 secretion. The single dose of LPS resulted in an increase in IL-6 secretion, however, 4 weeks of weekly LPS administration did not elevate the IL-6 response compared to untreated controls. The lack of sustained inflammation seen with regards to IL-6 and astrocytes, in response to chronic LPS dosing could possibly explain why there was no sustained neuronal cell death in

this model too. Therefore, while this study shows the impact of a single systemic LPS challenge on the nervous system, it also introduces the idea that repeated exposure may not lead to progressive neuroinflammation. Instead, they discuss that activated microglia seen in these models may be the M2 neuroprotective version (Perez-Dominguez *et al.*, 2019).

However, repeated administration for just seven days has induced enhanced pathognomonic signs. In their study, Zhao et al. (2019) showed that C57BL/6J male mice (11-12 weeks old) administered 500 µg/kg or 700 µg/kg consecutively for seven days showed decreased weight and mobility while also suffering from cognitive impairments. Like the i.c.v model, these mice also had an increase in IL-1β, TNF-α, COX-2 and NO in their serum and the brain. They too showed a decrease in neuronal viability within the hippocampus which could explain the cognitive impairment seen in the passive avoidance and Morris water maze test conducted daily 6 hours after the LPS administration. These mice models also had a decreased anti-inflammatory profile with the brain and serum, seen through decreased levels of IL-4 and IL-10, which could help propagate the neuroinflammation. The difference observed between Zhao *et al*. (2019) and Perez-Dominguez *et al.* (2019) could be the dosing regimen. While Zhao *et al.* (2019) opted for daily LPS challenge, the latter administered it only weekly.

Peripheral LPS can also encourage the production of Aβ plaques. This could be increasing the activity of β and γ-secretase. This has led to an increase in BACE and its product – the “99-residue carboxy-terminal fragment of APP” (C99), in ICR mice that were administered a single i.p injection of LPS (250 µg/kg) (Lee *et al.*, 2008). These changes together resulted in an increase in Aβ1–42 levels in the cortex and hippocampus. This increase in Aβ1–42 levels was further enhanced with the frequency of the LPS injections when given daily for three to seven days. The astrocytes within these mice were also more activated than the untreated control (Lee *et al.*, 2008). These changes within the brain could have led to the significant neuronal cell death observed, resulting in the cognitive

impairment seen using Passive avoidance test and water maze test. These mice had a decreased step latency; indicating they forgot the taught shock treatments therefore entered the dark room faster in the passive avoidance test. They also took longer to find the escape platforms and swam a longer distance to find the platform in the water maze test, despite being trained 6 times prior to LPS administration. However, LPS treatment did decrease the swimming speed, possibly due to systemic inflammation related sickness. This could partly explain the increased time taken to find the platform. This continued throughout the 3 days, although, they showed signs of some memory recovery or possibly learning again.

Furthermore, these mice also displayed an increase in iNOS and COX - 2 – another mediator of inflammation (Zhao *et al.*, 2019), and increased expression of GFAP. Increase in COX-2 in response to LPS has been shown to contribute to BBB disruption, increasing transcellular transport of small molecules. This was reported in male CD-1 mice that were administered LPS (3 mg/kg) via the i.p route. The BBB of these showed increased permeability to sucrose, which was inhibited using a COX inhibitor. Moreover, the COX inhibitor also inhibited the increased expression of GFAP, indicating that this could be mediated by the COX enzymes (Banks *et al.*, 2015).

Kahn S.M. *et al*. (2012) also evaluated the impact of prolonged exposure to LPS. C57BL/6 mice were administered LPS or saline consecutively for three or seven days. The mice administered LPS displayed distress signs and lost significant weight over four days. Their weight, however, started to increase again for the remainder of the experiment. The study also further evidenced the role of LPS in amyloid genesis, where the levels of Aβ1–42 were increased in the hippocampus of the mice given LPS for seven days. However, unlike the study by Lee et al. (2008), there was no such significant deposition of Aβ in mice given LPS for three days. This difference provides evidence that LPS-mediated effects can depend on the experimental design and strain of the mouse used.

Furthermore, the levels of Aβ peptides continued to be elevated in mice after 15 days post-LPS administration. This persistent increase indicates that the downstream signalling of peripheral LPS also damaged the Aβ clearance pathways (Kahn *et al*., 2012; Lee *et al*., 2008).

The study by Kahn *et al.* (2012) demonstrated that the levels of IL-1β were elevated after a single administration, much like the IL-6 levels, after four days of chronic administration. However, 24 hours after the seventh day of administration, serum and hippocampal IL-1β and IL-6 returned to baseline. This fast recovery from inflammation was postulated to be because the mice had gained tolerance to LPS. However, when behavioural and learning tests were conducted, the mice that received prolonged exposure to LPS did show memory impairment in hippocampus-dependent tasks.

These studies show that peripheral administration of LPS leads to systemic inflammation, neuroinflammation, activation of glial cells, and can increase Aβ 1 – 42 levels in the hippocampus. This production of Aβ is further enhanced by the increase in different inflammatory mediators, which also encourage the oligomerisation of Aβ. These changes are mainly seen within the hippocampus and cortex, eventually leading to cognitive impairment, gliosis, and neuronal cell death. However the neuroinflammatory changes seen can be acute and has the possibility to resolve.

While the central and peripheral injections of LPS have been commonly used techniques to induce neuroinflammation in the brain to neurodegeneration, these studies have a few downsides. With the cerebroventricular and stereotaxic injections, the mice usually have a longer recovery period due to the invasive nature of the technique. Challenges also arise with targeting the region of the brain accurately, meaning specialist training and tools would also be required (Zhao *et al.*, 2019; Landeck *et al.*, 2021), It can also be argued whether the inflammation seen within the brain, can be attributed to the trauma

resulting from the surgery or injection and not just the LPS (Del Pilar *et al.*, 2024; Herber *et al.*, 2006).

While the intraperitoneal route of administration is considerably less invasive and easy to conduct. However, it runs the risk of not delivering a sufficient amount of LPS into the brain, and not being able to control the anatomical region targeted (Skrzypczak-Wiercioch and Sałat, 2022).

The intranasal administration of LPS is a relatively less common and more recent route of administration, mainly used to study Parkinson's disease (PD), looking at the effects mainly looked at the effects of LPS on the olfactory bulb, substantia nigra and the striatum The advantage of this route is that it can access the brain directly bypassing the BBB. Furthermore, the role of LPS in environmental toxins and pollutants in neurodegenerative disease has come to light as patients suffering from AD and PD showing olfactory damages (Tang *et al.*, 2019). Therefore, the nasal stimulation of LPS also is a relevant model of AD, and possibly an easier and non-invasive method to stimulate the CNS (Song *et al.*, 2020; Keller, Merkel and Popp, 2022.)

Different paradigms exist in this model as well, with regards to whether LPS is administered bilaterally or unilaterally, and for how long it was administered. He *et al.* (2016) adopted a unilateral administration regimen, where they administered 10 µl of LPS (1 mg/ml) into 2-month-old, female C57BL/6 mice, every alternate day for 1 month. These mice showed PD associated changes such as a decrease in dopamine neurons and α-synuclein deposition within the substantia nigra and the olfactory bulb. There was also evidence of neuroinflammatory changes observed within the brain. An increase in NF-KB, iNOS from the pro-inflammatory M1 microglia and an increase in TNF-α were reported in the mice after a 1 month long chronic LPS intranasal administration (He *et al.*, 2016).

Another study that utilised a chronic intranasal treatment where LPS (10 µl of 1 mg/ml LPS) was administered to male C57BL/6J mice for five months. These mice showed impaired learning ability and weaker spatial

memory in Morris water maze tests by the third month, which became significant by the fourth month. These mouse models also showed an increase in GFAP-stained astrocytes compared to control mice that were given 10 µl of saline. However, the GFAP expression reduced from the olfactory bulb to the hippocampus. These models also showed an increase in inflammatory cytokines such as IL-1β, lL-6, IL-10, and TNF-α in the cerebral spinal fluid; however, this was not seen within the periphery (Tang *et al.*, 2019). This study proves that the intranasal route of LPS administration does look promising to model AD as it brings about significant changes to the CNS, as seen in AD. These changes were seen in the astrocytes within the hippocampus and the inflammatory profile, and it also did not induce any systemic inflammation.

In vitro studies using LPS

While LPS has been used to study neuroinflammation and neurodegeneration *in vivo*, as referenced above, *in vitro* studies that have utilised LPS as an inflammatory stimulant to challenge neurons, astrocytes, and microglial cells. Apart from confirming the effects of LPS seen *in vivo* these studies have also demonstrated the effects of LPS on each individual cell, and its effects on a molecular level.

For example, Banks *et al.* (2015) have utilised CD-1 mice primary brain microvascular endothelial cells to show that LPS (0.001 µg/ml - 10 µg/ml) can increase the permeability of the blood brain barrier, in a dose dependent manner. It increased the permeability of small molecules like sucrose (342 Da) through the paracellular pathway, and by disrupting the tight junction proteins occludin and ZO-1, it enabled larger molecules like albumin (65 kDa) to enter the brain through the transcellular pathways. More importantly, an *in vivo* conducted parallelly, showed that systemic inflammation induced by an i.p injection of LPS (3 mg/kg) was ameliorated by administering an anti-inflammatory drug, indomethacin, a COX inhibitor. However, this was not translated *in vitro.* Coupled with other data from microglia cells *in vivo,* the *in vitro* analysis indicates that unlike the peripheral inflammation, the central inflammation may not be COX mediated.

Through stimulation of differentiated mouse neural stem cells NE-4C-RA cells with LPS (10 ng/ml) for 48 hours D'Angelo *et al.* (2017) showed that LPS led to shorter neuronal branches and significant neuronal cell death. This was shown to be mediated through apoptosis. Further exploration revealed that the neuronal cells that entered apoptosis had also re-entered their cell cycle, which is not normally seen in differentiated cells (D'Angelo *et al.*, 2017).

In confirmation with *in vivo* studies, *in vitro* stimulation of LPS is also capable of inducing pro-inflammatory cytokines from immune cells. For example, RAW 264.7 macrophage cell lines have shown an increase in LPS induced TNF-α and NO synthesis is time and dose dependent as when stimulated with 0.3 ng/ml to 30 ng/ml of LPS (Tweedie *et al.*, 2012). An increase in IL-6, COX-2 mRNAs were also detected in BV-2 microglial cells, stimulated with LPS (200 ng/ml) for 5.5 hours. However, increasing the dose to 1000 ng/ml also upregulated IL-1β, and iNOS in these cells. It did not affect the TNF-α though. In primary C57BL/6 mouse microglial cells however, an increase in iNOS and TNF-α was also detected, along with the previous proinflammatory mediators, in response to 200 ng/ml of LPS for 5.5 hours. An upregulation of IL-1β, in addition to these were detected in primary mouse astrocytes and primary Sprague Dawley rat astrocytes (Ryu *et al.*, 2019).

Agreeing with *in vivo* results, LPS stimulation have also been shown to play a role in *in vitro* amyloid genesis, 2-day-old Sprague Dawley rat primary astrocytes and embryonic rat neuronal cultures that were stimulated with LPS (1 μg/ml) for 24 hours. Like the *in vivo* results, LPS upregulated the expression of BACE1, APP and the β secretase product – C99, as well as iNOS and COX 2. Using western Blot analysis Lee *et al.* (2008) was able to show that these changes were more prominent in astrocytes compared to neurons. These changes however were reversed in a concentration dependent manner, by an anti-inflammatory molecule, sulindac sulphide, demonstrating the potential of using LPS stimulated *in vitro* models to study anti-inflammatory molecules (Lee *et al.*, 2008).

A tri-culture model that included primary neurons, astrocytes, and microglia, obtained from B6C3F1 mice, also showed an increase in the expression of IL-1β, TNF-α and IL-6 in response to 100 ng/ml of LPS after a 48-hour stimulation period. In this model showed that LPS-induces IL-1β mediated autophagy in microglia, and also decrease the neuronal cell viability, although through another pathway. (François *et al.*, 2013).

A study conducted by Rodgers *et al.* (2020) also found that LPS mediated increase in TNF α and IL-1β mRNAs preceded that of IL-6 mRNA, and these increases were in a dose dependent manner (0.1 – 10 ng/ml LPS for 0-6 hours) in Sprague Dawley rat primary astrocytes. Additionally, LPS stimulation led to an increase in chemokines from the astrocytes, that could attract microglia and other leucocytes. Surprisingly this study reported an increase in astrocyte cell proliferation in a TNF α mediated way that was not reported in other studies. Instead, studies have reported that LPS does not affect the proliferation or cell viability of astrocytes *in vitro* (Ryu *et al.*, 2019; Brahmachari, Fung and Pahan, 2006; Dozio and Sanchez, 2018). This could possibly be a dose dependent response, as 50 ng/ml of LPS was shown to increase the proliferation of Human astrocytoma cell line, U373MG, after 24 hours. However, this increase was reversed with 100 ng/ml of LPS (Niranjan *et al.*, 2014).

These results suggest that LPS leads to NF-KB activation and subsequent expression of TNF-α, IL-1β, IL-6, NO, and chemokines. Its malicious effects on glial cells can be attributed to the increased ROS production, changes to the astrocytes cytoskeleton (increase in GFAP), and the pro-inflammatory transcriptional regulation it brings on (Nedzvetsky, Agca and Kyrychenko, 2017). Furthermore, LPS-induced cytokine expression has a temporal sequence, with the initial phase of the inflammation being brought about by TNF-a mRNA expression, followed by IL-1β and IL-6 (Rodgers *et al.*, 2020). The deleterious effects of LPS in AD are also because it encourages amyloid plaque genesis.

In addition to these, postmortem studies have provided significant knowledge on the role of LPS in AD. LPS is directly associated with the senile plaques. Zhan X. *et al*. (2016) discovered elevated levels of LPS

and other molecules specific to gram-negative bacteria within the Alzheimer's disease brain. This study showed that in AD, LPS can localise with several brain structures such as neurons, oligodendrocytes, oligodendrocyte progenitor cells and microglia. Furthermore, LPS colocalised with amyloid beta 1-40/42 molecules within clusters and blood vessels in the cortex. These clusters were surrounded by more LPS and astrocytes (Zhan *et al*., 2016).

1.4.4 Neuroprotective role of LPS

While the reviewed studies have shown the detrimental effects of LPS, it is essential to note that these effects depend on the dose used, exposure type, and route of administration. A few studies have shown that LPS can also be neuroprotective. While a single dose of LPS at a high enough concentration can induce a robust inflammatory response, repeated exposure to LPS can precondition the brain, resulting in tolerance that builds up or changes that can be neuroprotective.

A review conducted by Mizobuchi *et al*. (2021) showed that this dual effect of LPS is brought on by low doses and repeated exposure to LPS. This neuroprotective effect can be attributed to "immune training". Here, low-dose, repeated exposure to LPS elicits low concentrations of TNF-α and an increase in signalling molecules such as IL-10 and other antioxidant proteins.

For example, repeated systemic exposure to low-dose LPS induced tolerance in APP23 mice. A single i.p injection was followed by an acute inflammatory response in the periphery, which resolved upon the second injection. In the brain, however, TNF-α, IL-6 and IL-1β levels were shown to increase after the second injection, along with changes to the microglial gene profile. By the fourth injection, any upregulation of pro-inflammatory cytokines and glial cell activation markers were diminished entirely, indicating that the mice had gained tolerance. Additionally, levels of IL-10 were upregulated as well (Mizobuchi and Soma, 2021; Wendeln *et al.*, 2018)

In vitro, this has been shown by stimulating the C8 B4 cell line that was stimulated with 1 ng/ ml once or at three time points for 24 hours. Repeated low-dose microglia exposed to 1 ng/ml at three different time points showed a decrease in IL-6 and-TNF α secretion compared to a single low dose. That being said, they had an increased expression of other pro-inflammatory mediators, such as IL-12. These also expressed anti-inflammatory and neuroprotective molecules like IL-10 and BDNF compared to the single low-dose model. They were also shown to have a higher phagocytic activity (Mizobuchi *et al.*, 2020).

Therefore, depending on the exposure type, LPS can induce different effects.

1.5 Oxidative Stress

1.5.1 What is Oxidative Stress?

Oxidative stress results from an imbalance of reactive oxygen species/ reactive nitrogen species and the antioxidant systems. Reactive oxygen species (ROS) are molecular entities that contain oxygen radicals like the superoxide radicals (O2-) and oxidising agents like hydrogen peroxide. These species are typically produced during by the mitochondria during metabolism and other biological activities like gene expression. In normal physiological conditions, antioxidant enzymes like superoxide dismutase (SOD), catalase, glutathione peroxidase or non-enzymatic scavengers like Vitamin C and E, clear away the ROS hence regulating their production (Su *et al.*, 2008; Bayr, 2005).

However, during pathological conditions and in ageing, there is an increase in the production of ROS compared to its clearance mechanisms. This imbalance can be due to numerous reasons, for example - mitochondrial dysfunction, abnormal depletion of antioxidants or an increase in transition metals. This imbalance results in oxidative damage such as oxidation of deoxyribonucleic acid (DNA), lipid peroxidation, protein oxidation and other molecular changes within the cell. These damages are increased in ageing and in numerous pathological conditions like AD (Su *et al.*, 2008; Bayr, 2005).

Not only is oxidative stress damaging, but it is also self-propagating. The redox reactions that occur because of oxidative stress render proteins more prone to proteolysis, degradation of lipids, DNA mutations and other protein / DNA damages. These reactions produce more free radicals or ROS, which sustains oxidative stress and leads to further cellular damage (Salim, 2017; Betteridge, 2000).

The brain is highly susceptible to oxidative stress due to increased aerobic respiration. Its oxygen consumption is 20 % higher than regular tissues to produce the amount of Adenosine triphosphate (ATP) required to sustain its function. Therefore, it generates a large amount of ROS, which when combined with their lower antioxidant reservoir and a high amount of unsaturated lipids, makes them highly susceptible to oxidative damage (Milton, 2004; Su *et al.*, 2008; Huang, Zhang and Chen, 2016). To protect the brain, its antioxidant systems include enzymes such as SODs such as copper-zinc SOD and manganese, glyoxalase, glutathione reductase, glutathione peroxidase and catalase. The non-enzymatic antioxidants within the brain include glutathione, uric acid, vitamin C and melatonin (Salim, 2017).

1.5.2 Oxidative Stress in Alzheimer's disease

Like inflammation, oxidative stress is one of the earliest symptoms seen in AD. Studies conducted on Caenorhabditis elegans models of Alzheimer's disease have observed that oxidative stress develops much earlier to Aβ deposition, indicating that it could be an early marker of the disease (Milton, 2004). Increased levels of ROS, redox-active transition metals, glycoxidation products and oxidsed proteins, DNA, lipids are signs of oxidative damage associated with AD (Afsar *et al.*, 2023; Tabner *et al.*, 2005). A reduction in ROS scavengers, increased levels of mitochondrial damage and iron, has been seen in the hippocampus and cerebral cortex of the AD brain (Su *et al.*, 2008; Yang *et al.*, 2016).

A few sources of ROS in AD include A*β* (1-42) peptides, mitochondrial dysfunction and autophagy, transition metals, glial activation and

hyperphosphorylated tau proteins (Manoharan *et al.*, 2016; Su *et al.*, 2008). Each of these feed into each other forming a vicious cycle.

For example, during neuroinflammation, the respiratory burst that occurs because of microglial activation by amyloid β plaques produces superoxide radicals. This respiratory burst is brought on by the activation of nicotinamide adenine dinucleotide phosphate (NADPH) oxidase (Yang *et al.*, 2016). These superoxide radicals induce tissue damage and the production of more ROS species (Yang *et al.*, 2016). The damaged tissue further activates more microglia, leading to more ROS production. Microglial activation and amyloid β results in the activation of astrocytes as well. Activated glial cells release NO, another ROS capable of mediating further oxidative damage (Yang *et al.*, 2016). Additionally, cytokines such as IL-1β produced because of glial activation encourage the production and deposition of Aβ (1-42), leading to more ROS/ hydrogen peroxide production. Aβ (1-42) can also bind to mitochondria, causing mitochondrial dysfunction. Mitochondrial dysfunction leads to a loss in the mitochondrial potential, abnormal metabolism, and eventually mitochondrial autophagy, all of which result in more ROS production (Manoharan *et al.*, 2016; Afsar *et al.*, 2023; Yang *et al.*, 2016).

1.6 Hydrogen Peroxide

In order to study the effects of oxidative stress on astrocytes, in relation to AD, this study will utilise the oxidising agent and ROS hydrogen peroxide. Hydrogen peroxide is a stable, uncharged endogenous ROS, that is involved in both intercellular and intracellular signalling; and is transported across cells through the water channel aquaporin 3 (Milton, 2004; Rice, 2011; Miller, Dickinson and Chang, 2010). It is predominantly produced within the mitochondria and is made as a by product of aerobic respiration. During aerobic respiration, superoxide dismutase converts the oxide radicals produced by the mtiochondria into hydrogen peroxide and water. Then, in order to maintain the normal physioloigcal levels of hydrogen peroxide, glutathione peroxidase and catalase further reduce the hydrogen peroxide to water (Milton, 2004; Rice, 2011; Halliwell, Clement and Long, 2000).

Hydrogen peroxide is involved in numerous cellular activites and singalling pathways. It is involved in activating transcription factors, in cell differentiation, cell proliferation and apoptosis. It is produced during inflammation by leucocytes in a nicotinamide adenine dinucleotide phosphate (NADPH) oxidase mediated pathway, specifically by the acitvation of the NADPH oxidase 2 (NOX-2), that are expressed in the leucocytes. This hydrogen peroxide is converted to hypochlorous acid an antimicrobial agent (Wittmann *et al.*, 2012). They are also produced by the epithelial cells at the site of the injury by another NADPH oxidase enzyme called Dual Oxidase. This hydrogen peroxide is produced in a tissue scale gradient and functions to recruit more leucocytes at the site of the insult. Therefore, during inflammation, hydrogen peroxide plays a role in killing bacteria and in recuiting immune cells. (Wittmann *et al.*, 2012; Niethammer *et al.*, 2009; Halliwell, Clement and Long, 2000).

While excess hydrogen peroxide is readily scavenged by the peroxidases and catalase, an abnormal increase in hydrogen peroxide as a result of inflammation or other insults, results in oxidative stress. Unlike other ROS that are free radicals or ions, the stable nature of hydrogen peroxide does not allow them to directly damage tissues. However, in the presence of transition metals such as ferrous iron (Fe^{2+}), hydrogen peroxide is converted to the highly reactive and damaging OH^{-}, which mainly mediates the damages attributed to hydrogen peroxide (Rice, 2011; Milton, 2004). In order to mitigate this, transition metals are normally bound to proteins in order to sequester them from hydrogen peroxide, yet hydrogen peroxide is capable of liberating them and reacting with them to continue the cycle of ROS production (Halliwell, Clement and Long, 2000).

1.6.1 The role of Hydrogen peroxide in neuroinflammation and Alzhimer's disease

The actual concentrations of hydrogen peroxide present in the CNS in normal and AD paitients is yet to be determined. The half life of hydrogen peroxide in various cells is dependenton the levels of ROS scavengers within that cell; therefore as hydrogen peroxide can be rapidly degraded.

Most assays that are used to quantify the levels of hydrogen peroxide, measure the changes produced by hydrogen peroxide, for example changes in the activity of endogenous peroxidase enxymes. Therefore, measuring the concentration in AD brains using post mortem studies presents a challenge (Milton, 2004). Nevertheless, using transgenic mouse models, it has been shown that *in vivo* using imaging studies conducted on APP/PS1 mice and wild type mice, that the levels of hydrogen peroxide produced is significantly higher in the AD mouse model compared to the wild type mouse (Yang *et al.*, 2016).

Hydrogen peroxide is produced during the early stages of Aβ aggregation (Tabner *et al.*, 2005). In the study by Tabner *et al.* (2005), hydrogen peroxide was produced rapidly in the form of a “burst” as Aβ-(1–40) protofibrils were forming in PBS. The production of the hydrogen peroxide however plateued once mature fibrils formed and the monomeric Aβ peptides depleted. This provides an insight into how oxidative damage is an early pathological symptom associated with AD.

Another source of hydrogen peroxide arises from transition metals that bind onto amyloid beta peptides. Transition metals such as copper, zinc and iron are phsyiological relevant in the central nervous system for neuronal activity and for their catalytic role within Cu/Mn/Zn-SOD. Their reactivity is tightly regulated by metalo-proteins that bind onto them and keep them sequestered. In AD, not only is there an increase in unbound transition metals, instead, they are also found within the amyloid plaques. Studies have shown that these free copper, zinc and iron ions can bind onto the N terminal of Aβ peptides (Huang, Zhang and Chen, 2016). As seen in Figure 1.3, this metal co-ordination can then result in ROS synthesis (Cheignon *et al.*, 2018).

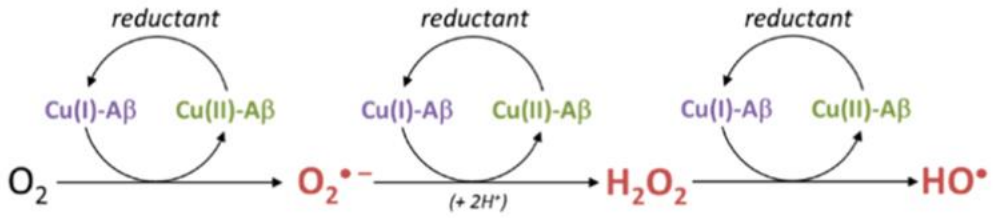

Fig 1.3: The co-ordination of copper ions with amyloid beta peptides and the resulting generation of ROS. When bound to Aβ, copper ions are constantly reduced and oxidised between Cu (II) and Cu (I) states in the presence of a reducing agent like ascorbate or Vitamin C. This chain of redox reaction produces superoxide radicals, hydrogen peroxide and the hydroxyl radicals. Source (Cheignon et al.).

Due to its ability to move intracellularly, as well as be transported across the plasma membrane through aquaporins, hydrogen peroxde has also been recognised as a pro-inflammatory second messenger. Stimulating Raw 264.7 mouse macrophage cell lines with a combination of LPS and IFNy in the presence of the peroxidase, catalase, there was an attenuation in the levels of NO and TNF-α produced, compared to in the absence of catalase. This study confirmed that catalase can't scanvenge the NO in the absence of a NF-KB related inflammatory stimuli. This indicates that hydrogen peroxide does have a role in NF-KB mediated inflammation, like that induced by LPS (Gunawardena, Raju and Münch, 2019). In their study they hypothesised that the superoxide radicals produced from the respiratory burst of macrophages, was converted to hydrogen peroxide by superoxide dismutase. This hydrogen peroxide then activates the NF-KB downstream signalling.

The pro-inflammatory nature of hydrogen peroxide was also characterised in microglial cells. In this study, rat primary microglial cells which were stimulated with TNF-α, IL-1β, and an NADPH oxidase activator underwent increased proliferation, a characteristic associated with reactive microglia. However, this was inhibited by catalase and NADPH oxidase inhibitors (Mander, Jekabsone and Brown, 2006). This

demonstrates that when stimulated with an inflammatory stimuli like the pro-inflammatory mediators or Aβ peptides, hydrogen peroxide is produced in an NADPH oxidase dependent manner and it propogates inflammation and oxidative stress (Jekabsone *et al.*, 2006).

Upon infection, astrocytes are also capable of producing hydrogen peroxide in monoamine oxidase B pathway (MAO-B), in conjunction with increase Gamma-aminobutyric acid (GABA), *in vivo* and *in vitro (*Chun *et al*., 2020).

Given the role of oxidative stress in neuroinflammation and AD, it is a suitable target for new AD therapies.

1.6.2 Astrocytes and Hydrogen peroixde

Astrocytes are generally resistant to hydrogen peroxide mediated toxicity due to their high antioxidant capacity. In a study using primary striatal neuronal cells from rats, increasing concentrations (10 µM to 100 µM) of hydrogen peroxide, for just 30 minutes or more, led to a dose and time dependent decrease in cell viability. On the other hand, combining these pure neuronal cells with primary striatal astrocytes and incubating them with 100 µM of hydrogen peroxide resulted in a higher survival of neuronal cells. This shows the neuroprotective role of astrocytes against hydrogen peroxide, as more hydrogen peroxide was taken up by the astrocytes and instantly degraded by the astrocytic catalase (Desagher, Glowinski and Premont, 1996). Nontheless, high concentrations of hydrogen peroxide are also reportedly detrimental to astrocytes. This phenonmenon was seen in rat C6 glial cells, where incubating the cells with 0.5 mM of hydrogen peroxide for 24 hours, was shown to decrease in cell viability of the C6 glioma cells, as analysed (Sahin and Ergul, 2022). A similar decrease in cell viability was also observed in a dose dependent manner in primary astrocytes isolated from C57BL/6 mice. These astrocytes were incubated in 50 µM – 300 µM of hydrogen peroxide for 1 hour when the decrease cell viability was observed. However, like the study by Desagher *et al.* (1996), the decrease in cell viability was not arrested after changing the cell medium. Instead it

continued for 3 hours. This shows that exposure to hydrogen peroxide, even for a relatively short period of time, can induce a continuous production of ROS, either from the hydroxyl radicals it can be converted to, or from the mitochondrial dysfucntion and other damages it causes (Amri *et al.*, 2017).

Moreover, Sahin and Ergul (2022) demonstrated that upon incubation with hydrogen peroxide, there was an increase in pro-apoptotic Bax-2 and a concomurrent decrease in anti-apoptotic Bcl-2. Furthermore, hydrogen peroxide also increased the levels of NF-KB, IL-1β, COX 1 and Cox 2 – demonstrating its pro-inflammaotry role. The study by Amri *et al.* (2007) also reprted an upregulation of COX 2, iNOS, and IL-6 genes.

Apart from being able to activate the NF-KB, hydrogen peroxide is also capable of inhibiting it.This was was demonstrated in rat primary astrocytes where a dose of 200 µM and above led to astrocyte cell death. This cell death was attributed to the inhibition of the constitive actication f NF-KB pathway induced by hydrogen peroxide (Choi *et al.*, 2007). However, how hydrogen peroxide modulates NF-KB differentially is yet to be understood.

In the study by Chun *et al*. (2020), activated astrocytes were able to produce hydrogen peroxide in a MAO-B mediated pathway. In addition to this they also showed that excessive hydrogen peroxide stimualtion on cultured astrocytes led to a significant increase in nitric oxide production (Chun *et al.*, 2020). Furthermore this study also showed that severe reactive astrocytes can lead to neuronal cell death intracellular tau phosphorylation in neurons, in a hydrogen peroxide mediated manner. Both these effects were resolved in response to a hydrogen peroxide scavenging compound, further demonstrating the pathological role of hydrogen peroxide in AD (Chun *et al.*, 2020).

1.7 Why astrocytes?

Astrocytes are the main antigen presenting cells within the CNS and they play an important role in maintaining the homeostasis, supporting the BBB and protecting the neurons. Therefore, their impaired function can

eventually lead to neuronal death (Li *et al.*, 2019). Given their misrepresentation as connective tissues of the central nervous system by the German pathologist Rudolf Virchow, the role of astrocytes has become only become more clearer since the late 20th century. Since then, importance in neuroinflammatory and neurodegenerative disorders is becoming into emphasis (Rodgers *et al.*, 2020).

These cells are a key component of the neurovascular unit. Through their long processes they mediate contact between the BBB vasculature and neurons (Li *et al.*, 2019). As stated in section 1.3, they play a crucial role in maintaining the BBB integrity, neuroprotection, and in synaptogenesis and pruning (Perez-Catalan, Doe and Ackerman, 2021). Therefore, any impairment in the physiological function of astrocytes can be detrimental to both neurons and synapses.

Reactive astrocytes are a seen during early stages of Alzheimer's disease, associated with Aβ peptides and plaques (Assefa, Gebre and Altaye, 2018). Inflammation and LPS induce this form of astrocytes, which are is capable of producing neurotoxic mediators, have aberrant glutamate metabolism, increase ROS species, and encourage the formation of Aβ. Additionally, transcriptomic analysis have shown that majority of the proinflammatory cytokines seen in AD is more upregulated in astrocytes compared to microglia (Li *et al.*, 2019; Zhan *et al.*, 2016). These phenomenon indicate that reversing or at least reducing the reactivity of astrocytes, could potentially benefit AD.

Previous studies have implied that astrocytes are activated by microglial cells in the CNS. As majority of the studies evaluate the effects of LPS on primary astrocyte cultures, that are not a 100 % pure, but contaminated with primary microglia, using immortalised astrocyte can allow a unique insight into how astrocytes behave independently (Kaur and Dufour, 2012). A main advantage of using immortalised cell lines is that it can undergo multiple passages for the duration of the experiments, however their biological relevance may be impaired. Immortalisation techniques and serial passaging that enable these cells to proliferate

unlimitedly can cause genetic heterogeneity, resulting in responses that may not be comparable to that seen in primary cells or *in vivo* (Kaur and Dufour, 2012). However, as these models are cost effective and easy to manipulate, and are more appropriate when testing a range of many drug doses (Preato *et al.*, 2024).

This study will utilise the SVG-A cells to study LPS mediated reactive astrocytes *in vitro*. These are immortalised human foetal cells from 8- to 12-week-old foetuses. immortalised by transfecting them with a plasmid containing an origin defective mutant of the simian tumour virus 40 (SV40). Their expression of GFAP helped identify these as foetal glial cells (Major *et al.*, 1985) . SVG-A cells are the astrocytic subclones of these cells (Farrell and Lahue, 2006). These cells have previously been used to model with different brain capillary endothelial cells to construct a reliable *in vitro* BBB model (Eigenmann *et al.*, 2013). They have also been used to study how HIV and JC polyomavirus affects the glial cells (Haley, O'Hara and Atwood, 2020; B. and W.J., 2001) . This is the first time these cells are used to study the response of astrocytes to LPS.

1.8 Aim and Objectives

The overall goal of this study was to evaluate the potential of LPS to induce reactive astrocytes in vivo using an intranasal approach and in vitro. Can these models be used to observe the neuroinflammatory traits associated, possibly due to the translocation of LPS to the brain, as seen in AD. Can they be leveraged to test potential anti-inflammatory therapeutics? Reactive astrocytes are identified by an increase in GFAP expression, and pro-inflammatory cytokine secretion. This study hypothesised that LPS would activate astrocytes *in vivo* and *in* vitro. *In vivo* this would be seen by an increase in GFAP expression *in vitro* LPS would induce an increase in IL-1β and IL-6 secretion from the SVG-A cells. As the SVG-A cells proved to be less sensitive to the LPS stimulation, the pro-oxidant hydrogen peroxide was utilised. In this part of the study, the hypothesis is that hydrogen peroxide will dose-dependently decrease the cell viability of the SVG-A cells, as well as

induce an increase in the expression of pro-inflammatory mediators. To test this hypothesis, the specific objectives of this study were:

1) To determine the area covered by DAB-stained GFAP-positive astrocytes in the hippocampus of C57BL/6 mice, 14 days post intranasal administration of an acute dose of LPS. To do this, wild-type C57BL/6 mice were treated with LPS or PBS (control), intranasally, where 10 µg of LPS or PBS was administered bilaterally, in 3 doses, over 24 hours. Two weeks post-treatment, the astrocytes within the hippocampus were labelled for GFAP using immunohistochemistry and were stained using 3, 3'-diaminobenzidine (DAB). The GFAP expression between LPS-treated and PBS-treated mice was then compared.

2) To treat SVG-A cells with increasing doses of LPS and then determine its effects on the cell viability and secretion of IL-6 and IL-1β, compared to untreated control samples. This could then be used to identify the best LPS dose that can be used to stimulate the SVG-A cells, to bring on its neuroinflammatory effects, against which a novel anti-inflammatory molecule can be tested in the future.

3) To incubate the SVG-A cells with increasing doses of hydrogen peroxide for 20 hours and obtain a dose-response curve showing the change in cell viability. This can then be used to identify non-lethal doses that can stimulate the SVG-A cells to produce an increase in IL-6 and IL-1β, compared to untreated samples. The potential of an anti-inflammatory molecule to inhibit the inflammatory changes to astrocytes and the oxidative stress brought on by hydrogen peroxide, concerning AD, can then be tested on these doses of hydrogen peroxide.

Chapter 2: Evaluating the effect of intranasal administration of Lipopolysaccharides on astrocytes of wild type mice.

2.1 Introduction

Astrocytes are important cells that are ubiquitously expressed within the CNS. They are involved in maintaining optimal conditions within the brain and regulate different aspects such as the permeability of the BBB, the synapses, the neuronal network, metabolism, and synthesis of neurotransmitters, as well as the glymphatic system. Apart from these functions, the astrocytes also have a role in the innate immune system as they are one of the main antigen-presenting cells within the brain and conduct inflammatory signalling (Li *et al*., 2019).

In neurodegenerative diseases, astrocytes become reactive and take on a more damaging role. These forms of astrocytes (A1) are neurotoxic and release NF-KB-regulated proinflammatory mediators and an unidentified neurotoxin that impacts the survival of neurons. One of the main characteristics of reactive astrocytes is an upregulation of GFAP – a structural component of the astrocyte cytoskeleton (Li *et al*., 2019; (Lee *et al.*, 2008).

Postmortem studies have revealed reactive astrocytes to be highly expressed in AD brains (Preston, Cervasio and Laughlin, 2019; Liddelow *et al*., 2017; Li *et al*., 2019). These forms of astrocytes are also shown to be induced by the immunostimulant LPS, *in* vivo (Ryu *et al.*, 2019). This endotoxin is the main component on the outer membrane of gram-negative bacteria and is found mainly in the gut along with hypertrophied reactive astrocytes, an increase in LPS surrounding the amyloid plaques has also been reported in the AD brain (Batista et al., 2019; Page, Kell and Pretorius, 2022; Zhan *et al*., 2016; Kim *et al*., 2021).

Given its presence in the AD pathology, and its ability to mimic the neuroinflammatory changes seen in neurodegenerative diseases, LPS is often used to stimulate the CNS and study such age-related neurodegenerative disorders that have an inflammatory tangent to its pathogenesis.

Previous studies have often used stereotaxic or peripheral injection techniques of LPS to model AD. However, due to the shortcomings of these techniques such as the invasive nature of the technique or the possible inability of LPS to cross the BBB, this study will look at stimulating wild-type APPswePS1dE9 mice with LPS through the nasal route. The intranasal administration of LPS has been used previously to model Parkinson's disease. Compared to stereotaxic central routes of administration, the nasal delivery system presents a non-invasive drug delivery method that can be modelled to have low systemic effects and does not require specialist training. In this method, the brain is targeted through the trigeminal or olfactory pathways, circumventing the BBB (Song *et al.*, 2020; Keller, Merkel and Popp, 2022). This is especially advantageous because while LPS can progressively mediate the breakdown of the BBB, it has been shown to have poor permeability across the murine BBB. However, different theories have been proposed on how it enters the brain in pathological amounts (Kim *et al.*, 2021; Banks and Robinson, 2010(Banks *et al.*, 2015).

This pilot study hypothesised that an LPS challenge would result in long-term activation of astrocytes as observed by an increase in GFAP expression. This hypothesis is based on studies that have shown an elevation in GFAP, 14 days after central administration of LPS in C57BL/6 mice (Herber *et al.*, 2006; Sharma, Patro and Patro, 2016). Furthermore, an increase in GFAP expression in response to chronic intranasal administration of LPS has been previously reported by Tang *et al.* (2019), indicating the potential of this technique. To this end, wild-type APPswePS1dE9 mice with a C57BL/6 genetic background were treated intranasally with three intranasal injections of LPS, at an experimental final dose of 60 µg, given bilaterally over a 24-hour window. The expression of GFAP after 14 days was then quantified within the hippocampus, an area of the brain related to cognitive ability and is severely atrophied in AD (Monterey *et al*., 2021).

2.2 Materials and Methods

2.2.1 Samples

Fourteen wild-type mice from the APPswePS1dE9 colony with a C57bl/6j background were bred and maintained by the University of Nottingham Biomedical Service Unit as previously described (Pardon *et al.*, 2016). They were treated blindly under project license PPL40/3601 by Dr. Marie Pardon. The mice were treated with 1 µg/ul LPS (Escherichia coli serotype Sigma 0111:B4, Sigma Aldrich) or PBS (Sigma Aldrich), administered by intranasal injections into each nostril at a volume of 10 µl. This dosing method has been shown to prevent LPS from entering the lungs (Ni *et al.*, 2023; Huang *et al.*, 2023). The treatment was administered at 3 different time points – 0, 6 and 24 hours. Fourteen days post-administration, the animals were culled by cervical dislocation, followed by PBS perfusion to flush out the blood.

The brains were post-fixed using 4 % paraformaldehyde and stored for at least 24 hours at 4–8 °C, before being embedded in paraffin wax on a tissue embedding station (Leica TP1020). Each brain was then mounted on APES coated slides, sectioned by 7µm thick sagittal cuts, in three different levels, twice at each level using a microtome (Microtome Slee Cut 4060), and dried overnight at 40 °C.

The astrocytes were stained for the astrocyte marker GFAP using the methods previously described. The sections were incubated with rabbit anti-GFAP antibody (Biogenix, cat.nr.AM020-5M, 1:4000 in PBS-T) for 1 hour at room temperature. They were then washed and incubated with biotinylated secondary antibody (Vectastain Elite ABC Kit, Rabbit IgG, Vector Labs, Burlingame, CA cat. nr. PK-6101, 1:200 in PBS-T) for 30 min(Pardon *et al.*, 2016). Each section was then washed incubated for 30 minutes with ABC-HRP reagent (Vectastain Elite ABC Kit R.T.U, Vector Labs, cat. nr. PK-7100) according to the manufacturer's instructions. The sections were then washed again and incubated with the DAB peroxidase substrate (Vector Labs cat. SK-4100), and counterstained using a haematoxylin and eosin protocol, by the lab as previously described (Pardon *et al.*, 2016). Images were then acquired

using a Hamamatsu NanoZoomer-XR 2.0-RS C10730 digital scanning system with TDI camera technology a NanoZoomer (Hamamatsu Photonics K.K. Systems, Japan) at 20× magnification and visualised using NDP.view2 (NanoZoomer Digital Photography).

2.2.2 Image analysis

Image analysis was performed using the ImageJ 64-bit software, supported by FIJI (Schindelin *et al.*, 2012). The mouse's hippocampus within each image was first identified using an interactive brain atlas. Each image included the entire sagittal section and was 15360 x 8640 pixels. To isolate the hippocampus accurately, the images were cropped using the same format. To do this, a rectangle selection with a width of 5456 pixels and a height of 6496 pixels was used to crop out the hippocampus. The size of the rectangle was determined using the biggest selection of hippocampus that would be used. This analysis did not use images that contained an overlay, or tissue processing damage or multiple regions of uneven staining as seen in figure 2.1.

Next, the hippocampus was drawn around using the freehand selection tool. This area was then labelled as the region of interest (ROI) and its co-ordinates were added to the ROI manager. Any dark background sections within this selection that could skew our results were also drawn over and flagged as an ROI into the ROI manager; these sections would be treated as an outlier in the calculations later. The image was then transformed to greyscale by converting it to an 8-bit image. Subsequently, to identify all the dark brown stained GFAP-positive astrocytes, manual thresholding was applied. To threshold the images, the darkest astrocytes and their projections were selected. The freehand selection of the hippocampus and the subsequent thresholding is shown in Figure 2.2.

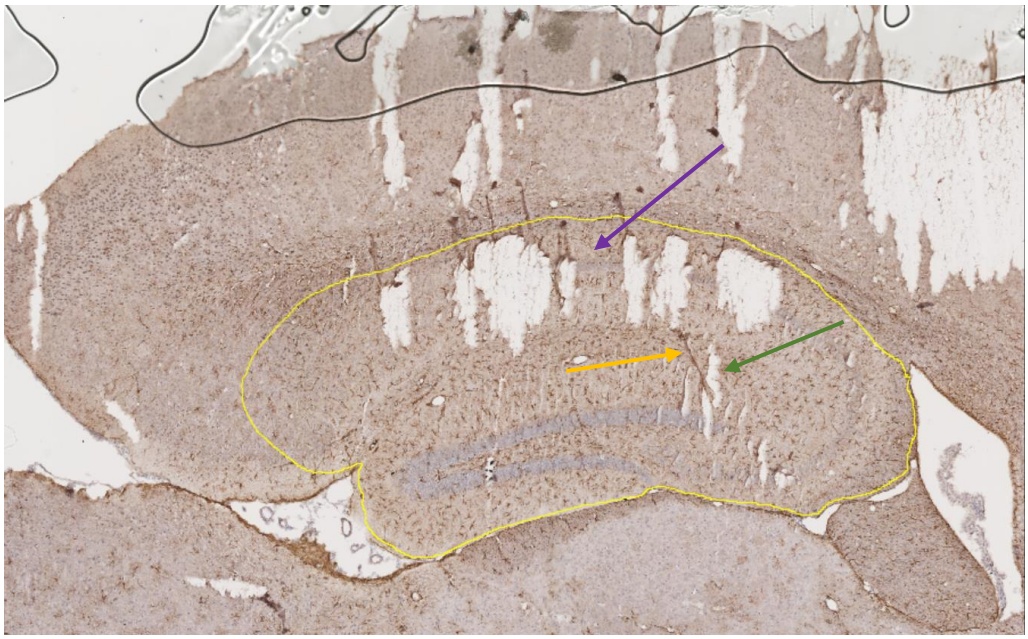

Figure 2.1: Excluded hippocampal image from wild type mice obtained 14 days after intranasal acute LPS exposure. *Images such as these that contained a significant area of damaged regions within the region of interest were excluded from the analysis. The DAPI stained nuclei of the pyramidal layer of the CA1 region (indicated by the purple arrow) that is used to spatially navigate the hippocampus is damaged and hence can't be used. Additionally, the excessive damaged regions (green arrow) or uneven staining regions (orange arrow) could potentially be missed thereby skewing the analysis.*

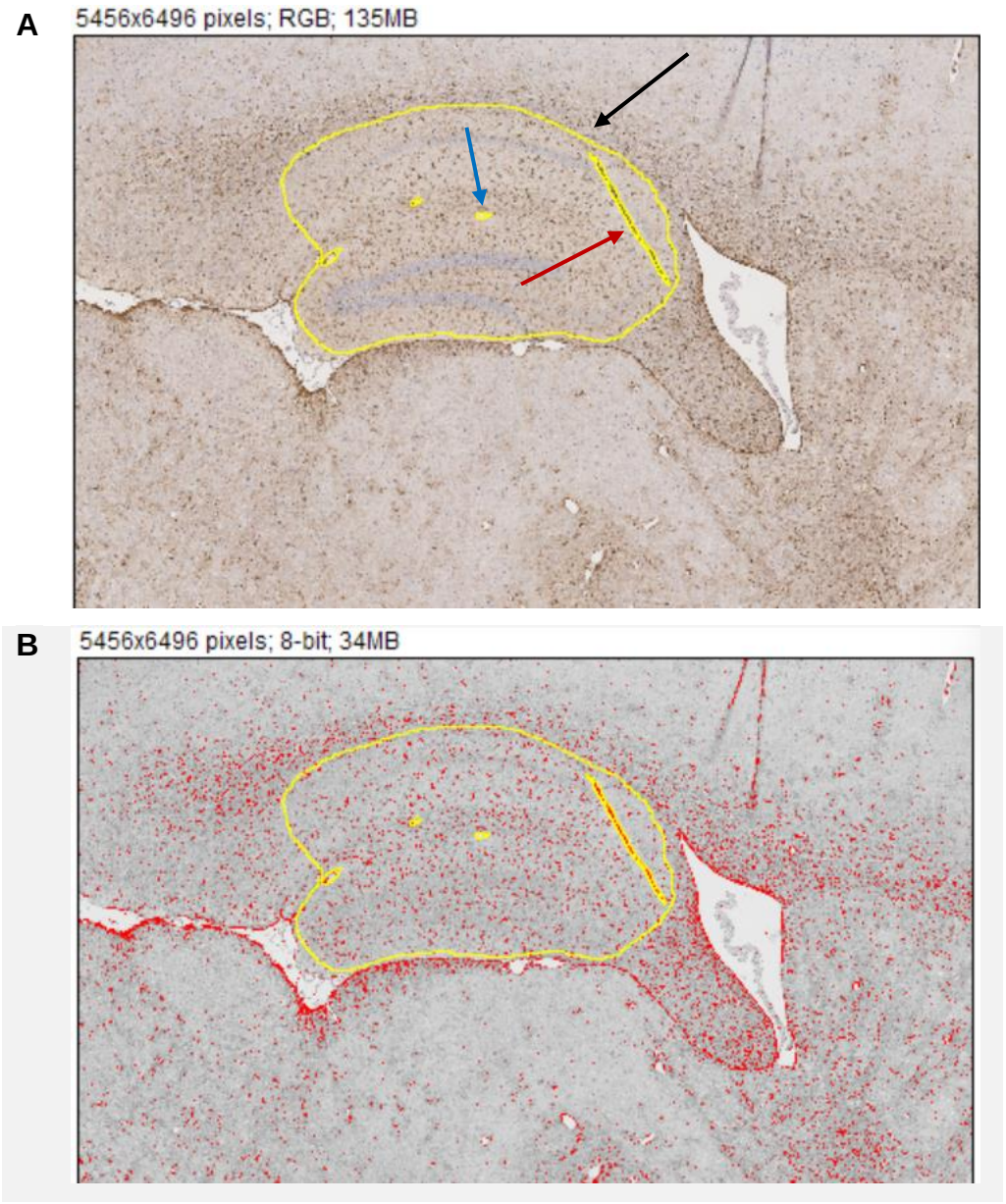

Figure 2.2 : Image J processing of hippocampal images from wild type mice obtained 14 days after intranasal LPS exposure*. A: The images were first cropped using a rectangle tool of the same size. This ensured that all the working images had the same pixels. The hippocampus (black arrow), as well as any holes (blue arrow) or regions with uneven staining (red arrow) were then drawn around using a free hand selection tool. B: The images were then converted to grey scale and thresholded manually. The DAB labelled regions were shaded red.*

To measure the percentage area stained, two area measurements were taken from the thresholded hippocampus – the total area of the ROIs **in pixels**, and the area of the ROIs **in pixels** 'limited to the threshold'. To do this, first, the measurements required were selected [Analyse > Set Measurements > Area and Area Fraction]. The total area of all the ROIs in pixels was then obtained [Analyse > Tools > ROI manager > Measure]. The total appropriate area of the hippocampus was then calculated using the equation –

$$\begin{aligned} &total\ area \\ &= total\ area\ of\ the\ hippocampus - (total\ area\ of\ the\ damages \\ &+ uneven\ staining) \end{aligned}$$

It should be noted that depending on the way the brain was sliced, the hippocampus can have two selections, which would be considered when calculating the total area of the hippocampus.

The measurements required were then reset to measure the area in pixels that were 'limited to threshold' [Analyse > Set Measurements > Area, Area Fraction, Limit to threshold]. The area of the ROIs in pixels limited to threshold was then obtained using a workflow like before [Analyse > Tools > ROI manager > Measure]. The total appropriate area in pixels limited to threshold was then calculated using the equation –

$$\begin{aligned} &Total\ approporate\ area\ (in\ pixels\ limited\ to\ threshold) \\ &= Total\ area\ of\ hippocampus\ (in\ pixels\ limited\ to\ threshold \\ &- (The\ total\ area\ of\ the\ damages \\ &+ unevenly\ stained\ regions\ (in\ pixels\ limited\ to\ threshold)) \end{aligned}$$

This gives the area that is stained within the image, according to the thresholds.

This analysis was done in a double-blind manner. The names of the mice and their corresponding image labels were then used to identify which image sections belonged to which mouse. Each mouse had up to six image sections; as stated earlier, each brain was cut in the sagittal plane

in three different levels, twice at each level, amounting to six different sections of the brain. The total area of the brain in pixels and in the pixels 'limited to threshold' was calculated by finding the sum of all the different sections. The percentage area showing DAB-stained GFAP astrocytes was calculated using the equation:

$$\frac{the\ total\ area\ in\ pixels\ limited\ to\ threshold}{total\ area\ of\ the\ hippocampus} \times 100$$

2.2.3 Data Analysis

Differences between the percentage area stained in mice treated with LPS and PBS were determined using the non-parametric Mann Whitney test. A p-value < 0.05 was considered significant. The letter 'n' is used to describe the number of mice analysed from each treatment group.

2.3 Results

To identify any changes in the expression of GFAP in astrocytes between mice treated with PBS and LPS, the data from nine different mice were used (PBS, n=4; LPS, n=5). The total % area stained was analysed using GraphPad prism. The data failed the Shapiro Wilk's normality test ($p=0.0218$, $n_1 = 4$, $n_2 = 5$), and was subsequently analysed using an unpaired Mann-Whitney test. The statistical analysis found that there were no significant differences (Mann Whitney $U = 10$ $p > 0.99$, $n_1 = 4$, $n_2 = 5$) in the GFAP expression, 14 days post treatment, in the PBS-treated mice (median = 4.979, $n_1 = 4$) and in the LPS treated mice (median =

4.617, n_2 = 5. These results have been graphically presented in Figure 2.3.

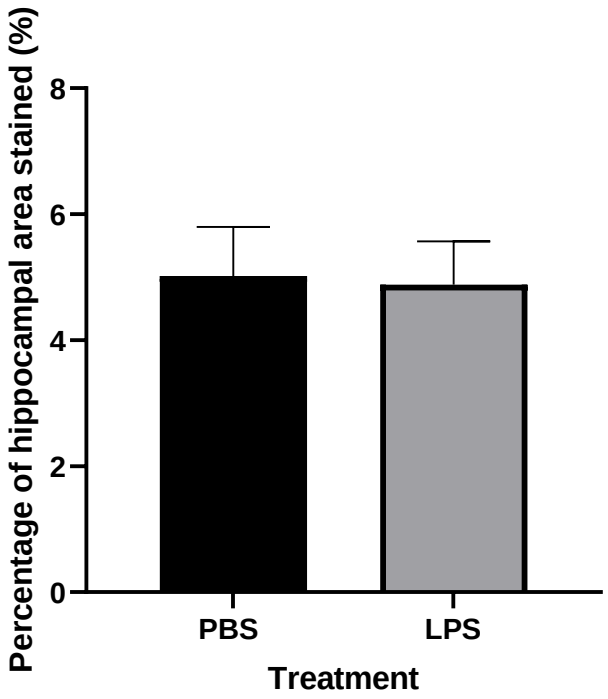

Figure 2.3: Percentage area occupied by GFAP expressing astrocytes in mouse hippocampus treated with LPS or PBS. *Whole brains of nine different wild type mice, that were randomly administered 60 µg of PBS or LPS through the nasal route, bilaterally, at t= 0, 6 and 24h, were assessed using GFAP immunostaining. The results showed that there were no significant differences in the hippocampal GFAP expression between the two treatments ($p > 0.99$, $n_1 = 4$, $n_2 = 5$). The data are expressed as mean ± standard deviation (SD) and was analysed using GraphPad prism 9.5.1.*

2.4 Discussion

2.4.1 Image analysis

This study adopted the intranasal route of administration due to its unique ability to bypass the BBB through the olfactory and trigeminal pathways (Keller, Merkel and Popp, 2022).

The results indicated that intranasal LPS in mice did not induce any long-term changes in the hippocampal GFAP expression compared to mice

treated with PBS. This does not align with other acute LPS stimulation models that were used to formulate the hypothesis and used a stereotaxic administration model. For example, the study by Hou *et al*. (2016) where bilateral intrahippocampal injection of 40 µg of LPS was administered to C57BL/6 mice showed increased GFAP expression that persisted for 21 days post-treatment. This study indicates that acute LPS exposure can induce long-term astrocyte changes. It could be argued that the long-term changes in the astrocytes seen in the study by Hou *et al.* (2016) are due to the intrahippocampal injection that offers a more direct route to stimulate the astrocytes.

One limitation of the present study is that it can't be said whether LPS did reach the desired location in the brain. Therefore, it can be argued that the lack of effects seen in this study could be because LPS did not reach the hippocampus. A study that administered LPS (1 µg/µl at a volume of 10 µl) intranasally into each nostril of C57BL/6 mice for six weeks did not detect any LPS in the olfactory bulb or the substantia nigra. This study argued that the microglial activation in the olfactory bulb and substantia nigra, and the resulting upregulation of IL-1β expression was due to the inflammation within the olfactory mucosa which was then sequentially propagated to the olfactory bulb and substantia nigra (Niu *et al.*, 2020). This has also been reported by Tang *et al.* (2019), where unilateral intranasal administration of LPS (10 µl at a dose of 1µg/µl) daily for 5 months resulted in an increase in GFAP expression that decreased from the olfactory bulb to the hippocampus. Furthermore, Niu *et al.* (2020) also looked at the time-dependent effects of intranasal LPS administration on microglia in different regions of the brain. In their study, stimulating the mice with chronic intranasal administration of LPS for 2 weeks, led to the activation of microglia within the olfactory bulb, however, not in the substantia nigra (Niu *et al.*, 2020). On the other hand, extending the LPS administration for 6 weeks activated the microglia within the striatum and the substantia nigra. This implies that to see the effects of LPS, especially in areas distal to the nostril, such as the striatum, substantia nigra and

hippocampus, LPS would have to be administered daily or on alternate days, for a prolonged period (Skrzypczak-Wiercioch and Sałat, 2022).

Another reason for the effects seen in this study could be that the acute dosing regimen only induced mild to moderate astrogliosis. This severity of activation is associated with mild inflammation that has the potential to recover over time or when the insult is resolved (Sofroniew and Vinters, 2009; Sofroniew, 2009)

2.4.2 Limitations and future studies

The immunohistochemical images were analysed using a manual thresholding technique, which can limit the reproducibility and consistency in identifying outliers. Therefore, an automated method of thresholding should be adopted to ensure that the analysis is robust.

To further understand the promise of using the intranasal model of LPS in AD, future studies can look at quantifying GFAP levels earlier, for example, 24 hours after the last LPS administration. This will show whether the intranasal administration of LPS can activate the astrocytes in the hippocampus, which then recover over time. To further investigate whether LPS given at this dose does reach the brain, immunohistochemical analysis can be done within 24 hours and 48 hours after the last administration. This study can label LPS in regions from the olfactory bulb to the hippocampus. Finally, increasing the period of LPS exposure can bring on a more progressive neuroinflammation model, which is more relevant to AD pathology.

Quantifying changes in the levels of activated microglial cells, pro-inflammatory cytokines, reactive oxygen species and amyloid beta peptides - two weeks after the same dosing regimen employed in this study - would also give an insight into whether the intranasal administration of LPS could model the other pathological conditions seen in AD.

2.5 Conclusion

To conclude, mice treated intranasally with 60 µg of LPS, administered at three different time points within 24 hours showed no changes in their

hippocampal GFAP expression compared to the control. These results indicate that the intranasal administration of LPS did not have any long-lasting effects on mouse astrocytes in the hippocampus. However, as the assessment was done 14 days post-treatment, with no markers utilised to indicate that the LPS had reached the desired region, this should only be taken as a preliminary result.

Chapter 3: Evaluating the effect of Lipopolysaccharides *in vitro* in SVG-A cells.

3.1 Introduction

Pro-inflammatory cytokines are a subgroup of cytokines that function to initiate and propagate inflammation within the body. These cytokines are mainly produced by activated immune cells and can act in paracrine, autocrine, or endocrine manner (Zhang and An, 2007).

The pro-inflammatory cytokines IL-1β and IL-6 have been implicated in the neurodegenerative Alzheimer's disease (AD). Previous meta-analysis has shown that the levels of these cytokines are elevated in the cerebral spinal fluid (CSF) and peripheral blood of AD patients (Ng *et al.*, 2018). Cytokines such as IL-1β and IL-6 are important in AD as they encourage formation of amyloid plaques. They do this by upregulating the expression of APP mRNA, phosphorylated tau mRNA and the amyloid processing secretases (Ogunmokun *et al.*, 2021).

Within the central nervous system, these cytokines are produced by neurons, microglia, astrocytes, and endothelial cells. Their expression is significantly upregulated during an infection or an insult that triggers inflammation. One molecule known to trigger increased production of these cytokines is the bacterial endotoxin LPS. LPS stimulates the innate immune system and encourages the production of pro-inflammatory cytokines by the CD-14 - TLR-4 – MYD88 -NF KB pathway (Page, Kell and Pretorius, 2022; Erta, Quintana and Hidalgo, 2012).

Previous studies have shown that astrocytes and microglial cells stimulated with LPS in vitro become activated and can produce pro-inflammatory mediators IL-6, IL–1β and TNF–α (Batista *et al.*, 2019). Based on these *in vitro* studies, I hypothesised that stimulating the immortalised human foetal astrocyte cell line – SVG-A- with LPS will activate the SVG-A cells. This will result in increased secretion of IL-6 and IL–1β. This can then be used as a neuroinflammatory model to test novel anti-inflammatory molecules against AD.

To this end, these cells were stimulated with increasing concentrations of LPS. The levels of IL–6 and IL-1β secreted after 3 hours of stimulation was then quantified. Similarly, to test the cytotoxicity of the LPS, a cell viability assessment was also conducted.

3.2 Materials and methods

3.2.1 Materials

Poly L lysine coated T75 flasks (75 cm^2 cell culture flask, canted neck, reference – 430641U, Cat -15350591) were obtained from Corning Incorporated, USA. Lipopolysaccharide (LPS, *Escherichia coli* serotype 0111: B4), Dulbecco's Modified Eagle Medium-high glucose (DMEM with 4500 mg/L glucose, L-glutamine, sodium pyruvate and sodium bicarbonate, Cat.# D6429 – 500 ml, Lot – RNBL2263, RNB25828, RNBL7451, RNBL8847), Dulbecco's phosphate buffered saline (DPBS without calcium chloride and magnesium chloride, Cat.# D8537-500ML, Lot – RNBL4055), Trypsin – EDTA solution 1x (0.5 g of porcine Trypsin and 0.2 g of EDTA, 4 Na/L of Hanks' Balanced salt solution with phenol red, Cat. # T3924 – 100 ML, Lot – SLCL6739), Foetal Bovine Serum (FBS, Heat inactivated, sterile filtered, Cat. # F9665-500ML), Penicillin – Streptomycin (Cat. # P0781-100ML), L glutamine (Cat.# G7513-100ML) were obtained from Sigma Alrich (Merck), St Louis, MO, USA. The 0.2 µm syringe filters (Lot – 16532 071387) were obtained from Sartorius Minisart®. For the 3-(4,5-dimethylthiazol-2-yl)-2,5-diphenyltetrazolium bromide (MTT) assay, the MTT kit (Cell Proliferation kit I, REF-11465007001, LOT- 64858300) was obtained from Roche Diagnostics, Mannheim, Germany. The ELISA kits used were - Duo Set Ancillary ELISA Reagent Kit 2 (Cat. # DY008B, Lot – P349065, P342934), Human IL-1β Duo Set ELISA (Cat. # DY201-5, Lot – P345640), Human IL-6 (Cat. # DY206-5, Lot – P336229), obtained from R&D Systems, Minneapolis, MN, USA.

For the immunofluorescence assay, PBS (Cat # X100-500ML) was from Oxoid, England while the Triton X 100 (TX-100), 4′,6-diamidino-2-phenylindole (DAPI) and Bovine serum albumin (BSA) were obtained from Merck. The primary antibodies that were used, recombinant GFAP

antibody (Cat # ab68428, Lot – 1002452-3) and anti-CD 14 antibody (Cat # ab181479, Lot – 1025708-1), were obtained from Abcam, USA while the TLR 4 polyclonal antibody (Cat # PA5-23124, Lot – XC3542889) was obtained from ThermoFisher Scientific Rockford, IL, USA. The secondary antibodies used, CF™ 488A conjugated anti Rabbit IgG (Cat # SAB4600036-250UL, Lot – 22C0208) and CF™ 633 conjugated Anti mouse IgG (Cat # SAB4600131-250UL, Lot – 19C0530), and the glycerol (Cat # 49770-1L, Lot – SZBE184BV) used for mounting were obtained from Sigma-Aldrich (Merck), USA. For the optimisation of this assay, the donkey serum (Cat # D9663 -10ML) was obtained from Sigma Aldrich (Merck), USA and the commercially available blocking solution, TNB, from was PerkinElmer, UK, FP1020. This solution is made up of Tris-HCl, NaCl and a blocking reagent and is part of their TSA Plus Fluorescence kit.

3.2.2 Cell culture

The human foetal astrocyte cells (SVG-A) were kindly provided by Sebastien Serres' lab at Queen Medical's Centre, Nottingham. These were cultured according to Dr. Serres' lab protocols. They were cultured in DMEM and supplemented with 2 % heat-inactivated FBS, and an additional 1 % Penicillin – Streptomycin and 1 % L glutamine. They were maintained in a humid incubator, in 5 % carbon dioxide at 37˚C and were placed in a new medium every two days. They were passaged every three to four days once they reached 70 % to 80 % confluency and were seeded in T75 flasks at a 1:5 dilution.

3.2.3 Lipopolysaccharide (LPS)

To analyse the effects of LPS on the SVG-A cells, the cells were stimulated with 0 ng/ml to 10,000 ng/ml (0 µg/ml to 10 µg/ml) of LPS (*Escherichia coli* serotype 0111: B4). Before the experiment, the LPS was reconstituted in complete media to a concentration of 1 mg/ml. On the day of the experiment, the stock solution was filtered through a 0.2 µm syringe filter and diluted by a factor of 10 to a working concentration

of 0.1 mg/ml. This was then further diluted to the required concentrations in complete medium.

3.2.3 MTT assay

The cell viability was measured using a commercially available MTT assay kit. The protocol used followed manufacturer's guidelines.

To evaluate the cell viability of the SVG-A cells when stimulated by LPS, the cells from three different flasks were detached using trypsin and seeded at a density of 5 x 10^5 cells/ml at a volume of 100 µl in 96-well plates. These were incubated overnight in 5 % carbon dioxide at 37˚C and allowed to adhere onto the plate. Each well was then briefly washed with DPBS, and their medium was replaced with DMEM containing LPS at doses of 0 ng/ml, 10 ng/ml, 100 ng/ml, 200 ng/ml, 500 ng/ml, 600 ng/ml, 800 ng/ml and 1000 ng/ml. A second 96 well plate containing six wells filled with just complete medium were used as blanks. A layout of the plates used is provided in figure 3.1. After 24 hours, the cells were treated with MTT labelling reagent at a final concentration of 0.5 mg/ml, for 4 hours. The purple formazan crystals formed were dissolved using 100 µl solubilisation solution provided with the kit. This was left overnight to incubate in 5 % carbon dioxide and 37˚C, as per the manufacturer's instructions. The absorbance levels were read using a microplate reader (SPECTRO star Nano plate reader, version 3.33, BMG Labtech) and its associated software for analysis (MARS software for analysis, version 3.33) set at 450 nm.

3.2.4 Enzyme linked immunosorbent assay (ELISA)

Cells were seeded onto 24 well plates at a density of 1 x 10^5 cells / ml and left overnight to adhere in an incubator set to 5% carbon dioxide and 37˚C. The seeding density was used according the guidelines from Thermo Fisher Scientific for 24 well plates (Thermo Fisher Scientific, n.d.).

After a brief wash with DPBS, their medium was replaced with medium containing LPS at doses of 0 µg/ml, 0.01 µg/ml, 0.1 µg/ml, 0.2 µg/ml, 0.5 µg/ml, 0.6 µg/ml, 0.8 µg/ml, and 10 µg/ml. The medium per well was then

acquired after 3 hours and centrifuged at 1200 g for 20 minutes at 4˚C. The supernatant was then aliquoted and either maintained at 2-8 ˚C or were snap frozen using dry ice before being stored at -80 C. On the day of the experiment, these samples were diluted by a factor of 2 and their concentrations of IL-1β and IL-6 were quantified using commercially available ELISA kits, according to manufacturer's instructions. The IL-1β and IL-6 assays had a sensitivity of 3.91 pg/ml to 125 pg/ml and 9.38 pg/ml to 600 pg/ml respectively. To ensure the proteins did not degrade during the experiment, the samples were maintained on ice. The absorbance levels were read using a microplate reader (SPECTRO star Nano plate reader, version 3.33, BMG Labtech) and its associated software for analysis (MARS software for analysis, version 3.33) set at 450 nm.

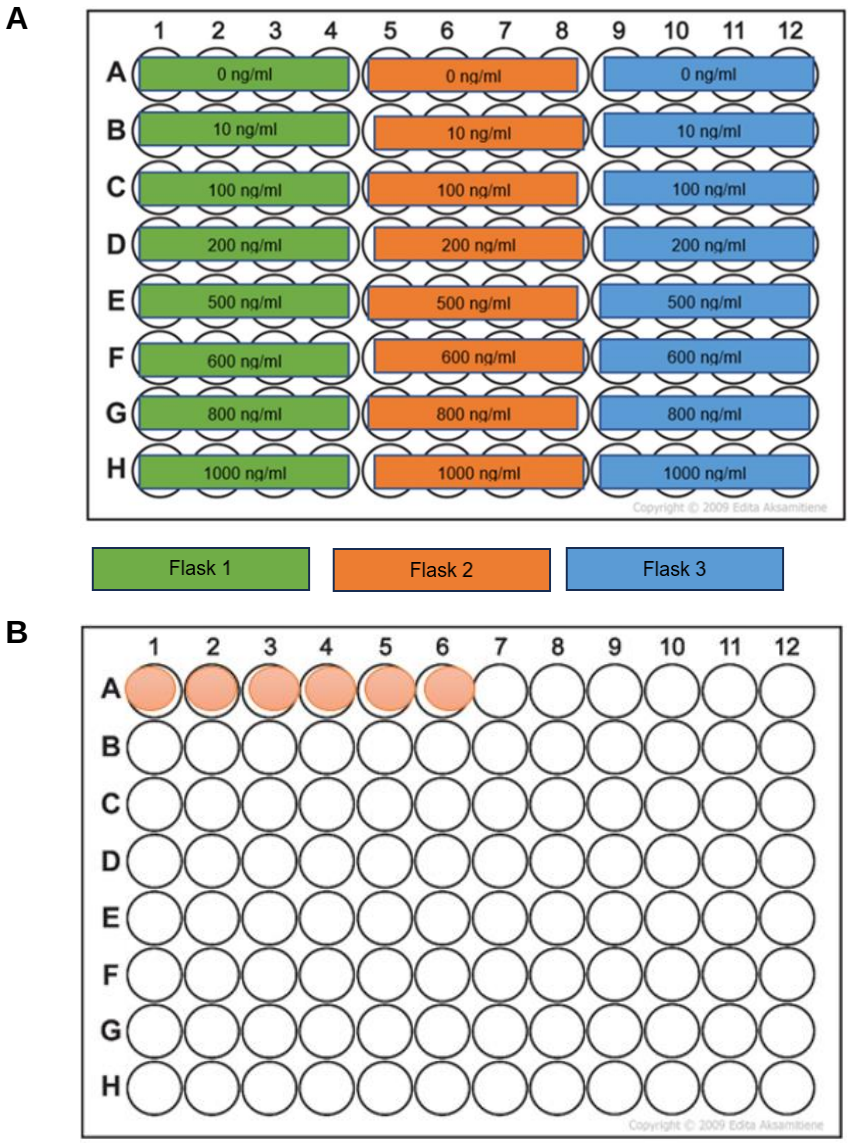

Figure 3.1: Plate layout used to measure the cell viability of SVG-A cells at increasing LPS concentrations. *A) SVG-A cells from three different flasks were plated at a density of 5 x 10^5 cells/ml, on a 96 well plate. Each flask was treated independently as three biological replicates, and plated with four internal repeats. B) 100 µl of complete medium was plated onto six wells of a 96 well plate. These were treated as blanks and were void of any cells and LPS.*

3.2.5 Immunofluorescence

Pilot study

SVG-A cells were seeded onto autoclaved glass coverslips in 12 well plates, at a density of 0.3 x 10^6 cells/ well. The cells were washed once with PBS and fixed using 4 % paraformaldehyde (kindly given by Dr Sheridan's lab) for 20 minutes. They were then permeabilised with 0.5 % TX-100 and blocked with 2 % BSA for 1 hour. After the incubation period, the cells were incubated overnight, at 4° C in recombinant GFAP antibody (1:1000), TLR-4 polyclonal antibody (2 µg/ml) and anti-CD 14 antibody (1:500) primary antibodies made up in 1% BSA and 0.1 % TX 100.

After the overnight incubation, the cells were then washed in PBS four times for a period of five minutes each and incubated with secondary antibodies – CF™ 488A conjugated anti Rabbit IgG (1:2000) and CF™ 633 conjugated Anti mouse IgG (1:2000) - as well as DAPI; made up in 1 % BSA and 0.1 % TX 100 at room temperature for 4 hours. They were then mounted onto labelled microscope slides using glycerol.

Optimisation

Due to the presence of significant background staining in the pilot study, the immunofluorescence assay was optimised either by blocking with an increased concentration of BSA, using donkey serum (Im *et al.*, 2019), or by using the commercially available blocking reagent TNB that was kindly provided by Dr Sebastien Serres' lab.

SVG-A cells and human macrophage cells, which Dr Luisa Martinez-Pomares' lab kindly provided, were seeded on 12 well plates at a density of 0.3 x 10^6 cells/well. The cells were washed once with PBS and fixed using 4 % paraformaldehyde for 20 minutes. Then, the cells were washed again four times with PBS and blocked using either 5 % BSA or 10 % donkey serum or a commercially available blocking solution, TNB for 1 hour and permeabilised with 0.1 % Triton X (TX-100). The cells were then washed two times, for 5 minutes each and incubated at 4° C overnight with the primary antibodies made up in either 5 % BSA, 500 µl of TNB or 5 % donkey serum and 0.1% TX-100. The primary antibodies used were

Recombinant GFAP antibody (1:100) TLR 4 polyclonal antibody (3 µg/ml) and Anti CD 14 antibody (1:300).

Following the incubation with the primary antibodies, the cells were washed four times, 5 minutes each with PBS. They were then incubated overnight in the dark at 4° C with the donkey-derived secondary antibodies made up in either 5 % BSA, 500 µl of TNB or 5 % donkey serum and 0.1 % TX 100. The same secondary antibodies used for the pilot study were also used for this optimisation step, CF™ 488A conjugated anti rabbit IgG (1: 2000) and CF™ 633 conjugated anti mouse IgG (1:2000).

After the overnight incubation in the secondary antibodies, the cells were washed six times, for 8 minutes each wash, on a rocker and then mounted using glycerol, on labelled microscope slides. The microscope slides were then visualised using a Zeiss Excitor widefield microscope at 20X/0.75 objective, using the channels FITC and CY5 at exposures of 200 milliseconds and 150 milliseconds, respectively.

3.2.6 Data Analysis

To analyse the cell viability MTT assay, the raw data from the plate containing the SVG-A cells (figure 3.1A) experiment was first corrected using the blanks plated (figure 3.1B) . The blanks were plated in six wells, on a different 96 well plate were free of cells and contained only complete medium, MTT labelling reagent and the solubilisation solution. First, the average of these six blanks was calculated. Each raw data value from the experimental plate was then subtracted from the average if the blanks to give the blank corrected data. The average optical density (OD) per flask at each concentration was then calculated. This was done using the equation:

$$Average\ OD\ of\ flask\ 1\ at\ concentration\ A\ of\ LPS = \frac{\sum OD\ from\ wells\ containing\ cells\ from\ flask\ 1\ at\ concentration\ A}{4}$$

Subsequently, the percentage OD per flask at each concentration was calculated. This was done using the equation:

$$\%\ OD = \frac{Average\ OD\ of\ flask\ 1\ at\ concentration\ A\ of\ LPS}{Average\ optical\ denisty\ of\ flask\ 1\ at\ 0\ ng/ml} \times 100$$

Since the cell viability is directly linked to the OD, % cell viability at each dose was calculated as the % OD seen at each concentration relative to the control.

The data from the ELISA experiments were analysed using the 'Four Parameter Logistic Curve' online data analysis tool from My Assays Ltd. The concentrations acquired were then analysed using GraphPad Prism 9.5.1.

Differences between groups were analysed using a Kruskal Wallis test. A $p < 0.05$ was considered significant. This was done using GraphPad Prism 9.5.1. The letter 'n' is used to describe the number of biological replicates analysed.

3.3 Results

LPS had no effect on the cell viability of the SVG-A cells.

To investigate the effect of LPS on the cell viability of the SVG-A cells, these cells were incubated with 0 ng/ml to 1000 ng/ml of LPS for 24 hours. As seen in Figure 3.2, the results showed that there was significant difference in cell viability of the SVG-A cells with increasing concentrations of LPS ($p = 0.3118$, $n = 3$). At 1000 ng/ml the cell viability of these cells, had also increased by 67 %, although this was not a significant increase compared to the untreated (0 ng/ml) samples.

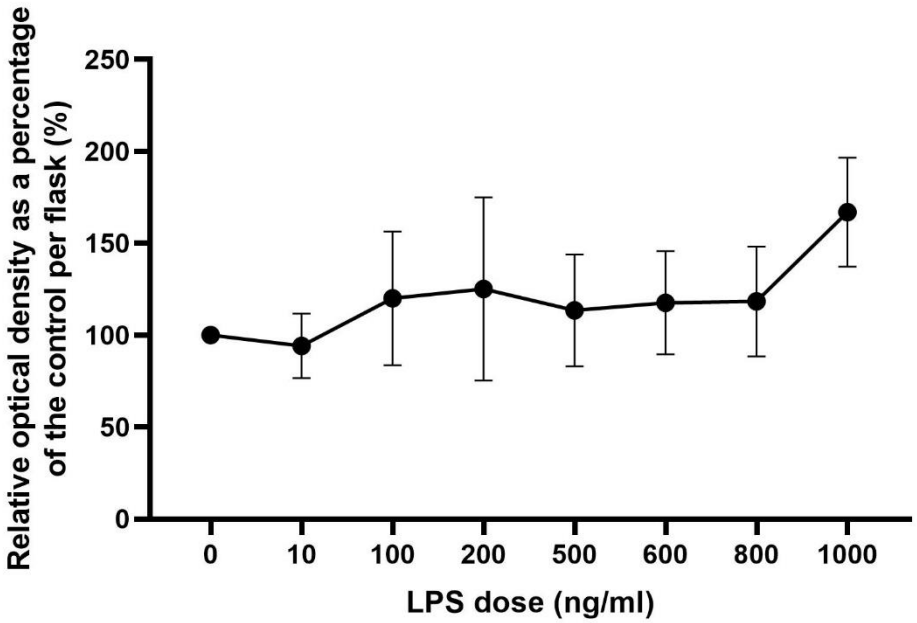

Figure 3.2: The effect of LPS on the cell viability of SVG-A cells. *There was no significant change in the cell viability of SVG-A cells that were incubated in 0 ng/ml to 1000 ng/ml of LPS (p = 0.3118, n = 3). The data was analysed using a Kruskal-Wallis test and the results are presented as mean ±SD.*

LPS led to an increase in IL-6 at a dose of 10 µg/ml

There was a significant difference in the amount of IL-6 produced by the SVG-A cells in response to 0 µg/ml to 10 µg/ml of LPS (p=0.0020, n=6, Kruskal Wallis test), as seen in figure 3.3. A post hoc analysis using a Dunn's multiple comparison test which compared the median IL-6 secreted at each increasing LPS concentration with the control (0 µg/ml) indicated that 10 µg/ml of LPS led to a significant increase in IL-6 (p = 0.0017, n = 6). At 0 µg/ml the median of IL-6 secreted was 67.93 pg/ml, and at 10 µg/ml it was 110.7 pg/ml; therefore, 10 µg/ml was able to elicit 62.96 % increase in the IL-6 secretion.

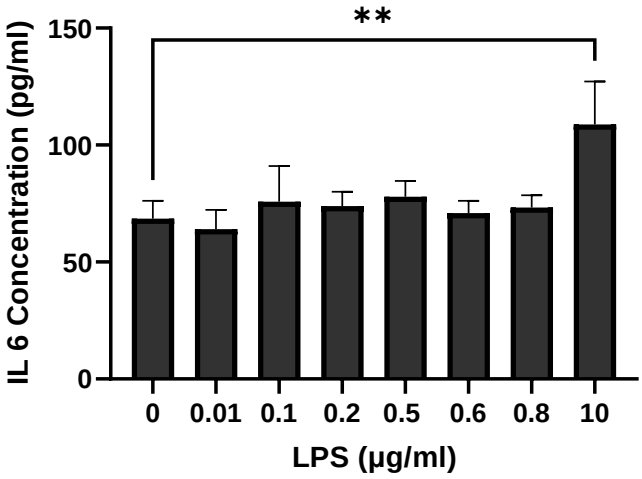

Figure 3.3: Levels of IL-6 secreted by SVG-A cells when stimulated by increasing concentrations of LPS . *SVG-A cells from six different flasks were stimulated with LPS, at doses ranging from 0 µg/ml to 10 µg/ml. At 10 µg/ml of LPS there was a significant increase in the level of IL-6 secreted, compared to the control (p = 0.0017, n = 6). The data was analysed using a Kruskal Wallis test and a subsequent Dunn's test, on GraphPad prism. The results are presented as a mean ±SD.*

The levels of IL-1β secreted by the SVG-A cells after stimulation with LPS, at doses of 0 µg/ml, 0.01 µg/ml, 0.1 µg/ml, 0.2 µg/ml, 0.5 µg/ml, 0.6 µg/ml, 0.8 µg/ml, and 10 µg/ml, were also quantified using ELISA. However, the IL-1β secreted were unable to be read by the assay.

Immunofluorescence staining of GFAP, CD-14 and TLR-4

To determine whether the SVG-A cells expressed GFAP, CD-14 and TLR-4 the cells were immunolabelled using fluorescent antibodies targeting GFAP, CD-14 and TLR-4. As seen in Figure 3.4, the 'secondary antibody controls' from the pilot study, containing only SVG-A cells incubated in secondary antibodies and DAPI showed significant staining.

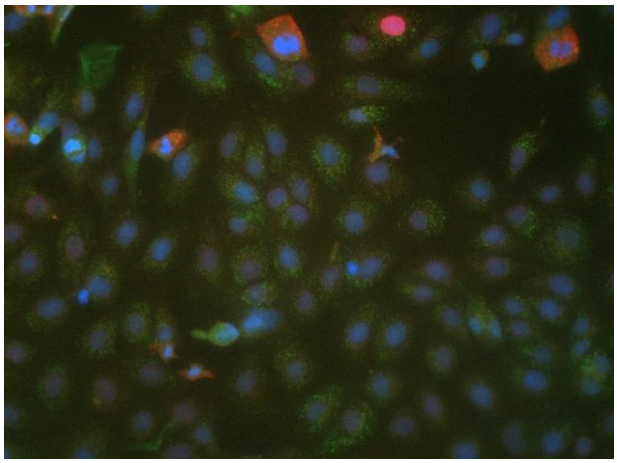

Figure 3.4: Immunofluorescence staining of a 'secondary antibody control' containing only SVG-A cells that were incubated with CF™ 633 conjugated anti-mouse IgG (red) and CF™ 488A conjugated anti-rabbit IgG (green) secondary antibodies, in the absence of any primary antibodies. *These cells were blocked in 2 % BSA and 0.5 % TX 100 and the donkey derived secondary antibodies, were made in 1 % BSA and 0.1 % TX 100. The nucleus was counterstained with DAPI. The labelled cells were viewed at a magnification of 20X.*

To avoid this nonspecific staining in the absence of the primary antibodies, three different blocking solutions were tested, prior to incubation with the antibodies. This was to see which blocking solution could eliminate the non-specific signal. However, as seen in Figure 3.5 and 3.6, blocking the CF™ 488A conjugated anti-rabbit IgG and CF™ 633 conjugated anti-mouse IgG controls with either 5 % BSA or a commercially available blocking serum - TNB or donkey serum still generated a signal. However, upon contrast adjustment, donkey serum produced the least amount of background signal.

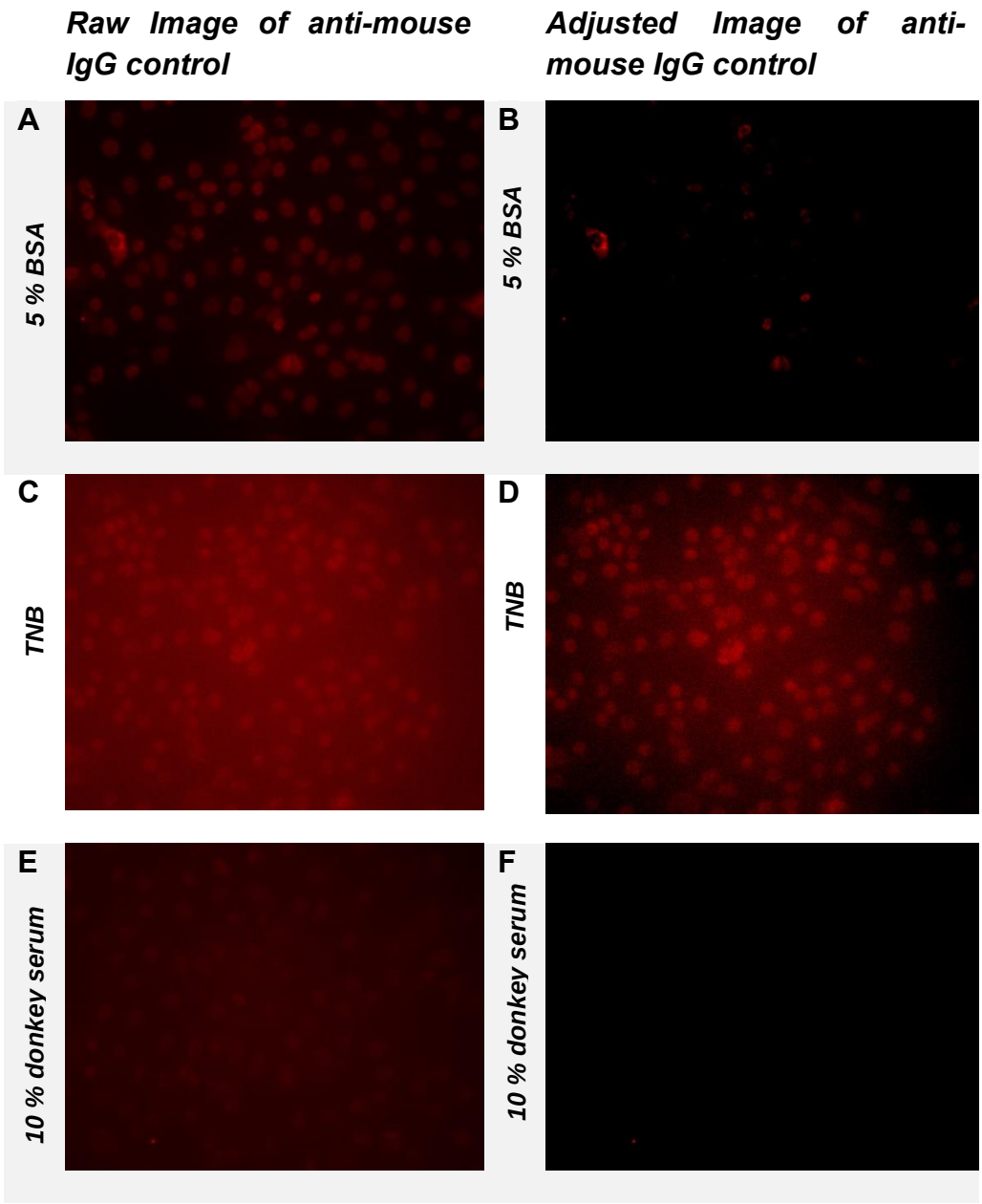

Figure 3.5: Immunofluorescence staining of the CF™ 633 conjugated anti-mouse IgG antibody controls in A – B) 5 % BSA and 0.1 % TX -100, C-D) TNB and 0.1 % TX -100, E-F) 10 % donkey serum and 0.1 % TX 100. *The left panel (A,C,E) shows the raw images without any manipulation, while the right panel (B,D,F) shows images with adjusted contrast (minimum / maximum intensity = 68/186). Images were captured using Zeiss Excitor Widefield microscope at a 20X magnification, using the CY5 (red) channel.*

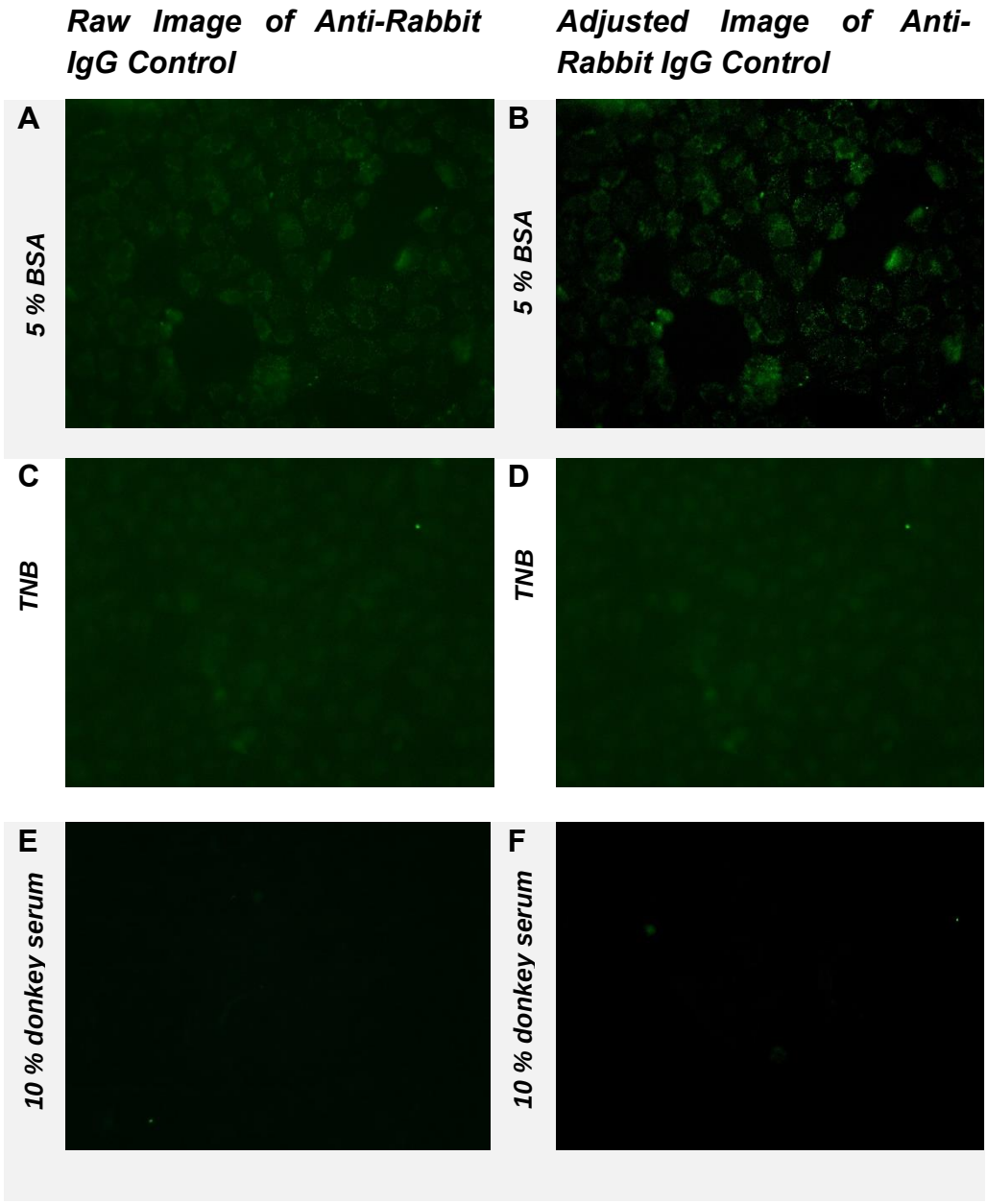

Figure 3.6: Immunofluorescence staining of the CF™ 488A conjugated anti-rabbit IgG antibody controls in A - B) 5 % BSA and 0.1 % TX -100, B - C) TNB and 0.1 % TX -100 C) 10 % donkey serum and 0.1 % TX 100. *The left panel (A,C,E) shows the raw images without any manipulation, while the right panel (B,D,F) shows images with adjusted contrast (minimum / maximum intensity = 22/232). Images were captured using Zeiss Excitor Widefield microscope at a 20X magnification, using the FITC (green) channel.*

SVG-A cells express GFAP, and the TLR-4 and CD-14 receptors.

Figure 3.7, 3.8 and 3.9 clearly demonstrates that the SVG-A cells express GFAP, and the key LPS receptors TLR-4 and CD-14 respectively. When

comparing the different blocking solutions, the results show that these proteins were visualised best when the cells were blocked with 10 % donkey serum. The experimental images containing both primary and secondary antibody labelling were adjusted to an appropriate brightness and contrast using Image J. For reliable comparisons, the secondary antibody controls, adjusted to the same contrast as the experimental figures are shown alongside the experimental images. Given that blocking the cells in 10 % donkey serum resulted in minimum non-specific staining in the secondary antibody controls, as seen in figure 3.5 and 3.6, the intensity adjustments for all images were calibrated based on the brightness and contrast levels required to visualise signals in the donkey serum - blocked samples.

The results show that all three blocking solutions blocked the non-specific staining in cells incubated with the CF™ 488A conjugated anti Rabbit IgG, when the intensities were adjusted. However, only the donkey serum could produce a reliable signal in the SVG-A cells incubated with CF™ 633 conjugated Anti mouse IgG secondary antibody. In the cells that were blocked with 5 % BSA and incubated with the CF™ 633 conjugated Anti mouse IgG, it resulted in a high background, even after adjusting the brightness and contrast levels, whereas blocking these cells in 500 µl of TNB resulted in low signal that could not be detected.

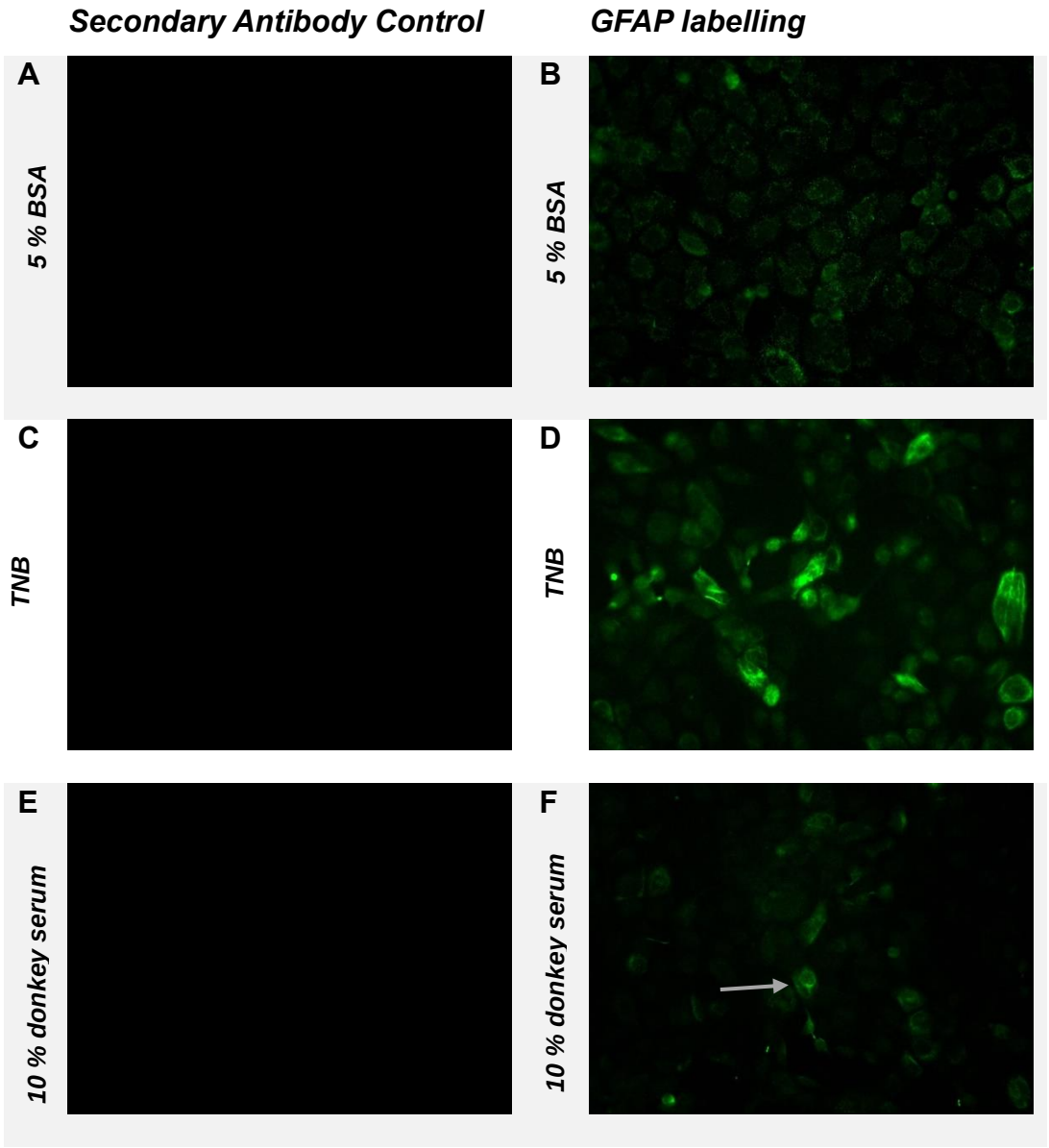

Figure 3.7: Immunofluorescence labelling of GFAP in SVG-A cells blocked in A) 5 % BSA and 0.1 % TX -100, B) TNB and 0.1 % TX -100 C) 10 % donkey serum and 0.1 % TX 100. *The SVG-A cells were seeded at a density of 0.3 x 10^6 cells/ well in a 12 well plate. They were incubated in Recombinant GFAP primary antibody and CF™ 488A conjugated anti Rabbit IgG, made up in 5 % BSA, TNB or 5 % donkey serum overnight at 4˚C. The experimental images and their controls were adjusted for contrast (minimum / maximum intensity = 473/1347, for reliable comparison). Images were captured using Zeiss Excitor Widefield microscope at a 20X magnification, using the FITC (green) channel. The grey arrow points to the GFAP labelling seen in the cells blocked with 10 % donkey serum.*

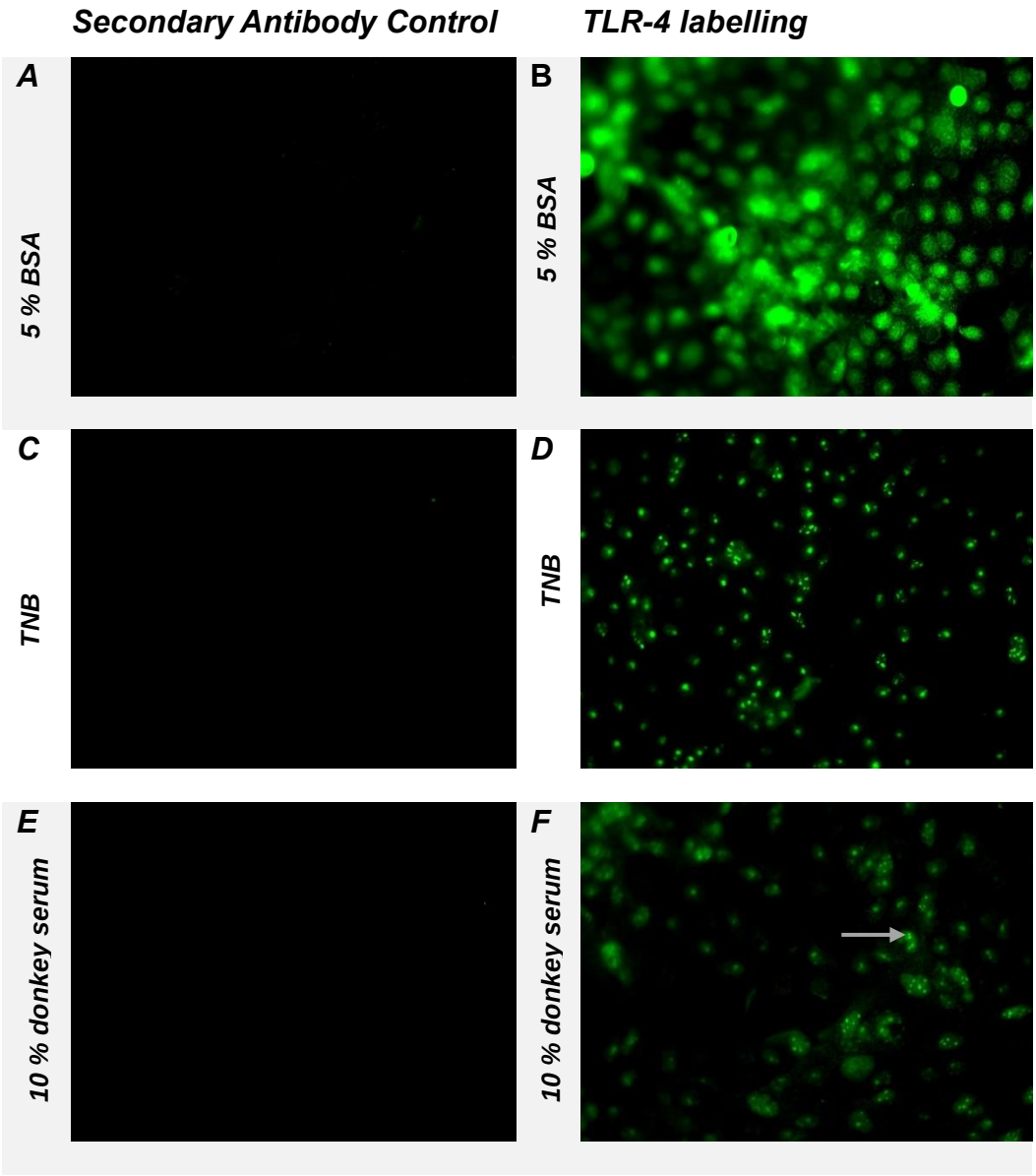

Figure 3.8: Immunofluorescence labelling of TLR4 in SVG-A cells blocked in A-B) 5 % BSA and 0.1 % TX -100, b) TNB and 0.1 % TX -100 c) 10 % donkey serum and 0.1 % TX 100. *The SVG-A cells were seeded at a density of 0.3 x 10^6 cells/ well in a 12 well plate. They were incubated in TLR 4 polyclonal primary antibody and CF™ 488A conjugated anti Rabbit IgG secondary antibody made up in 5 % BSA, TNB or 5 % donkey serum overnight at 4˚C. The experimental images and their controls were adjusted for contrast (minimum / maximum intensity = 658 / 2282), for reliable comparison). Images were captured using Zeiss Excitor Widefield microscope at a 20X magnification, using the FITC (green) channel. The grey arrow points to the TLR-4 labelling in 10 % donkey serum.*

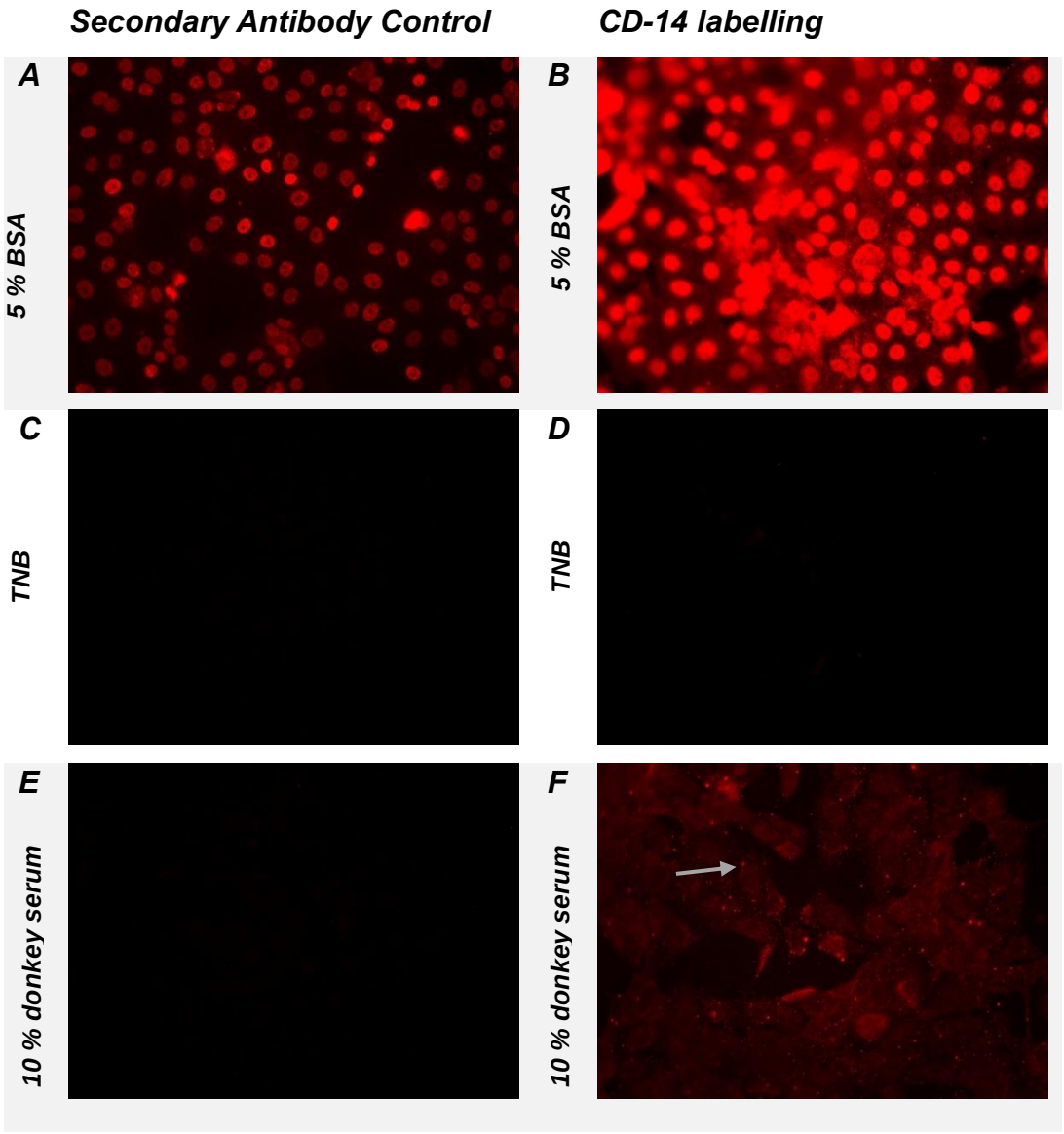

Figure 3.9: Immunofluorescence labelling of CD-14 in SVG-A cells blocked in A) 5 % BSA and 0.1 % TX -100, B) TNB and 0.1 % TX -100 C) 10 % donkey serum and 0.1 % TX 100. *The SVG-A cells were seeded at a density of 0.3 x 10^6 cells/ well in a 12 well plate. They were incubated in anti-CD-14 primary antibody and CF™ 633 conjugated Anti mouse IgG secondary antibody made up in 5 % BSA, TNB or 5 % donkey serum overnight at 4˚C. The experimental images and their controls were adjusted for contrast (minimum / maximum intensity = 392/2090), for reliable comparison. Images were captured using Zeiss Excitor Widefield microscope at a 20X magnification, using the Cy5 (red) channel. The grey arrow points to the CD-14 labelling in cells blocked using 10 % donkey serum.*

Positive controls for TLR-4 and CD-14 expression

Primary human macrophage cells were used as a positive control to visualise the expression of TLR-4 and CD-14, as well as to validate the antibodies used. These cells were fixed with 4% paraformaldehyde and provided by Dr Lusia Martinez's lab. They were treated the exact same way as the SVG-A cells and were labelled for TLR-4 and CD-14 receptors. Figure 3.10 shows the expression of these receptors in human macrophages that were blocked with 10 % donkey serum.

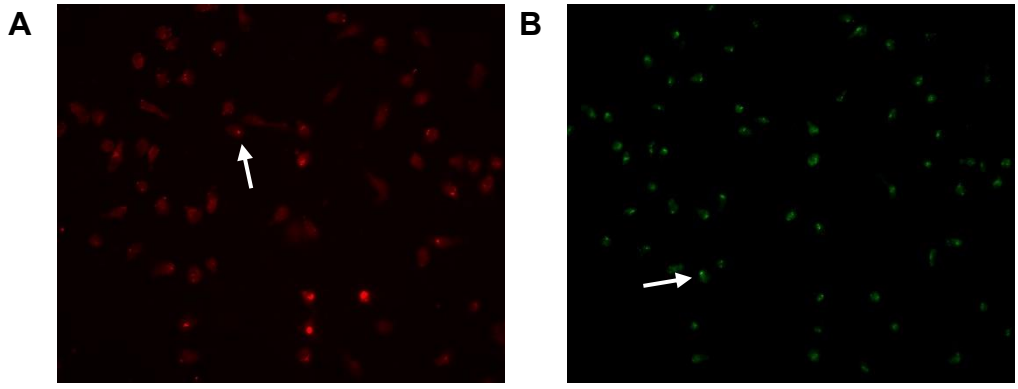

Figure 3.10: Immunofluorescence staining of A) CD-14 and B) TLR-4 receptors in human macrophages blocked in 10 % donkey serum and 0.1 % TX 100. *The white arrow points to the CD-14 and TLR-4 labelling in cells blocked using 10 % donkey serum. Images were captured using Zeiss Excitor Widefield microscope at a 20X magnification, using the Cy5 (red) and the FITC (green) channel. These are raw images, whose intensities have not been adjusted.*

3.4 Discussion

The MTT assay is a colorimetric assay that assumes only metabolically active cells are viable cells, provides a quick and easy method of analysing cell viability. (Ghasemi *et al.*, 2021; Stockert *et al.*, 2018). Previous studies have demonstrated that LPS does not affect the cell viability of murine astrocytes and normal human astrocytes (Ryu *et al.*, 2019; Brahmachari, Fung and Pahan, 2006; Zhang *et al.*, 2017). Similarly, 0 ng/ml – 1000 ng/ml of LPS used in this study had no significant effect on the cell viability of the SVG-A cells. This result aligns with a study conducted on immortalised foetal astrocytes that showed

100 ng/ ml of LPS had no effect on the cell viability of the cells, as determined by a MTS [3-(4,5-dimethylthiazol-2-yl)-5-(3-carboxymethoxyphenyl)-2-(4-sulfophenyl)-2H-tetrazolium] assay (Dozio and Sanchez, 2018). A study conducted on primary astrocytes obtained from the C57BL6 strain that were treated with LPS in the same dose range as our study and utilised the MTT cell viability assay showed no difference in the cell viability of the cells either (Brahmachari, Fung and Pahan, 2006).

Unregulated and increased expression of inflammatory cytokines that occur alongside increase NO synthesis and GFAP upregulation, are biomarkers of reactive gliosis and neuroinflammation (Niranjan *et al.*, 2014; Li *et al.*, 2019). In primary human foetal astrocytes, 0.001 µg/ml – 1 µg/ml of LPS, dose dependently increased the IL-6 secretion after 24 hours (Park *et al.*, 2017). Similarly, 1 µg/ml of LPS was able to induce IL-6 secretion in primary mouse and rat astrocytes after 5.5 hours of stimulation (Ryu *et al.*, 2019). However, as seen in this study 0 µg/ml – 0.8 µg/ml of LPS did not significantly increase the IL-6 secretion compared to control, after a stimulation period of three hours. Instead, the maximum dose of LPS used, 10 µg/ml, was able to significantly upregulate the secretion of IL-6, compared to the untreated control.

Another study that aimed to profile the cytokines secreted by LPS in immortalised human foetal astrocytes, supplemented with 10 % FBS, a higher amount than that used to culture SVG-A cells in this study, showed that 10 µg/ml of LPS had no effect on stimulating IL-6 release but rather increased the secretion of IL -1β and other cytokines after 24 hours (Dozio and Sanchez, 2018). This contradicts the effects seen with the SVG-A cells. In the current study , 0 µg/ml – to 10 µg/ml LPS failed to produce any detectable levels of IL-1β but led to an increase in IL-6.

In this study, IL-6 and IL-1β secretion from SVG-A cells was determined at 3 hours. It could be hypothesised that this is possibly too early detect IL-1β levels. On the other hand, stimulating primary normal human astrocytes (90 % purity), with 0.5 µg/ml of LPS showed that IL-1β

secretion was only detected by ELISA after 4 hours which increased for 24 hours (Sharif *et al.*, 1993). Therefore, it can be hypothesised that IL-β was not detected in these cells due to the time window at which it was quantified.

The ability of human foetal astrocytes to respond to LPS has been much debated in previous literature. A study conducted by Tarassishin *et al*. (2014) found that 0.1 µg/ml and 1 µg/ml of LPS failed to produce any IL-1 proteins (IL-1α and IL-1β) in primary human foetal astrocytes after a 22-hour stimulation period. Further experiments narrowed this down to the absence of CD-14 expression in human foetal astrocytes. The effects seen in the SVG-A cells in my study aligns with this observation. While the study by Tarassishin *et al*. (2014) used primary foetal astrocytes, they conducted their study in low serum media (0.5 %). The SVG-A cells used in my study was also cultured in low serum media, using only 2 % of FBS when compared to the more commonly used 10 % of FBS. This could be important as the study conducted by Yang *et al*. (2020) showed that in low serum conditions – 0 % or 1 % FBS – NCI-H292, lung epithelial cells become hyporesponsive to LPS stimulation when compared to conditions with 10 % FBS-supplemented media.

This effect of FBS is supported by a study conducted by Park *et al*. (2017) that showed NF-KB activation by LPS was completely abolished in serum-free media. The activation of this pathway mediates the production of pro-inflammatory cytokines like IL-6 and IL-1β. Park *et al.* (2017) further reported that the NF-KB pathway activation was restored in a dose-dependent manner when soluble CD-14 (sCD-14) was supplemented externally. FBS contains several cytokines, proteins and growth factors that provide the missing endogenous constituents required for normal cell behaviour. In cells that do not endogenously produce membrane-anchored CD-14 or sCD-14, the serum could provide this protein, enabling the cells to respond to LPS. Therefore, having less FBS could mean less sCD-14 in human foetal astrocyte cell culture that was previously suspected to lack a CD-14 expression (Tarassishin, Suh and Lee, 2014)Yang, Sin and Dorscheid, 2020).

Previous studies have also reported that in cells that lack CD-14 but express TLR-4, the sensitivity of the cells to LPS is massively decreased. However, a high concentration of LPS at ranges of 100 ng/ml or 1000 ng/ml could induce a response (Page, Kell and Pretorius, 2022). This could be seen in our study, where a high concentration of 10,000 ng/ml (10 µg/ml) did lead to an elevation in the IL-6 secreted by the cells. Given this reduced sensitivity seen with LPS, it could be mean that the SVG-A cells lack key LPS sensing receptors within the SVG-A cells.

TLR-4 and CD-14 are two important receptors involved in the LPS sensing mechanism. CD-14 obtains circulating LPS bound to lipid-binding proteins (LBP) and transfers this to the TLR-4/MD-2 receptor complex. This triggers the TLR-4/MD-2 receptor complex activation, initiating multiple downstream signalling processes (Page, Kell and Pretorius, 2022). Therefore, to determine whether the hypo-responsiveness of SVG-A cells to LPS was due to a lack of CD-14 and TLR-4 receptors, their expression were determined using immunocytochemistry.

The SVG-A cells were first labelled for GFAP, the astrocyte marker. As expected, the SVG-A cells did GFAP, which aligns with previous studies that have reported GFAP expression in SVG-A cells, marking them as astrocytes (Farrell and Lahue, 2006). The cells were also positively stained for both TLR-4 and CD-14 receptors, confirming their expression in these cells. My study is the first to report the expression of these receptors within these cells. As MD-2 is another important receptor required to recognise LPS, future studies can be directed to visualise the expression of these receptors.

Furthermore, it cannot be concluded that the CD-14 – TLR-4 / MD-2 receptors are not expressed as there is still IL-6 secretion with LPS stimulation, even though the IL-1β secreted was below what could be detected using the ELISA kit used in this study. One reason the SVG-A cells failed to secrete a detectable amount of IL -1β but secreted IL-6 at a quantifiable level could be due to differences in how the supernatants

were stored prior to quantification. Supernatants used to detect IL -1β were stored at 4˚C, whereas the supernatants used to quantify the IL-6 were stored at -80 ˚C. However, cytokines are more stable upon refrigeration compared to freezing. Therefore, it could be postulated that the storage technique was irrelevant with regards to the low IL-1β secretion (Liu *et al.*, 2021).

The sufficient release of IL-6 instead of IL-1β might mean that the receptors are not working the way they should, as both IL-1β and IL-6 are induced by the activation of the CD14-LPS-TLR-4/MD-2-MYD88 mediated NF kB pathway (Page, Kell and Pretorius, 2022). Secondly, unlike IL-6, which is secreted as soon as the protein is translated, IL-1β must go through further activation by the NLRP3 inflammasome and caspase 1 (Lopez-Castejon and Brough, 2011).

Yang *et al*. (2020) also utilised an immortalised cell line, 1HAEo-, a normal lung epithelial cell line that was immortalised by the transfection of SV40, like the SVG-A cells. These cells were hypo-responsive to LPS compared to NCI-H292 cell lines that were immortalised differently. They both were treated in the same conditions. Therefore, it could be postulated that non-intentional mutations may have occurred in these lines during the immortalisation procedure by SV-40 that led to their hypo-responsiveness. Additionally, compared to other cell lines, the hypo-responsiveness seen with the SVG-A cell lines could also be attributed to differential LPS response depending on the cell line, the passage used or the experimental conditions.

Limitations and future studies

Only one independent experiment was done for the MTT assay, where in one 96-well plate, three biological replicates, each consisting of four internal repeats, were plated. To ensure the reproducibility of the results, more independent experiments are needed to be done. Therefore, the statistical analysis must be interpreted as a preliminary outlook.

In the IL-6 ELISA, certain limitations associated with the experimental design should be considered. First, the supernatants from six different

flasks were plated on two 96-well ELISA plates, each with a column for IL-6 standards. However, one of the standards was skipped in one of the 96 well plates and hence was plated twice on the second plate. To mitigate any variability introduced by plate-plate differences, the values for the standards from both plates were averaged to draw a standard curve at the start of the data analysis. Nevertheless, this method can still introduce potential inconsistencies in the results. Additionally, all six biological replicates were processed on a single experimental day. This approach might limit the strength of the statistical analysis. This is because independent experiments conducted on separate days might offer a more reliable representation of the effects observed by eliminating any variability due to human or instrumental error.

Secondly, since the ELISA experiments checked the levels of IL-6 secreted at 0 µg/ml, 0.01 µg/ml, 0.1 µg/ml, 0.2 µg/ml, 0.5 µg/ml, 0.6 µg/ml, 0.8 µg/ml, and 10 µg/ml, we cannot determine whether 1 µg/ml would have led to an IL-6 secretion.

Another possible limitation with the IL-1β ELISA should also be noted. During the experimental session, the capture antibodies plated at the start of the IL-1β experiment were incubated for 48 hours rather than 24 hours. To avoid the capture antibody from drying up, they were stored at 2 – 8 ˚C. Despite this, the standard curve generated was within an expected range (125 pg/ml – 3.82 pg/ml) with an R^2= 1. However, repeating the experiment a few more times, using the manufacturer suggested incubation period can confirm the consistency in the results. A different ELISA kit can also be utilised to detect the IL-1β levels.

Regarding the immunofluorescence staining, the pilot studies found significant non-specific staining in the secondary antibody controls. To overcome this issue, the experiment was optimised using different blocking reagents. Therefore, a higher concentration of BSA or a commercially available blocking reagent (TNB) or donkey serum was utilised. Since the secondary antibodies were derived from the host species - donkey –it was hypothesised that blocking with donkey serum

would provide the least amount of non-specific staining. The donkey serum did indeed produce the least amount of non-specific staining for both the secondary antibodies used. However, as these optimised studies did not include DAPI, it limits how much we can interpret from the staining. TLR-4 is a membrane-bound receptor; hence, their expression should be on the cell membrane. Including DAPI in future studies will help confirm that the appropriate receptors are stained. Including DAPI in future experiment could also ensure that the cells haven't been washed away during the washing procedure.

To identify if the hypo-responsiveness despite the presence of TLR-4 and CD-14 is because of a non-functional mutation in these receptors or in any of the other downstream signalling molecules, a quantitative polymerase chain reaction (qPCR) can be done to identify any mutations that may be present in these cells. A third immunostaining and qPCR can also be done to evaluate the expression of MD-2 receptors in these cells. For example, previous studies have shown that, the presence of an alanine substitution in the human CD-14 protein which impair its ability to bind to LPS, or a point mutation in the highly conserved cysteine residue in position 95 of MD-2 protein, can affect the cell's ability to respond to LPS (Stelter *et al.*, 1997; Schromm *et al.*, 2001).

3.5 Conclusion

In conclusion, this study shows that LPS does not affect the cell viability of the SVG-A cells, in line with previous studies conducted on primary and immortalised astrocytes. On the other hand, this study shows for the first time that the SVG-A cells express important LPS sensing receptors, the TLR-4 and CD-14 receptors. Nevertheless, these cells seem to be hypo-responsive to LPS, as only the highest dose used in this study, 10 µg/ml, increased the IL-6 secretion. Furthermore, no detectable levels of IL-1β was secreted. Taken together, this study aligns with those studies that suggest that human foetal astrocytes have a decreased sensitivity to LPS. This contributes to the differential responses seen when different types of cells are stimulated with LPS.

Chapter 4: Effect of Hydrogen Peroxide on the cell viability of SVG-A cells

4.1 Introduction

Oxidative stress and inflammation are two early pathological symptoms seen in the AD brain. Due to their high antioxidant capacity, astrocytes are generally resistant to oxidative stress. However, an overwhelming production of ROS as seen in pathological conditions such as AD, activate astrocytes and can also lead to cell death (Amri *et al.*, 2017). Due to their protective and supportive role, any damage that occurs to astrocytes can result in neuronal loss as seen in AD, therefore, understanding how oxidative stress affects them and how the effects can be ameliorated is important (Lee *et al.*, 2005).

One of the early ROS produced in AD is hydrogen peroxide which is formed during the initial aggregation phases of the Aβ peptides (Tabner *et al.*, 2005). It is also formed during infections or the Aβ peptide activation of the monoamine oxidase B (MAO B) pathway in astrocytes and through NADPH oxidase-mediated inflammatory response of the microglial cells (Su *et al.*, 2008; Picca *et al.*, 2020; Chun *et al.*, 2020). This oxidising agent can further synthesise more ROS, such as the OH^- radical and NO species (Milton, 2004). Furthermore, due to is also a modulation of NF-KB, it can also encourage the production COX 1,2, and IL-1β cytokines (Sahin and Ergul, 2022). .

This study aims to stimulate the immortalised human foetal astrocyte cell line – SVG-A cells – with hydrogen peroxide-induced oxidative stress and inflammation. To do that, it is important to identify the non-lethal doses of hydrogen peroxide that induce around 40 – 60 % decrease in cell viability and ROS production. These doses can then be used in future studies to induce the secretion of IL-6 and IL-1β.

Based on previous *in-vitro* studies, hydrogen peroxide was hypothesised to dose dependently decrease the cell viability of SVG-A cells (Amri *et al.*, 2017). To test this, SVG-A cells were incubated with increasing concentrations of hydrogen peroxide (0 µM to 1 mM).

4.2 Materials and methods

4.2.1 Materials

For trypsinisation, Trypsin – EDTA solution 1x made using DPBS and Trypsin – EDTA 10 x (Cat. # T4174 – 100 ML, Lot – SLM1804) from Sigma Aldrich, US (Merck) was used. Similarly, hydrogen peroxide with stabiliser (30 % (w/w) in H_2O_2, Cat. # H1009 – 500 ML, PCode – 102560504, Source – STBL0036) was obtained from Sigma Aldrich (Merck).

4.2.2 Cell culture

The human foetal astrocyte cells (SVG-A) were cultured using the technique mentioned in Chapter 3, section 3.2.1.

4.2.2 Hydrogen peroxide

The SVG-A cells were stimulated with a stabilised hydrogen peroxide solution that was made fresh on the day of the experiments. The stock solution of hydrogen peroxide at a concentration of 9.8 M was first diluted down to a working concentration of 0.1 M using autoclaved, distilled water, this was then made up to 0 µM - 1 mM in complete medium.

4.2.3 MTT assay

To evaluate the viability of these cells in hydrogen peroxide, the cells were detached from the T 75 flasks using trypsin. They were then spun at 280 g for 5 minutes to remove the trypsin as per the instructions of Mattea Finelli's lab. Cells from two different flasks were divided between two 96 well plates. The plate layout was set up so that half of each plate contained cells from one flask, while the other half contained cells from the second flask. This method reduces any variability that is introduced by different plates. This was done with cells from a total of four different flasks. They were plated at a density of 67360 cells/ml in a 96 well plate, as per the instructions from Mattea Finelli's lab. After plating, the cells were allowed to adhere overnight in an incubator set to 5 % carbon dioxide at 37˚C. The next day their medium was removed, and each well

was washed once with DPBS. The medium was then replaced with medium containing 0 µM to 1mM of hydrogen peroxide.

The cells were incubated again for a period of 20 hours in 5 % carbon dioxide at 37˚C. They were treated with MTT labelling reagent at a concentration of 0.5 mg/ml for 4 hours as per the manufacturer's instructions. Any purple formazan crystals that formed were dissolved using the solubilisation solution provided with the kit. This was left overnight to incubate at 5 % carbon dioxide and 37˚C. The absorbance levels were read using a microplate reader (SPECTRO star Nano plate reader, version 3.33, BMG Labtech) and its associated software for analysis (MARS software for analysis, version 3.33) set at 450 nm.

4.2.4 Data analysis

The data was analysed using a method like that referenced in Chapter 3, section 3.2.6. The raw data per plate was initially subtracted from the blanks plated on the same plate. The raw data was then consolidated and grouped according to the concentration of hydrogen peroxide used and the flask they came from. The average optical density (OD) of the controls (0 µM) per flask was then quantified. Using this, OD as a percentage of the control was calculated using the same equation cited in Chapter 3, section 3.2.6. As the OD is related to the cell viability, a higher the optical density means greater a cell viability.

The differences between the cell viabilities at each concentration were then analysed using the Kruskal Wallis test, conducted using GraphPad Prism 9.5.1. A p-value lower that 0.05 was considered significant. The letter 'n' defines the number of data sets analysed.

4.3 Results

Hydrogen peroxide decreased the cell viability of the SVG-A cells.

Incubating the SVG-A cells with increasing concentrations of hydrogen peroxide dose dependently decreased the cell viability of the SVG-A cells. The data analysed using a Kruskal Wallis test indicated a significant difference in the cell viability of SVG-A cells at varying concentrations of

hydrogen peroxide ($p < 0.0001$, $n = 4$). A further analysis using Dunn's multiple comparisons test, indicated that the 800 µM ($p = 0.0154$, $n = 4$), 900 µM ($p = 0.0008$, $n = 4$) and 1 mM ($p = 0.0007$, $n = 4$) led to a significant decrease in the cell viabilities compared to the control (0 µM). The medians for the doses 800 µM, 900 µM and 1 mM are 42.23 %, 2.0 % and 2.51 %. The associated interquartile ranges for the doses 800 µM, 900 µM and 1 mM are 17.83 – 57.97, 0.16 – 18.54, 0.86 – 6.82. At 600 µM and 700 µM of hydrogen peroxide, the median OD was 62.26 % and 59.65 %, and their interquartile ranges are 53.13 – 73.41 and 44.88 – 70.53. Since in MTT assay the optical density is directly proportional to the cell viability, it can be assumed that at 600 µM and 700 µM, there was 37.74 % to 40.35 % respectively.

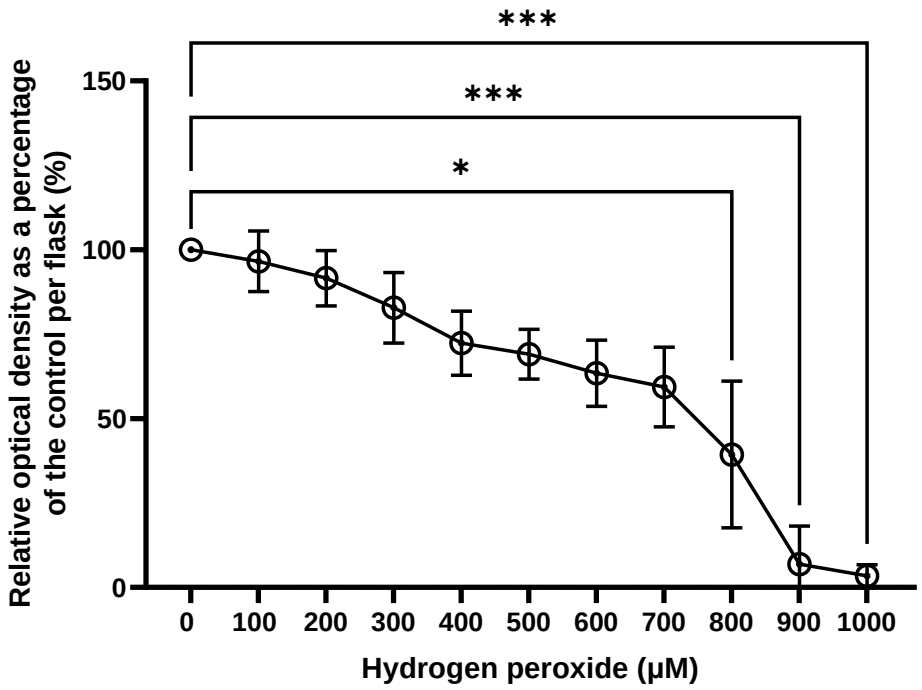

Figure 4.1: The effect of hydrogen peroxide on the cell viability of the SVG – A cells. *There was a dose dependent decrease in the cell viability of the SVG-A cells when incubated with hydrogen peroxide at increasing concentrations, 0 µM - 1 mM ($p < 0.0001$, $n = 4$). The doses 800 µM, 900 µM and 1 mM led to a significant decrease in cell viability compared to the control (0 µM) The data was analysed using a Kruskal*

Wallis test and a further Dunn's multiple comparisons test using GraphPad Prism 9.5.1. It is graphically presented as the mean and SD.

4.4 Discussion

Due to their higher antioxidant capacity compared to neurons, astrocytes are more resistant to oxidative stress (Desagher, Glowinski and Premont, 1996). Nevertheless, exposing them to hydrogen peroxide at doses higher than 200 µM has been shown to induce cell death. In agreement with these studies, our results show that high concentrations of hydrogen peroxide induce cell death in astrocytes in a dose-dependent manner, increasing significantly at concentrations above 800 µM after 20 hours.

A study conducted on cortical astrocytes, isolated from 2-4 day old Sprague Dawley rats, exposed the cells to serum-free media containing hydrogen peroxide at doses ranging from 200 µM to 1000 µM for either 0.5 hours or 3 hours. The cell viability measured using an MTT assay showed a significant decrease in cell viability in a dose and time-dependent manner from 200 µM compared to the controls (Juknat *et al.*, 2005). While these studies align with ours and show a dose dependent decrease in the astrocyte cell viability, the hypo-responsiveness of the SVG-A cells to hydrogen peroxide – evidenced by the high dose required even at a higher time point is noteworthy. This could be attributed to the serum-deprived experimental design used in the study by Junkat *et al.* (2005). The serum-free media can also induce oxidative stress, which can suggest why the primary rat astrocytes used in this study were more responsive to hydrogen peroxide stimulation (Pandey, Lopez and Jammu, 2003). The differences in cell-cell response between the studies can also be attributed to the different cell types used in these studies. This can be seen in the study by Desagher *et al.* (1996), whether the

Studies conducted on human glioblastoma cell lines, A172, have also reported hydrogen peroxide mediated decrease in cell viability. Like the study by Junkat *et al.* (2005), these cells were exposed to varying doses of hydrogen peroxide (0-1 mM) for 24 hours, in a serum free media. Like

its effects on the SVG-A cells, hydrogen peroxide led to a dose dependent decrease in cell viability of the A172 cells (Lee *et al.*, 2005).

Limitations and future studies

One limitation of this study is that these experiments were conducted over two experimental sessions. Therefore, more experimental sessions can improve the reliability of the statistical analysis by considering any instrumental or human error.

To see if hydrogen peroxide-induced oxidative stress can also induce inflammatory changes, the next step would be to examine the ROS, IL-6 and IL-1β levels secreted at the appropriate concentrations. Since this experiment aimed to find hydrogen peroxide concentrations that resulted in only 40 % - 60 % cell death, 600 µM, 700 µM and 800 µM could be used in subsequent experiments. Furthermore, morphological analysis and transcriptomic analysis can give further insights into whether the astrocytes seen after exposure to hydrogen peroxide reflect that seen in activated astrocytes in AD.

4.5 Conclusion

In conclusion, this study shows that hydrogen peroxide-mediated oxidative stress can reduce the viability of SVG-A cells in a dose-dependent manner, as seen in other astrocytic cells. Future studies can be directed to analyse whether hydrogen peroxide can elicit neuroinflammatory characteristics in these cells by using an optimum dose selected from the above dose response curve. This could then be used as an *in vitro* model of oxidative stress and neuroinflammation to test potential therapeutics that target these two characteristics of AD.

Chapter 5: Final Discussion and Conclusion

As reviewed in Chapter 1, section 1.4.3, the most used LPS administration methods have been i.p or i.c.v injections. While these can replicate significant hallmarks of AD, they can pose a challenge when either assessing the direct effects of LPS only in the brain due to its poor BBB permeability, and the direct application of LPS can result in acute and immediate neuroinflammation, that does not necessarily model the progressive neuroinflammation present in AD. Injections directly into the hippocampus and the cerebroventricular region also require surgical expertise, have a more extended recovery period and a lower survival rate (Tang *et al.*, 2019; Zhao *et al.*, 2019).

The intranasal administration model used in this study, aimed to target the hippocampus through the nasal route, while circumventing the BBB in a non-invasive route. While LPS showed no changes to the GFAP expression in this model, with treatment regimen utilised, it can't yet be concluded that LPS did not cross the BBB. Further studies that can label LPS within the hippocampus, at early intervals, can give further insight into whether LPS did successfully cross the BBB and whether the effects seen in the wild type mice are due to resolution of inflammation, or simply because the treatment regimen was too short. There currently is a significant lack of literature as to whether LPS can enter the brain and whether it mediates it effects by directly activating the glial cells. While chronic LPS dose for 5 months have failed to detect LPS within the hippocampus (Niu *et al.*, 2020), a single intranasal dose of LPS of 10 µg can induce activation of microglia and increase in hippocampal cytokines within 5 hours, in C57BL/6 mice (Huang *et al.*, 2023). Therefore, in order to validate the intranasal model, future studies can look at the increase in GFAP, NO, IL-1β, TNF α, as well as label LPS at time points as early as 5 hours post treatment. Moreover, measuring other parameters of neuroinflammation and AD, such as learning and memory impairment, microglia activation, the expression of different cytokines, and Aβ will give more holistic information on this model.

In vivo studies are frequently accompanied by *in vitro* studies. These give a clearer idea as to how LPS affects astrocytes independently. *In vivo* activation or astrocytes and microglia occur together, and can be induced by each other (Liddelow *et al.*, 2017), therefore using immortalised astrocytes that are not contaminated with microglia can give a clearer idea as to how astrocytes are involved in LPS mediated neuroinflammation and propagation of AD. To this end, the immortalised human foetal astrocyte cell line SVG-A cells were utilised.

The ability of human foetal astrocytes to respond to LPS has been widely debated in literature. Primary human astrocytes obtained from 16 – 20-week-old foetuses have been shown to respond to 10 ng/ml of LPS. These primary human astrocytes could secrete IL-6, IL-1β and TNF-α, among other cytokines. However, in our studies, LPS stimulation in the SVG-A cells did not increase the IL-6 secretion at 10 ng/ml (0.01 µg/ml); it elicited an increase in IL-6 at 10,000 ng/ml (10 µg/ml). Furthermore, the levels of IL-1β secreted by these cells, with or without LPS, were undetectable. Immortalised normal human astrocytes have also been shown to respond to LPS by secreting IL-1β and IL-6 (Zhou *et al.*, 2022). However, in other studies utilising human foetal astrocytes, LPS stimulated the secretion of some cytokines, such as IL-1β but not IL-6. In another study, the human foetal astrocytes did not show any increase in secretion of any cytokines in response to LPS (Tarassishin, Suh and Lee, 2014). As discussed in Chapter 3, section 3.4, this difference could be attributed to the immortalisation procedure introducing mutations in this cell line or the fewer CD-14 proteins available to facilitate the LPS-mediated TLR-4 activation. However, the expression of other essential proteins involved in the TLR-4/MD-2 sensing mechanism and further downstream processes must be assessed.

Furthermore, studies that use primary astrocyte cultures try to grow enriched astrocyte cultures; however, these are never really 100 % pure (Saura, 2007; Choi *et al.*, 2007). Therefore, these cultures are potentially contaminated by at least 1 % microglia. As microglia are highly potent to LPS compared to astrocytes and can activate astrocytes, they can further

enhance any response produced by LPS (Jack *et al.*, 2005; Saura, 2007). Therefore, the experimental design can also be optimised to reflect more *in vivo* characteristics by priming the SVG-A cells first using cytokines released from M1-type microglia induced by LPS (Dozio and Sanchez, 2018).

One disadvantage of using immortalised cell lines is that their genetic integrity is unreliable compared to primary cells. Due to serial passaging and manipulation to induce the immortality, they tend to have an altered genotype and even phenotype (Kaur and Dufour, 2012). This is evidenced in the MTT assay conducted in this study. While LPS did not alter the cell viability of SVG-A cells, as seen in several other *in vitro* analysis (Brahmachari, Fung and Pahan, 2006), these results are starkly different from *in-vivo* studies showing many astrocytes undergoing glutamate mediated apoptosis(Sharma, Patro and Patro, 2016). This inconsistency can question the predictive validity of these *in vitro* models of AD. It brings up the possibility that *in vivo* astrocyte cell death can be attributed to the inflammatory role of LPS and a secondary mechanism, such as oxidative stress (Yue *et al.*, 2008).

LPS has been shown to encourage the expression of NO, and it can also stimulate the release of other reactive oxygen species by activating the microglia. Studies have also shown that during the initial phase of AD, during the Aβ aggregation phase, hydrogen peroxide is produced in bursts (Tabner *et al.*, 2005). To understand how the SVG-A cells would respond to hydrogen peroxide-mediated oxidative stress, we stimulated them with increasing concentrations of hydrogen peroxide. This resulted in a dose-dependent decrease in astrocyte cell viability. This shows that the SVG-A cells are better at modelling the oxidative stress phase of AD using hydrogen peroxide compared to LPS-induced neuroinflammation. However, future experiments can potentially try to combine both these stressors. T98G astrocytoma cells showed that pre-treatment with LPS led to a potentiated response to hydrogen peroxide-induced oxidative stress (Yue *et al.*, 2008). This experimental approach could consider how inflammation can activate glial cells and induce Aβ expression, setting

the cells up for the oxidative stress seen in AD. It would give a better insight into how these processes work together to bring out the deleterious effects in astrocytes, as seen in AD.

In conclusion, this study adds to the existing knowledge on the role of LPS-mediated inflammation and oxidative stress induced by hydrogen peroxide on astrocytes. It also provides new insights into using SVG-A cells to study AD. Additionally it also characterises the long-term effects of an acute dosing regimen of intranasal LPS in astrocytes by looking at the percentage hippocampal area populated by GFAP stained astrocytes.

References

Afsar, A., Chacon Castro, M. D. C., Soladogun, A. S. and Zhang, L. (2023) 'Recent Development in the Understanding of Molecular and Cellular Mechanisms Underlying the Etiopathogenesis of Alzheimer's Disease', *International Journal of Molecular Sciences,* 24(8), pp. 7258.

Akira, S., Uematsu, S. and Takeuchi, O. (2006) 'Pathogen Recognition and Innate Immunity', *Cell,* 124(4), pp. 783-801.

Amri, F., Ghouili, I., Amri, M., Carrier, A. and Masmoudi-Kouki, O. (2017) 'Neuroglobin protects astroglial cells from hydrogen peroxide-induced oxidative stress and apoptotic cell death', *Journal of Neurochemistry,* 140(1), pp. 151-169.

Ashraf, G. M., Tarasov, V. V., Makhmutova, A., Chubarev, V. N., Avila-Rodriguez, M., Bachurin, S. O. and Aliev, G. (2019) 'The Possibility of an Infectious Etiology of Alzheimer Disease', *Molecular neurobiology,* 56(6), pp. 4479-4491.

Assefa, B. T., Gebre, A. K. and Altaye, B. M. (2018) 'Reactive Astrocytes as Drug Target in Alzheimer's Disease', *BioMed Research International,* 2018, pp. 1-10.

B., S. and W.J., A. (2001) 'HIV Type 1 Infection of Human Astrocytes Is Restricted by Inefficient Viral Entry', *AIDs Research And Human Reteroviruses,* 17(12).

Banks, W. A., Gray, A. M., Erickson, M. A., Salameh, T. S., Damodarasamy, M., Sheibani, N., Meabon, J. S., Wing, E. E., Morofuji, Y., Cook, D. G. and Reed, M. J. (2015) 'Lipopolysaccharide-induced blood-brain barrier disruption: roles of cyclooxygenase, oxidative stress, neuroinflammation, and elements of the neurovascular unit', *Journal of Neuroinflammation,* 12(1).

Batista, C. R. A., Gomes, G. F., Candelario-Jalil, E., Fiebich, B. L. and De Oliveira, A. C. P. (2019) 'Lipopolysaccharide-Induced Neuroinflammation as a Bridge to Understand Neurodegeneration', *International Journal of Molecular Sciences,* 20(9), pp. 2293.

Bayr, H. (2005) 'Reactive oxygen species', *Critical care medicine,* 33(12 Suppl), pp. S498-S501.

Beom Seok, P., Dong Hyun, S., Ho Min, K. I. M., Choi, B.-S., Lee, H. and Lee, J.-O. (2009) 'The structural basis of lipopolysaccharide recognition by the TLR4-MD-2 complex', *Nature,* 458(7242), pp. 1191-1195.

Betteridge, D. J. (2000) 'What is oxidative stress?', *Metabolism, clinical and experimental,* 49(2), pp. 3-8.

Beurel, E. and Jope, R. S. (2009) 'Lipopolysaccharide-induced interleukin-6 production is controlled by glycogen synthase kinase-3 and STAT3 in the brain', *Journal of Neuroinflammation,* 6(1), pp. 9.

Blasko, I., Stampfer-Kountchev, M., Robatscher, P., Veerhuis, R., Eikelenboom, P. and Grubeck-Loebenstein, B. (2004) 'How chronic inflammation can affect the brain and support the development of Alzheimers disease in old age: the role of microglia and astrocytes', *Aging cell,* 3(4), pp. 169-176.

Brahmachari, S., Fung, Y. K. and Pahan, K. (2006) 'Induction of Glial Fibrillary Acidic Protein Expression in Astrocytes by Nitric Oxide', *The Journal of neuroscience,* 26(18), pp. 4930-4939.

Brown, G. C. (2019) 'The endotoxin hypothesis of neurodegeneration', *Journal of Neuroinflammation,* 16(1).

Cheignon, C., Tomas, M., Bonnefont-Rousselot, D., Faller, P., Hureau, C. and Collin, F. (2018) 'Oxidative stress and the amyloid beta peptide in Alzheimer's disease', *Redox biology,* 14, pp. 450-464.

Choi, J.-J., Choi, J.-J., Choi, J., Choi, J.-J., Choi, J., Kang, C.-D., Chen, X., Wu, C.-F., Ko, K. H. and Kim, W.-K. (2007) 'Hydrogen peroxide induces the death of astrocytes through the down-regulation of the constitutive nuclear factor-kappaB activity', *Free Radical Research,* 41(5), pp. 555-562.

Chun, H., Im, H., Kang, Y. J., Kim, Y., Shin, J. H., Won, W., Lim, J., Ju, Y., Park, Y. M., Kim, S., Lee, S. E., Lee, J., Woo, J., Hwang, Y., Cho, H., Jo, S., Park, J.-H., Kim, D., Kim, D. Y., Seo, J.-S., Gwag, B. J., Kim, Y. S., Park, K. D., Kaang, B.-K., Cho, H., Ryu, H. and Lee, C. J. (2020) 'Severe reactive astrocytes precipitate pathological hallmarks of Alzheimer's disease via H2O2− production', *Nature Neuroscience,* 23(12), pp. 1555-1566.

Cunningham, C. and Hennessy, E. (2015) 'Co-morbidity and systemic inflammation as drivers of cognitive decline: new experimental models adopting a broader paradigm in dementia research', *Alzheimer's Research & Therapy,* 7(1), pp. 33.

D'Angelo, B., Astarita, C., Boffo, S., Massaro-Giordano, M., Antonella Ianuzzi, C., Caporaso, A., Macaluso, M. and Giordano, A. (2017) 'LPS-induced inflammatory response triggers cell cycle reactivation in murine neuronal cells through retinoblastoma proteins induction', *Cell cycle (Georgetown, Tex.),* 16(24), pp. 2330-2336.

Del Pilar, C., Garrido-Matilla, L., Del Pozo-Filíu, L., Lebrón-Galán, R., Arias, R. F., Clemente, D., Alonso, J. R., Weruaga, E. and Díaz, D. (2024) 'Intracerebellar injection of monocytic immature myeloid cells prevents the adverse effects caused by stereotactic surgery in a model of cerebellar neurodegeneration', *Journal of neuroinflammation,* 21(1), pp. 49-49.

Desagher, S., Glowinski, J. and Premont, J. (1996) 'Astrocytes protect neurons from hydrogen peroxide toxicity', *The Journal of Neuroscience,* 16(8), pp. 2553-2562.

Dozio, V. and Sanchez, J.-C. (2018) 'Profiling the proteomic inflammatory state of human astrocytes using DIA mass spectrometry', *Journal of Neuroinflammation,* 15(1).

Eigenmann, D. E., Xue, G., Kim, K. S., Moses, A. V., Hamburger, M. and Oufir, M. (2013) 'Comparative study of four immortalized human brain capillary endothelial cell lines, hCMEC/D3, hBMEC, TY10, and BB19, and optimization of culture conditions, for an in vitro blood-brain barrier model for drug permeability studies', *Fluids and barriers of the CNS,* 10(1), pp. 33-33.

Erta, M., Quintana, A. and Hidalgo, J. (2012) 'Interleukin-6, a Major Cytokine in the Central Nervous System', *International Journal of Biological Sciences,* 8(9), pp. 1254-1266.

Farrell, B. T. and Lahue, R. S. (2006) 'CAG·CTG repeat instability in cultured human astrocytes', *Nucleic Acids Research,* 34(16), pp. 4495-4505.

Fenn, A. M., Henry, C. J., Huang, Y., Dugan, A. and Godbout, J. P. (2012) 'Lipopolysaccharide-induced interleukin (IL)-4 receptor-α expression and corresponding sensitivity to the M2 promoting effects of IL-4 are impaired in microglia of aged mice', *Brain, behavior, and immunity,* 26(5), pp. 766-777.

François, A., Terro, F., Janet, T., Bilan, A. R., Paccalin, M. and Page, G. (2013) 'Involvement of interleukin-1β in the autophagic process of microglia: relevance to Alzheimer's disease', *Journal of Neuroinflammation,* 10(1), pp. 151.

Galea, I. (2021) 'The blood-brain barrier in systemic infection and inflammation', *Cellular & molecular immunology,* 18(11), pp. 2489-2501.

Ghasemi, M., Turnbull, T., Sebastian, S. and Kempson, I. (2021) 'The MTT Assay: Utility, Limitations, Pitfalls, and Interpretation in Bulk and Single-Cell Analysis', *International journal of molecular sciences,* 22(23), pp. 12827.

Ghosh, S., Lertwattanarak, R., Garduño, J. d. J., Galeana, J. J., Li, J., Zamarripa, F., Lancaster, J. L., Mohan, S., Hussey, S. and Musi, N. (2015) 'Elevated muscle TLR4 expression and metabolic endotoxemia in human aging', *The journals of gerontology. Series A, Biological sciences and medical sciences,* 70(2), pp. 232-246.

González-Reyes, R. E., Nava-Mesa, M. O., Vargas-Sánchez, K., Ariza-Salamanca, D. and Mora-Muñoz, L. (2017) 'Involvement of Astrocytes in Alzheimer's Disease from a Neuroinflammatory and Oxidative Stress Perspective', *Frontiers in molecular neuroscience,* 10, pp. 427-427.

Gunawardena, D., Raju, R. and Münch, G. (2019) 'Hydrogen peroxide mediates pro-inflammatory cell-to-cell signaling: a new therapeutic target for inflammation?', *Neural regeneration research,* 14(8), pp. 1430-1437.

Guo, S., Wang, H. and Yin, Y. (2022) 'Microglia Polarization From M1 to M2 in Neurodegenerative Diseases', *Frontiers in aging neuroscience,* 14, pp. 815347-815347.

Haley, S. A., O'Hara, B. A. and Atwood, W. J. (2020) 'Adipocyte Plasma Membrane Protein (APMAP) promotes JC Virus (JCPyV) infection in human glial cells', *Virology (New York, N.Y.),* 548, pp. 17-24.

Halliwell, B., Clement, M. V. and Long, L. H. (2000) 'Hydrogen peroxide in the human body', *FEBS Letters,* 486(1), pp. 10-13.

Hampel, H., Hardy, J., Blennow, K., Chen, C., Perry, G., Kim, S. H., Villemagne, V. L., Aisen, P., Vendruscolo, M., Iwatsubo, T., Masters, C. L., Cho, M., Lannfelt, L., Cummings, J. L. and Vergallo, A. (2021) 'The Amyloid-β Pathway in Alzheimer's Disease', *Molecular Psychiatry,* 26(10), pp. 5481-5503.

He, Q., Li, Y. H., Guo, S. S., Wang, Y., Lin, W., Zhang, Q., Wang, J., Ma, C. G. and Xiao, B. G. (2016) 'Inhibition of Rho-kinase by Fasudil protects dopamine neurons and attenuates inflammatory response in an intranasal lipopolysaccharide-mediated Parkinson's model', *European Journal of Neuroscience,* 43(1), pp. 41-52.

Heneka, M. T., Carson, M. J., Khoury, J. E., Landreth, G. E., Brosseron, F., Feinstein, D. L., Jacobs, A. H., Wyss-Coray, T., Vitorica, J., Ransohoff, R. M., Herrup, K., Frautschy, S. A., Finsen, B., Brown, G. C., Verkhratsky, A., Yamanaka, K., Koistinaho, J., Latz, E., Halle, A., Petzold, G. C., Town, T., Morgan, D., Shinohara, M. L., Perry, V. H., Holmes, C., Bazan, N. G., Brooks, D. J., Hunot, S., Joseph, B., Deigendesch, N., Garaschuk, O., Boddeke, E., Dinarello, C. A., Breitner, J. C., Cole, G. M., Golenbock, D. T. and Kummer, M. P. (2015) 'Neuroinflammation in Alzheimer's disease', *The Lancet Neurology,* 14(4), pp. 388-405.

Herber, D. L., Maloney, J. L., Roth, L. M., Freeman, M. J., Morgan, D. and Gordon, M. N. (2006) 'Diverse microglial responses after intrahippocampal administration of lipopolysaccharide', *Glia,* 53(4), pp. 382-391.

Hou, Y., Xie, G., Liu, X., Li, G., Jia, C., Xu, J. and Wang, B. (2016) 'Minocycline protects against lipopolysaccharide-induced cognitive impairment in mice', *Psychopharmacology,* 233(5), pp. 905-916.

Huang, C., Ye, T., Chen, B., Chen, Z., Ye, Y. and Liu, H. (2023) 'Intranasal administration of lipopolysaccharide reverses chronic stress-induced depression-like behavior in mice by microglial stimulation', *International immunopharmacology,* 120, pp. 110347-110347.

Huang, W.-J., Zhang, X. and Chen, W.-W. (2016) 'Role of oxidative stress in Alzheimer's disease', *Biomedical Reports,* 4(5), pp. 519-522.

Im, K., Mareninov, S., Diaz, M. F. P. and Yong, W. H. (2019) 'An Introduction to Performing Immunofluorescence Staining', *Methods in Molecular Biology*: Springer New York, pp. 299-311.

Jack, C. S., Arbour, N., Manusow, J., Montgrain, V., Blain, M., McCrea, E., Shapiro, A. and Antel, J. P. (2005) 'TLR Signaling Tailors Innate Immune Responses in Human Microglia and Astrocytes', *Journal of Immunology,* 175(7), pp. 4320-4330.

Jekabsone, A., Mander, P. K., Tickler, A., Sharpe, M. and Brown, G. C. (2006) 'Fibrillar beta-amyloid peptide Aβ1–40 activates microglial proliferation via stimulating TNF-α release and H2O2 derived from NADPH oxidase: a cell culture study', *Journal of Neuroinflammation,* 3(1), pp. 24.

Jemimah, S., Chabib, C. M. M., Hadjileontiadis, L. and Alshehhi, A. (2023) 'Gut microbiome dysbiosis in Alzheimer's disease and mild cognitive impairment: A systematic review and meta-analysis', *PLOS ONE,* 18(5), pp. e0285346.

Jesus, A., Jose, L. J., Mar, P. and Felix, H. (2004) 'Role of Tau Protein in Both Physiological and Pathological Conditions', *Physiological Reviews,* 84(2), pp. 361-384.

Juknat, A. A., Méndez, M. d. V. A., Quaglino, A., Fameli, C. I., Mena, M. and Kotler, M. L. (2005) 'Melatonin prevents hydrogen peroxide-induced Bax expression in cultured rat astrocytes', *Journal of pineal research,* 38(2), pp. 84-92.

Kahn, M. S., Kranjac, D., Alonzo, C. A., Haase, J. H., Cedillos, R. O., McLinden, K. A., Boehm, G. W. and Chumley, M. J. (2012) 'Prolonged elevation in hippocampal Aβ and cognitive deficits following repeated endotoxin exposure in the mouse', *Behavioural brain research,* 229(1), pp. 176-184.

Kaur, G. and Dufour, J. M. (2012) 'Cell lines', *Spermatogenesis,* 2(1), pp. 1-5.

Kim, H. S., Kim, S., Shin, S. J., Park, Y. H., Nam, Y., Kim, C. W., Lee, K. W., Kim, S.-M., Jung, I. D., Yang, H. D., Park, Y.-M. and Moon, M. (2021)

'Gram-negative bacteria and their lipopolysaccharides in Alzheimer's disease: pathologic roles and therapeutic implications', *Translational Neurodegeneration,* 10(1).

Kim, K.-A., Jeong, J.-J., Yoo, S.-Y. and Kim, D.-H. (2016) 'Gut microbiota lipopolysaccharide accelerates inflamm-aging in mice', *BMC microbiology,* 16(6), pp. 9-9.

Kinney, J. W., Bemiller, S. M., Murtishaw, A. S., Leisgang, A. M., Salazar, A. M. and Lamb, B. T. (2018) 'Inflammation as a central mechanism in Alzheimer's disease', *Alzheimer's & Dementia: Translational Research & Clinical Interventions,* 4(1), pp. 575-590.

Kumar, H., Kawai, T. and Akira, S. (2009) 'Toll-like receptors and innate immunity', *Biochemical and biophysical research communications,* 388(4), pp. 621-625.

Landeck, N., Mazza, M. C., Duffy, M., Bishop, C., Sortwell, C. E. and Cookson, M. R. (2021) 'Stereotaxic Intracranial Delivery of Chemicals, Proteins or Viral Vectors to Study Parkinson's Disease', *Journal of visualized experiments,* (168).

Lee, J. W., Lee, Y. K., Yuk, D. Y., Choi, D. Y., Ban, S. B., Oh, K. W. and Hong, J. T. (2008) 'Neuro-inflammation induced by lipopolysaccharide causes cognitive impairment through enhancement of beta-amyloid generation', *Journal of Neuroinflammation,* 5(1), pp. 37.

Lee, W. C., Choi, C. H., Cha, S. H., Oh, H. L. and Kim, Y. K. (2005) 'Role of ERK in hydrogen peroxide-induced cell death of human glioma cells', *Neurochemical research,* 30(2), pp. 263-270.

Li, K., Li, J., Zheng, J. and Qin, S. (2019) 'Reactive Astrocytes in Neurodegenerative Diseases', *Aging and disease,* 10(3), pp. 664-675.

Liddelow, S. A. and Barres, B. A. (2017) 'Reactive Astrocytes: Production, Function, and Therapeutic Potential', *Immunity,* 46(6), pp. 957-967.

Liddelow, S. A., Guttenplan, K. A., Clarke, L. E., Bennett, F. C., Bohlen, C. J., Schirmer, L., Bennett, M. L., Münch, A. E., Chung, W.-S., Peterson, T. C., Wilton, D. K., Frouin, A., Napier, B. A., Panicker, N., Kumar, M., Buckwalter, M. S., Rowitch, D. H., Dawson, V. L., Dawson, T. M.,

Stevens, B. and Barres, B. A. (2017) 'Neurotoxic reactive astrocytes are induced by activated microglia', *Nature,* 541(7638), pp. 481-487.

Liu, C., Chu, D., Kalantar-Zadeh, K., George, J., Young, H. A. and Liu, G. (2021) 'Cytokines: From Clinical Significance to Quantification', *Advanced science,* 8(15), pp. e2004433-n/a.

Lopez-Castejon, G. and Brough, D. (2011) 'Understanding the mechanism of IL-1β secretion', *Cytokine & growth factor reviews,* 22(4), pp. 189-195.

Lyman, M., Lloyd, D. G., Ji, X., Vizcaychipi, M. P. and Ma, D. (2014) 'Neuroinflammation: the role and consequences', *Neuroscience research,* 79, pp. 1-12.

Major, E. O., Miller, A. E., Mourrain, P., Traub, R. G., De Widt, E. and Sever, J. (1985) 'Establishment of a Line of Human Fetal Glial Cells That Supports JC Virus Multiplication', *Proceedings of the National Academy of Sciences - PNAS,* 82(4), pp. 1257-1261.

Mander, P. K., Jekabsone, A. and Brown, G. C. (2006) 'Microglia Proliferation Is Regulated by Hydrogen Peroxide from NADPH Oxidase', *Journal of Immunology,* 176(2), pp. 1046-1052.

Manoharan, S., Guillemin, G. J., Abiramasundari, R. S., Essa, M. M., Akbar, M. and Akbar, M. D. (2016) 'The Role of Reactive Oxygen Species in the Pathogenesis of Alzheimer’s Disease, Parkinson’s Disease, and Huntington’s Disease: A Mini Review', *Oxidative Medicine and Cellular Longevity,* 2016, pp. 1-15.

McGeer, E. G. and McGeer, P. L. (1997) 'Inflammatory Cytokines in the CNS: Possible Role in the Pathogenesis of Neurodegenerative Disorders and Therapeutic Implications', *CNS drugs,* 7(3), pp. 214-228.

Miller, E. W., Dickinson, B. C. and Chang, C. J. (2010) 'Aquaporin-3 mediates hydrogen peroxide uptake to regulate downstream intracellular signaling', *Proceedings of the National Academy of Sciences - PNAS,* 107(36), pp. 15681-15686.

Milton, N. G. N. (2004) 'Role of Hydrogen Peroxide in the Aetiology of Alzheimer's Disease', *Drugs & Aging,* 21(2), pp. 81-100.

Mizobuchi, H. and Soma, G.-I. (2021) 'Low-dose lipopolysaccharide as an immune regulator for homeostasis maintenance in the central nervous

system through transformation to neuroprotective microglia', *Neural regeneration research,* 16(10), pp. 1928-1934.

Mizobuchi, H., Yamamoto, K., Tsutsui, S., Yamashita, M., Nakata, Y., Inagawa, H., Kohchi, C. and Soma, G.-I. (2020) 'A unique hybrid characteristic having both pro- and anti-inflammatory phenotype transformed by repetitive low-dose lipopolysaccharide in C8-B4 microglia', *Scientific Reports,* 10(1).

Monterey, M. D., Wei, H., Wu, X. and Wu, J. Q. (2021) 'The Many Faces of Astrocytes in Alzheimer's Disease', *Frontiers in neurology,* 12, pp. 619626-619626.

Nagai, Y., Takatsu, K. and Watson, R. R. (2014) 'Chapter 26 - Role of the Immune System in Obesity-Associated Inflammation and Insulin Resistance', *Nutrition in the Prevention and Treatment of Abdominal Obesity*. San Diego: Academic Press, pp. 281-293.

Nedzvetsky, V. S., Agca, C. A. and Kyrychenko, S. V. (2017) 'Neuroprotective Effect of Curcumin on LPS-activated Astrocytes Is Related to the Prevention of GFAP and NF-κB Upregulation', *Neurophysiology (New York),* 49(4), pp. 305-307.

Newton, K. and Dixit, V. M. (2012) 'Signaling in Innate Immunity and Inflammation', *Cold Spring Harbor Perspectives in Biology,* 4(3), pp. a006049-a006049.

Ng, A., Tam, W. W., Zhang, M. W., Ho, C. S., Husain, S. F., Mcintyre, R. S. and Ho, R. C. (2018) 'IL-1β, IL-6, TNF- α and CRP in Elderly Patients with Depression or Alzheimer's disease: Systematic Review and Meta-Analysis', *Scientific Reports,* 8(1).

Ni, M., Zheng, M., Chen, B., Lu, X., Zhao, H., Zhu, T., Cheng, L., Han, H., Ye, T., Liu, H., Ye, Y., Huang, C. and Yuan, X. (2023) 'Microglial stimulation triggered by intranasal lipopolysaccharide administration produces antidepressant-like effect through ERK1/2-mediated BDNF synthesis in the hippocampus', *Neuropharmacology,* 240, pp. 109693-109693.

Niethammer, P., Grabher, C., Look, A. T. and Mitchison, T. J. (2009) 'A tissue-scale gradient of hydrogen peroxide mediates rapid wound detection in zebrafish', *Nature,* 459(7249), pp. 996-999.

Niranjan, R., Nagarajan, R., Hanif, K., Nath, C. and Shukla, R. (2014) 'LPS induces mediators of neuroinflammation, cell proliferation, and GFAP expression in human astrocytoma cells U373MG: the anti-inflammatory and anti-proliferative effect of guggulipid', *Neurological sciences,* 35(3), pp. 409-414.

Niu, H., Wang, Q., Zhao, W., Liu, J., Wang, D., Muhammad, B., Liu, X., Quan, N., Zhang, H., Zhang, F., Wang, Y., Li, H. and Yang, R. (2020) 'IL-1β/IL-1R1 signaling induced by intranasal lipopolysaccharide infusion regulates alpha-Synuclein pathology in the olfactory bulb, substantia nigra and striatum', *Brain Pathology,* 30(6), pp. 1102-1118.

Ogunmokun, G., Dewanjee, S., Chakraborty, P., Valupadas, C., Chaudhary, A., Kolli, V., Anand, U., Vallamkondu, J., Goel, P., Paluru, H. P. R., Gill, K. D., Reddy, P. H., De Feo, V. and Kandimalla, R. (2021) 'The Potential Role of Cytokines and Growth Factors in the Pathogenesis of Alzheimer's Disease', *Cells,* 10(10), pp. 2790.

Ohsawa, K., Imai, Y., Sasaki, Y. and Kohsaka, S. (2004) 'Microglia/macrophage-specific protein Iba1 binds to fimbrin and enhances its actin-bundling activity', *Journal of neurochemistry,* 88(4), pp. 844-856.

Page, M. J., Kell, D. B. and Pretorius, E. (2022) 'The Role of Lipopolysaccharide-Induced Cell Signalling in Chronic Inflammation', *Chronic Stress,* 6, pp. 247054702210763.

Pardon, M.-C., Yanez Lopez, M., Yuchun, D., Marjańska, M., Prior, M., Brignell, C., Parhizkar, S., Agostini, A., Bai, L., Auer, D. P. and Faas, H. M. (2016) 'Magnetic Resonance Spectroscopy discriminates the response to microglial stimulation of wild type and Alzheimer's disease models', *Scientific Reports,* 6(1), pp. 19880.

Park, J. Y., Lee, K.-H., Park, H. S. and Choi, S. J. (2017) 'LPS Sensing Mechanism of Human Astrocytes: Evidence of Functional TLR4 Expression and Requirement of Soluble CD14', *Journal of Bacteriology and Virology,* 47(4), pp. 189.

Perez-Catalan, N. A., Doe, C. Q. and Ackerman, S. D. (2021) 'The role of astrocyte-mediated plasticity in neural circuit development and function', *Neural Development,* 16(1).

Perez-Dominguez, M., Ávila-Muñoz, E., Domínguez-Rivas, E. and Zepeda, A. (2019) 'The detrimental effects of lipopolysaccharide-induced neuroinflammation on adult hippocampal neurogenesis depend on the duration of the pro-inflammatory response', *Neural regeneration research,* 14(5), pp. 817-825.

Perez-Nievas, B. G., Stein, T. D., Tai, H.-C., Dols-Icardo, O., Scotton, T. C., Barroeta-Espar, I., Fernandez-Carballo, L., De Munain, E. L., Perez, J., Marquie, M., Serrano-Pozo, A., Frosch, M. P., Lowe, V., Parisi, J. E., Petersen, R. C., Ikonomovic, M. D., López, O. L., Klunk, W., Hyman, B. T. and Gómez-Isla, T. (2013) 'Dissecting phenotypic traits linked to human resilience to Alzheimer's pathology', *Brain,* 136(8), pp. 2510-2526.

Picca, A., Calvani, R., Coelho-Junior, H. J., Landi, F., Bernabei, R. and Marzetti, E. (2020) 'Mitochondrial Dysfunction, Oxidative Stress, and Neuroinflammation: Intertwined Roads to Neurodegeneration', *Antioxidants,* 9(8), pp. 647.

Preato, A. M., Pinheiro, E. d. S., Rosenstock, T. R. and Glezer, I. (2024) 'The Relevance of Astrocytic Cell Culture Models for Neuroinflammation in Neurodegeneration Research', *Neuroglia (Basel, Switzerland),* 5(1), pp. 27-49.

Preston, A. N., Cervasio, D. A. and Laughlin, S. T. (2019) 'Visualizing the brain's astrocytes', *Methods in enzymology,* 622, pp. 129-151.

Rice, M. E. (2011) 'H2O2: A Dynamic Neuromodulator', *The Neuroscientist,* 17(4), pp. 389-406.

Rodgers, K. R., Lin, Y., Langan, T. J., Iwakura, Y. and Chou, R. C. (2020) 'Innate Immune Functions of Astrocytes are Dependent Upon Tumor Necrosis Factor-Alpha', *Scientific reports,* 10(1), pp. 7047-7047.

Ryu, J.-K., Kim, S. J., Rah, S.-H., Kang, J. I., Jung, H. E., Lee, D., Lee, H. K., Lee, J.-O., Park, B. S., Yoon, T.-Y. and Kim, H. M. (2017) 'Reconstruction of LPS Transfer Cascade Reveals Structural Determinants within LBP, CD14, and TLR4-MD2 for Efficient LPS Recognition and Transfer', *Immunity,* 46(1), pp. 38-50.

Ryu, K.-Y., Lee, H.-J., Woo, H., Kang, R.-J., Han, K.-M., Park, H., Lee, S. M., Lee, J.-Y., Jeong, Y. J., Nam, H.-W., Nam, Y. and Hoe, H.-S.

(2019) 'Dasatinib regulates LPS-induced microglial and astrocytic neuroinflammatory responses by inhibiting AKT/STAT3 signaling', *Journal of neuroinflammation,* 16(1), pp. 190-190.

Saha, S., Pupo, E., Zariri, A. and van der Ley, P. (2022) 'Lipid A heterogeneity and its role in the host interactions with pathogenic and commensal bacteria', *microLife,* 3, pp. uqac011-uqac011.

Sahin, B. and Ergul, M. (2022) 'Captopril exhibits protective effects through anti-inflammatory and anti-apoptotic pathways against hydrogen peroxide-induced oxidative stress in C6 glioma cells', *Metabolic Brain Disease,* 37(4), pp. 1221-1230.

Salim, S. (2017) 'Oxidative stress and the central nervous system', *The Journal of pharmacology and experimental therapeutics,* 360(1), pp. 201-205.

Saura, J. (2007) 'Microglial cells in astroglial cultures: a cautionary note', *Journal of Neuroinflammation,* 4(1), pp. 26.

Schindelin, J., Arganda-Carreras, I., Frise, E., Kaynig, V., Longair, M., Pietzsch, T., Preibisch, S., Rueden, C., Saalfeld, S., Schmid, B., Tinevez, J.-Y., White, D. J., Hartenstein, V., Eliceiri, K., Tomancak, P. and Cardona, A. (2012) 'Fiji: an open-source platform for biological-image analysis', *Nature Methods,* 9(7), pp. 676-682.

Schromm, A. B., Lien, E., Henneke, P., Chow, J. C., Yoshimura, A., Heine, H., Latz, E., Monks, B. G., Schwartz, D. A., Miyake, K. and Golenbock, D. T. (2001) 'Molecular Genetic Analysis of an Endotoxin Nonresponder Mutant Cell Line', *The Journal of Experimental Medicine,* 194(1), pp. 79-88.

Semmler, A., Hermann, S., Mormann, F., Weberpals, M., Paxian, S. A., Okulla, T., Schäfers, M., Kummer, M. P., Klockgether, T. and Heneka, M. T. (2008) 'Sepsis causes neuroinflammation and concomitant decrease of cerebral metabolism', *Journal of Neuroinflammation,* 5(1), pp. 38.

Sharif, S. F., Hariri, R. J., Chang, V. A., Barie, P. S., Wang, R. S. and Ghajar, J. B. G. (1993) 'Human astrocyte production of tumour necrosis factor-α, interleukin-1β, and interleukin-6 following exposure to lipopolysaccharide endotoxin', *Neurological Research,* 15(2), pp. 109-112.

Sharma, A., Patro, N. and Patro, I. K. (2016) 'Lipopolysaccharide-Induced Apoptosis of Astrocytes: Therapeutic Intervention by Minocycline', *Cellular and molecular neurobiology,* 36(4), pp. 577-592.

Skrzypczak-Wiercioch, A. and Sałat, K. (2022) 'Lipopolysaccharide-Induced Model of Neuroinflammation: Mechanisms of Action, Research Application and Future Directions for Its Use', *Molecules,* 27(17), pp. 5481.

Stelter, F., Bernheiden, M., Menzel, R., Jack, R. S., Witt, S., Fan, X., Pfister, M. and Schütt, C. (1997) 'Mutation of Amino Acids 39–44 of Human CD14 Abrogates Binding of Lipopolysaccharide and Escherichia coli', *European journal of biochemistry,* 243(1-2), pp. 100-109.

Stockert, J. C., Horobin, R. W., Colombo, L. L. and Blázquez-Castro, A. (2018) 'Tetrazolium salts and formazan products in Cell Biology: Viability assessment, fluorescence imaging, and labeling perspectives', *Acta histochemica,* 120(3), pp. 159-167.

Su, B., Wang, X., Nunomura, A., Moreira, P., Lee, H.-G., Perry, G., Smith, M. and Zhu, X. (2008) 'Oxidative Stress Signaling in Alzheimers Disease', *Current Alzheimer Research,* 5(6), pp. 525-532.

Sun, E., Motolani, A., Campos, L. and Lu, T. (2022) 'The Pivotal Role of NF-kB in the Pathogenesis and Therapeutics of Alzheimer's Disease', *International Journal of Molecular Sciences,* 23(16), pp. 8972.

Tabner, B. J., El-Agnaf, O. M. A., Turnbull, S., German, M. J., Paleologou, K. E., Hayashi, Y., Cooper, L. J., Fullwood, N. J. and Allsop, D. (2005) 'Hydrogen Peroxide Is Generated during the Very Early Stages of Aggregation of the Amyloid Peptides Implicated in Alzheimer Disease and Familial British Dementia', *Journal of Biological Chemistry,* 280(43), pp. 35789-35792.

Tan, Y. and Kagan, Jonathan C. (2014) 'A Cross-Disciplinary Perspective on the Innate Immune Responses to Bacterial Lipopolysaccharide', *Molecular cell,* 54(2), pp. 212-223.

Tang, L., Liu, L., Li, G., Jiang, P., Wang, Y. and Li, J. (2019) 'Expression Profiles of Long Noncoding RNAs in Intranasal LPS-Mediated Alzheimer's Disease Model in Mice', *BioMed research international,* 2019, pp. 9642589-14.

Tarassishin, L., Suh, H.-S. and Lee, S. C. (2014) 'LPS and IL-1 differentially activate mouse and human astrocytes: Role of CD14', *Glia,* 62(6), pp. 999-1013.

Trzeciak, A., Lerman, Y. V., Kim, T.-H., Kim, M. R., Mai, N., Halterman, M. W. and Kim, M. (2019) 'Long-Term Microgliosis Driven by Acute Systemic Inflammation', *The Journal of immunology (1950),* 203(11), pp. 2979-2989.

Tweedie, D., Ferguson, R. A., Fishman, K., Frankola, K. A., Van Praag, H., Holloway, H. W., Luo, W., Li, Y., Caracciolo, L., Russo, I., Barlati, S., Ray, B., Lahiri, D. K., Bosetti, F., Greig, N. H. and Rosi, S. (2012) 'Tumor necrosis factor-α synthesis inhibitor 3,6′-dithiothalidomide attenuates markers of inflammation, Alzheimer pathology and behavioral deficits in animal models of neuroinflammation and Alzheimer's disease', *Journal of Neuroinflammation,* 9(1), pp. 106.

Wang, M., Feng, L.-R., Li, Z.-L., Ma, K.-G., Chang, K.-W., Chen, X.-L., Yang, P.-B., Ji, S.-F., Ma, Y.-B., Han, H., Ruganzua, J. B., Yang, W.-N. and Qian, Y.-H. (2021) 'Thymosin β4 reverses phenotypic polarization of glial cells and cognitive impairment via negative regulation of NF-κB signaling axis in APP/PS1 mice', *Journal of Neuroinflammation,* 18(1).

Wassenaar, T. M. and Zimmermann, K. (2018) 'Lipopolysaccharides in Food, Food Supplements, and Probiotics: Should We be Worried?', *European journal of microbiology & immunology,* 8(3), pp. 63-69.

Wendeln, A.-C., Degenhardt, K., Kaurani, L., Gertig, M., Ulas, T., Jain, G., Wagner, J., Häsler, L. M., Wild, K., Skodras, A., Blank, T., Staszewski, O., Datta, M., Centeno, T. P., Capece, V., Islam, M. R., Kerimoglu, C., Staufenbiel, M., Schultze, J. L., Beyer, M., Prinz, M., Jucker, M., Fischer, A. and Neher, J. J. (2018) 'Innate immune memory in the brain shapes neurological disease hallmarks', *Nature,* 556(7701), pp. 332-338.

Wittmann, C., Chockley, P., Singh, S. K., Pase, L., Lieschke, G. J. and Grabher, C. (2012) 'Hydrogen Peroxide in Inflammation: Messenger, Guide, and Assassin', *Advances in Hematology,* 2012, pp. 1-6.

Xie, J., Van Hoecke, L. and Vandenbroucke, R. E. (2021) 'The Impact of Systemic Inflammation on Alzheimer's Disease Pathology', *Frontiers in immunology,* 12, pp. 796867-796867.

Yang, J., Yang, J., Liang, S. H., Xu, Y., Moore, A. and Ran, C. (2016) 'Imaging hydrogen peroxide in Alzheimer's disease via cascade signal amplification', *Scientific Reports,* 6(1), pp. 35613.

Yue, G., Shi, G., Azaro, M. A., Yang, Q., Hu, G., Luo, M., Yin, K., Nagele, R. G., Fine, D. H., Yang, J.-M. and Li, H. (2008) 'Lipopolysaccharide (LPS) potentiates hydrogen peroxide toxicity in T98G astrocytoma cells by suppression of anti-oxidative and growth factor gene expression', *BMC Genomics,* 9(1), pp. 608.

Zhan, X., Stamova, B., Jin, L.-W., Decarli, C., Phinney, B. and Sharp, F. R. (2016) 'Gram-negative bacterial molecules associate with Alzheimer disease pathology', *Neurology,* 87(22), pp. 2324-2332.

Zhang, J.-M. and An, J. (2007) 'Cytokines, inflammation, and pain', *International anesthesiology clinics,* 45(2), pp. 27-37.

Zhang, K., Wu, S., Li, Z. and Zhou, J. (2017) 'MicroRNA-211/BDNF axis regulates LPS-induced proliferation of normal human astrocyte through PI3K/AKT pathway', *Bioscience Reports,* 37(4).

Zhang, R., Miller, R. G., Gascon, R., Champion, S., Katz, J., Lancero, M., Narvaez, A., Honrada, R., Ruvalcaba, D. and Mcgrath, M. S. (2009) 'Circulating endotoxin and systemic immune activation in sporadic amyotrophic lateral sclerosis (sALS)', *Journal of Neuroimmunology,* 206(1-2), pp. 121-124.

Zhao, J., Bi, W., Xiao, S., Lan, X., Cheng, X., Zhang, J., Lu, D., Wei, W., Wang, Y., Li, H., Fu, Y. and Zhu, L. (2019) 'Neuroinflammation induced by lipopolysaccharide causes cognitive impairment in mice', *Scientific Reports,* 9(1).

Zhao, Y., Jaber, V. R., Pogue, A. I., Sharfman, N. M., Taylor, C. and Lukiw, W. J. (2022) 'Lipopolysaccharides (LPSs) as Potent Neurotoxic Glycolipids in Alzheimer's Disease (AD)', *International Journal of Molecular Sciences,* 23(20), pp. 12671.

Zhou, J., Xiang, W., Zhang, K., Zhao, Q., Xu, Z. and Li, Z. (2022) 'IL1RAP Knockdown in LPS-Stimulated Normal Human Astrocytes Suppresses

LPS-Induced Reactive Astrogliosis and Promotes Neuronal Cell Proliferation', *Neurochemical Research*.